Kinematics and Dynamics of Roller Chain Drives

PhD Thesis

$$(EIv'')'' = q - \rho A\ddot{v}$$

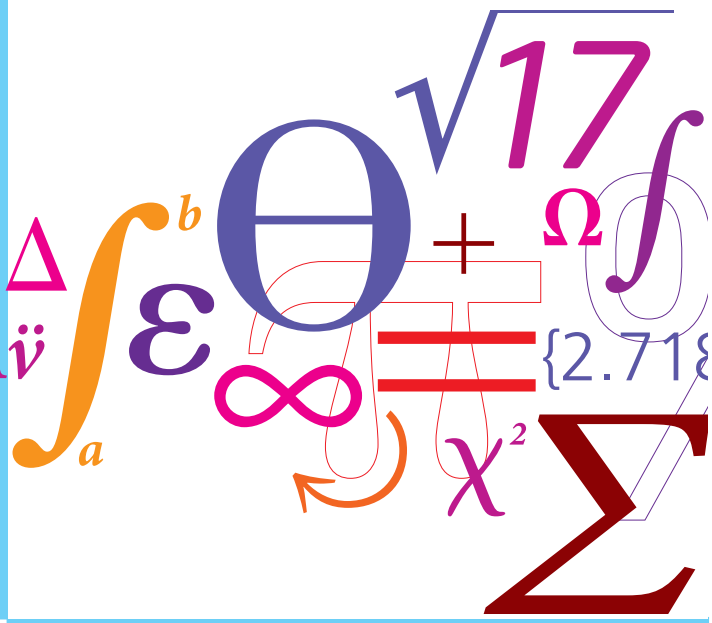

Niels Fuglede
DCAMM Special Report No. S175
July 2014

DTU Mechanical Engineering
Department of Mechanical Engineering

Kinematics and Dynamics of Roller Chain Drives

by

Niels Fuglede

Preface

This thesis is submitted as partial fulfillment of the requirements for being awarded the Danish ph.d. degree. Employed part time only, the work has been carried out from January 2010 to July 2014 at the Department of Mechanical Engineering at the Technical University of Denmark. The project has been supervised by associate professor dr.techn. Jon Juel Thomsen. For the initial phase of the project Peter Orthmann from MAN Diesel A/S provided valuable input in terms of discussions and most importantly, all the written relevant documentation the company had available on the subject of roller chain drives. Although not directly involved with the project, I wish to show my respect for the thorough and well documented work on the simulation of roller chain drives carried out by Sine L. Pedersen.

The program SIMCH developed by Sine, as well as the data provided by Peter has provided a very valuable source of input for me to understand the challenges in the practical design and operation of roller chain drives.

During my ph.d. studies I had the pleasure of visiting Li-Qun Chen and his research team at Shanghai University, Peoples Republic of China. It was a very warm welcome and a fruitful experience on many levels. During my foreign stay I also took the opportunity to meet professor Robert G. Parker, who at the time worked at the University of Michigan-Shanghai Jiao Tong University Joint Institute. His guidance in gyroscopic systems was much appreciated.

Needless to say I am truly grateful to Jon for having patiently supervised my work for nearly a decade, and for providing me with tons of knowledge that remains useful for me, also personally. I would like also to thank all my co-workers, students and friends at the department, who are too many to mention by name, for contributing to a nice atmosphere. Finally, I thank my friends and family for their love and support.

Vesterbro, July 31st 2014 Niels Fuglede

Abstract

There are two main subjects of this work: Kinematic and dynamic modeling and analysis of roller chain drives. In the kinematic analysis we contribute first with a complete treatment of the roller chain drive modeled as a four-bar mechanism. This includes a general, exact and approximate analysis with a clear derivation of the seating and release configurations, as well as the driven sprocket angular position, velocity and discontinuous acceleration. The approximate analysis allows for simple expressions describing the seating and release configurations and shows the influence of main design parameters which is useful for predicting the characteristic loading of the roller chain drive. As a completely novel contribution, a kinematic model and analysis is presented which includes both spans and sprockets in a simple chain drive system. A general procedure for determination of the total wrapping length is presented, which also allows for exact sprocket center positions for a chain with a given number of links. Results show that the total chain wrapping length varies periodically with the tooth frequency. These results are of practical importance to both the design, installation and operation of roller chain drives.

For the analysis of roller chain drive dynamics we present a novel model of a chain drive that couples the vibrations of the chain spans and the driven sprocket. This also includes contributions to the studies of axially moving materials, as the chain is modeled as a string with a variable length supported by moving boundaries. A stationary operating state is introduced for the dynamic model and employing a perturbation method for the analysis of the approximate model results show a multitude of internal and external resonance conditions, thereby identifying critical operating conditions for real chain drives. Examples are presented of both decoupled and coupled motion. Together, the kinematic and dynamic model and analytical results provides a framework for numerical and experimental investigations of roller chain drive motion and deepens the understanding of roller chain drive operation.

Resumé

For denne afhandling er der to hovedtemaer: Kinematisk og dynamisk modellering og analyse af kædetræk. Det første bidrag i den kinematiske analyse er et komplet studie af et kædetræk modelleret som en fire-leds mekanisme. En generel, eksakt og approksimativ analyse præsenteres med en klar udledning for de konfigurationer hvor kæderullerne opnår og mister kontakt med kædehjulene, samt det drevne kædehjuls vinkel-position, hastighed og diskontinuerte acceleration. Med approksimativ analyse opnås simple analytiske udtryk for konfigurationerne hvor kæderullerne opnår og mister kontakt med kædehjulene. Den kinematiske analyse demonstrerer indflydelsen af de vigtigste design parametre og resultaterne kan anvendes til at bestemme den karakteristiske belastning af kædetræk. Som et nyt og originalt bidrag præsenterers en kinematisk model og analyse der inkluderer begge kædespan og kædehjul i et kædetræk. For dette system gives en generel procedure til at bestemme en kædes samlede omslyngede længde, hvilket giver mulighed for beregne den præcise placering af kædehjulenes centrum for en kæde med et givent antal led. Analysen viser at kædens omslyngede længde varierer periodisk med tandfrekvensen. Resultaterne har betydning både for design, montering og drift af kædetræk.
I analysen af kædetræks dynamik præsenteres en ny model hvor vibrationer af kædespan og det drevne kædehjulder kobles. Dette inkluderer også et bidrag til studierne af aksialt bevægede legemer, da kæden modelleres som en streng med variabel længde og bevægende understøtninger. For den dynamiske model introduceres en stationær drift-tilstand og ved at benytte en perturbationsmetode i analysen af den approksimative model opnås betingelser for intern og extern resonans. Resultaterne illustreres med eksempler på både koblede og isolerede svingninger. Tilsammen danner den kinematiske og dynamiske model, analyse og resultater et fundament for videre eksperimentelle og numeriske undersøgelser og bidrager til en dybere forståelse af kædetræks drift.

List of Publications

The following publications are a part of this thesis:

[P1] N. Fuglede and J. J. Thomsen. Kinematics of roller chain drives - exact and approximate analysis. *Submitted for Journal Publication*, 2014. (Can be found on page 71)

[P2] N. Fuglede and J. J. Thomsen. Kinematic and dynamic modeling and approximate analysis of a roller chain drives. *Submitted for Journal Publication*, 2014. (Can be found on page 109)

[P3] N. Fuglede and J. J. Thomsen. Roller chain drive vibration analysis based on a string model with boundaries moving non-smoothly. In *3rd International Conference on Vibro Impact Systems and Systems with Non-smooth Interactions*, 22-26/7/2013, Leinsweiler, Germany. (Can be found on page 167)

[P4] N. Fuglede and J. J. Thomsen. Vibrations of axially moving strings with in-plane oscillating supports. In *1st International Colloquium on Time-periodic Systems, Current trends in theory and application*, 27-30/8/2012, Frankfurt, Germany. (Can be found on page 169)

[P5] N. Fuglede and J. J. Thomsen. Roller chain drive analysis: simplified modeling and analysis of the dynamic effects of meshing. In *7th European Nonlinear Dynamics Conference*, 24-29/7/2011, Rome, Italy. (Can be found on page 175)

Contents

1 Introduction

Motivated by mechanical failure of roller chain drives in low-speed marine propulsion engines, this thesis aims at providing a better theoretical understanding of roller chain drive characteristics. The engineering challenges of designing and operating roller chain drives, to achieve an optimal performance, are significant. The present study focuses on the subjects of kinematics and dynamics of roller chain drives. Kinematic studies deal with the chain drive properties introduced by the geometry of the drive, i.e. shaft center distance, chain pitch length, and number of teeth on the sprockets. Dynamic studies deal with the properties derived mainly from mass, stiffness and damping properties of the drive components, and the loading of the roller chain drive. Since the work carried out in this thesis is of a general theoretical character, it may also be of academic interest to related fields such as belt drive dynamics, band saws etc.

In 2004 Sine L. Pedersen completed a ph.d. project on the multi-body simulation and analysis of roller chain drive systems. In the engineering application of this program, for large chain drives applied in low-speed ship propulsion engines, it became apparent that interpreting the results were difficult, and making suggestions for design improvements equally challenging. Furthermore, it was difficult to design (numerical) experiments, which would produce the kind of vibratory motion experienced in practical roller chain drives to be detrimental. Planning such experiments requires a strong theoretical understanding of the dynamic phenomena, and successful interpretation of the simulation and measurement results requires a good understanding of the chain drive kinematics.

Roller chain drive kinematics take into consideration that roller chains are made out of a series of discrete connected links. In the kinematic analysis of chain drives, it is traditionally assumed that there are no deformation of the chain drive components, i.e. all chain and sprocket elements are rigid. Since roller chains are characterized by having a high axial stiffness, compared to related drives such as belts, the axial deformations are very small compared to the link length, and the kinematic predictions of e.g. positions are practically useful. Furthermore, roller chains are non-uniform, and the most characteristic feature is the uneven bending stiffness EI as well as non-uniform axial stiffness EA and mass distributions ρA, schematized as a function of the span length x in Figure 1.1. The discrete properties are difficult to handle analytically, but throughout the project these properties have been taken into consideration, in order to ensure that the produced research would be directly relevant to the field of roller roller chain drives.

As a consequence of the roller chain discrete properties, a chain wrapped around sprockets form polygons rather than circles, as illustrated in Figure 1.2. The collected effects that chain discreteness introduces are known as polygonal action, and generally include: A periodically varying span length, non-smooth changes of span endpoint velocities leading to impulsive loading at the span endpoints, and a non-smooth driven sprocket angular velocity, even when the driver sprocket angular velocity is constant. This last effect is also apparent in cardan-joints, but in roller chain drives this variation is non-smooth. A thorough study of the chain drive modeled as a four-bar mechanism is carried out in this study. As an original contribution to the effects of polygonal action, it is demonstrated in this work that the total length of a chain wrapping around two sprockets generally varies, due to the sprockets being effectively eccentric. The study of roller chain drive kinematics is not a very large, or currently active field; the latest contribution was published in 1988.

Due to the effects of polygonal action, roller chain drives are inherently prone to vibration and noise, and especially the discontinuous effects of polygonal action makes the subject challenging. Despite this, roller chain drives are used in many mechanical applications due to numerous reasons: Large power transmitting capabilities, the possibility of obtaining a very high efficiency ($> 98\%$), the flexibility in choosing shaft center distances, the successful application in harsh operating environments, the ease of both installation, inspection and maintenance, as well as the option of replacing worn chain drive components at a relatively low cost. Together these properties make roller chain drives attractive in many applications. There are currently no better alternatives to roller chain drives applied in low-speed

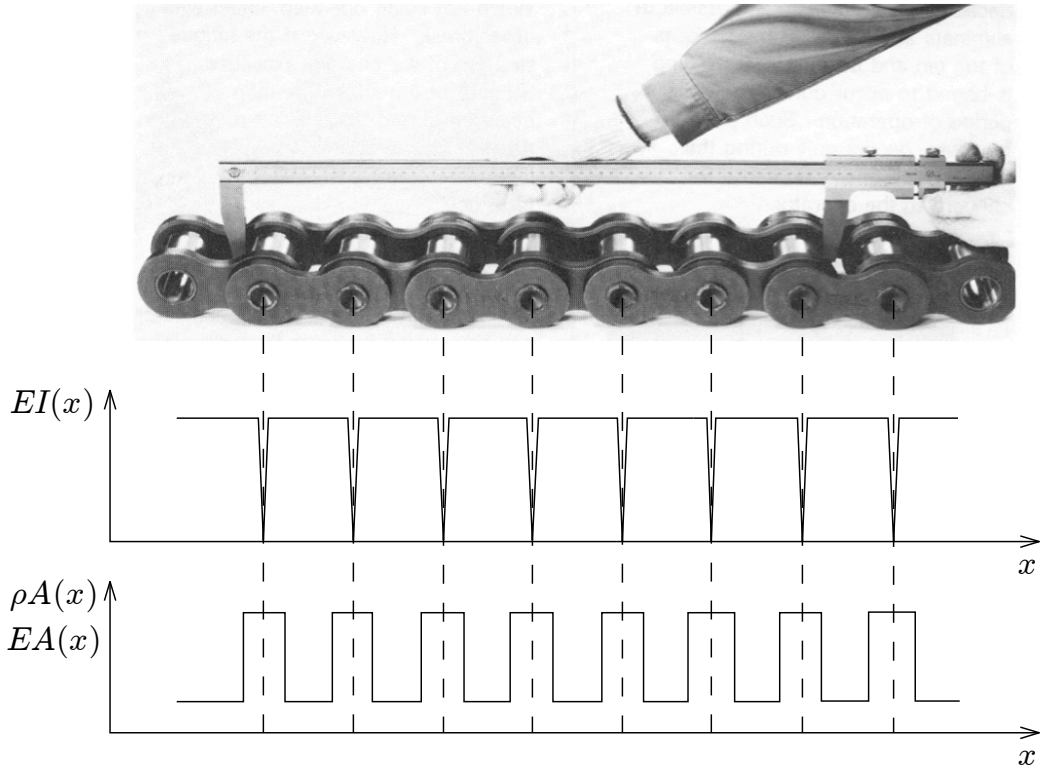

Figure 1.1: Picture showing a chain from a marine diesel engine, and a sketch of the non-uniform properties of roller chains. The bending stiffness EI of each link is very large, but vanishing at the pin joints. Also the mass distribution ρA, and the axial stiffness EA, are non-uniform along the chain length.

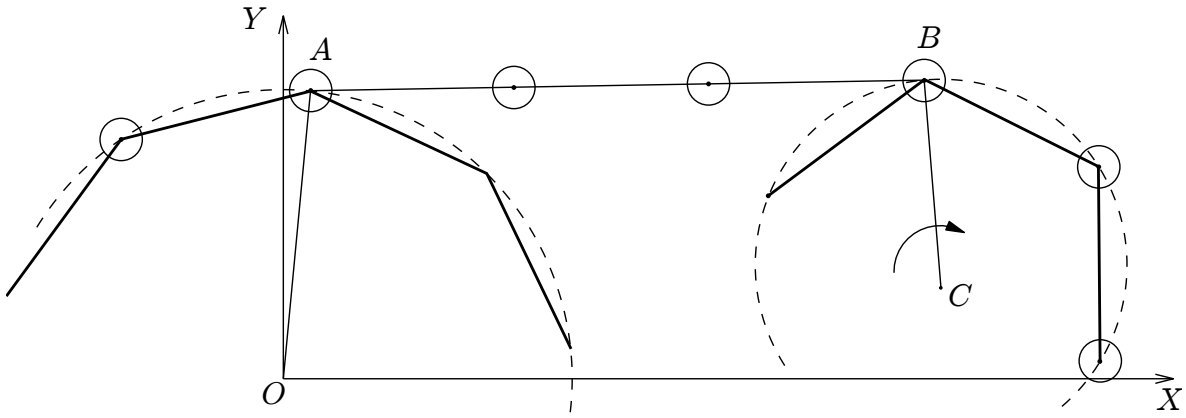

Figure 1.2: Sketch of a roller chain consisting of discrete links connecting two sprockets. A chain wrapped on a sprocket forms a polygon, and therefore the velocity ratio between two sprockets vary during one tooth period. The span endpoints A and B move in the plane as the sprockets rotate, and the chain is subject to impulsive loading when meshing with the sprockets. As the sprockets rotate, and links enter and leave the span, the span length $|AB|$ varies. The effects that the discreteness of a chain introduces are referred to as polygonal action.

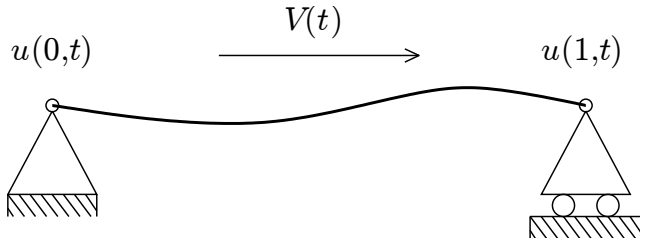

Figure 1.3: Sketch of uncoupled axially moving string traveling with velocity $V(t)$ between boundaries with prescribed endpoint longitudinal displacements $u(0,t)$ and $u(1,t)$. In this type of analysis there is no dynamic coupling to the surrounding system. In the present study, the dynamic coupling between a driven sprocket and two connecting chain spans will be treated analytically.

marine propulsion engines, and they are expected to be the best choice within the foreseeable future.

In the limit, when the number of links is increased and the pitch length decreases, the dynamics of a roller chain span can be studied by modeling the span as an axially moving string. A decoupled axially moving string is illustrated in Figure 1.3. From the considerations of polygonal action there are numerous excitation sources to both longitudinal, and transverse vibration of a chain span. The most often studied sources of longitudinal excitation of strings are either the varying transport velocity, or excitation coming from the prescribed relative motion of the string endpoints. In a chain drive, this corresponds to prescribing both the angular position of the driver and the driven sprocket, and assuming those to be unaffected by the dynamic response of the chain span. In the study of decoupled axially moving strings, the relative endpoint displacements of the string are prescribed through statements such as: *"The relative longitudinal motion of the endpoints* $u(1,t) - u(0,1)$ *is specified. In serpentine belt drives, it is calculated from dynamic analysis of the discrete pulley rotations induced by crankshaft excitations and dynamic accessory torques."* [6]. When statements like these are put forward, it is done without reference to how, in this case, the discrete pulley rotations are calculated. To the designer of chain drives this makes for a significant limitation, since the decoupling appear to be difficult to realize in both laboratory experiments, and practical applications. The coupled dynamic motion may also introduce important phenomena of both practical and academic interest.

A lot of research has been aimed towards the study of belt drives; supported and motivated by the application in the automotive industry. The research on belt drives also included analytical models which accounted for the coupling between

span and sprocket dynamics. However, these models were non-linear and comprehensive; including up to ten coupled partial and ordinary differential equations, and therefore difficult to solve. When analyzed analytically, it was done by making simplifications leading to complete decoupling. Otherwise, solutions were obtained by direct numerical simulation.

This has motivated the formulation of a new mathematical model; undertaken in this study, which include the dynamic coupling, but still allows for analytical solutions. In this work a model of a chain drive is derived, which includes the coupling between two chain spans transverse vibrations and the driven sprocket angular vibration. The model is non-linear, but approximate analytical solutions can be obtained, and demonstrate e.g. under which conditions the dynamics of a chain can be treated as decoupled. Using the model, insight can also be gained into the resonance phenomena that can occur. Approximate analytical solutions show results of great practical relevance, and contribute significantly to the understanding of roller chain drive dynamics.

1.1 Literature review

As indicated in the motivational and informal introduction above, there are several research areas under the headline of roller chain drives. Naturally, the subjects are overlapping, but for providing a better overview, these studies are categorized according to their main focus: Kinematics, roller impact and noise, load distributions, coupled sprocket and span dynamics, full system (multi-body) simulation models, axially moving materials, and finally published reviews covering these different topics. In the following, the literature on these subjects is grouped and reviewed.

Kinematic studies consider the chain drive components to be rigid, and examines the resulting motion of the sprockets and chain span. Bartlett 1931 [7] was the first to realize that a chain wrapping around a sprocket could be compared with that of a non-slippable belt traveling over a prism, i.e. a sprocket could be modeled as a polygon. He derived analytical expressions for the minimum and maximum variation of velocity ratios, and showed that these occur for span lengths equal to an integer number of pitch lengths, or an odd number of pitch lengths, respectively. The concept of treating the kinematic motion of the chain drive to happen through a series of four-bar mechanisms was introduced by Morrison 1952 [8]. An expression for the shaft center distance of the sprockets giving the smallest velocity ratio variation was derived. The four-bar mechanism is made out by points $OABC$ in

Figure 1.2, and the use of this modeling approach has been central to the studies of chain drive kinematics. Radzimovsky 1955 [9] suggested a mechanism for eliminating the velocity pulsation occuring in drives with a small number of teeth. A full monograph was on roller chain drives was written by Binder 1956 [10], in which many subjects relevant for chain drive designers were presented, including; velocity variations, standard tooth geometry, static loading, friction, and wear. Bouillon and Tordion 1965 [11] presented both numerical and experimental investigations of the periodic fluctuation of the driven sprocket angular velocity. They concluded that for drives with average velocity ratios smaller than 1/4, the velocity variations are insensitive to the shaft center distance. It was shown that the angular- velocity and displacement errors decrease approximately as the square and cube, respectively, of the number of teeth on the driver sprocket. Turnbull and Fawcett 1975 [12] carried out an approximate analysis of the driven sprocket angular velocity using a series expansion, and illustrated the influence of the number of expansion terms for different tooth ratios and centre distances. Chen and Freudenstein 1988 [13] gave a more general kinematic analysis, where the center distance could be arbitrary. The discontinuous span length, driven sprocket angular- velocity and accelerations were considered, and the configurations for a roller seating on the driver sprocket were introduced. However, the presentation by [13] was not given in sufficient detail to make it possible to derive the analytical solutions presented, and the work was incomplete in that only the seating configuration was presented. This motivated a more thorough, complete and full kinematic analysis of the roller chain drive modeled as a four-bar mechanism, which was undertaken in the present study. A common motivation mentioned in the above studies is that the kinematic properties are relevant for the dynamic loading of the chain drive, although the dynamics were not considered.

Impact studies concerns the forcing and response of roller and span, due to a non-zero relative velocity between rollers and sprockets at the instant of meshing. Binder and Covert 1948 [14] presented different expressions for the relative impact velocities between a seating roller and a sprocket. The given formulas were derived under the assumptions of; both sprockets having the same size, sprocket pitch equal to chain pitch, constant sprocket angular velocity, and the chain span always being parallel to the line of sprocket centers. The study also presented results of wear and failure tests. Archibald 1946 [15] studied energy losses in chain drives due to impact using energy considerations. A series of experimental and theoretical studies on the uneven transmission by roller chain drives were carried out by Okoshi and Uehara 1959 [16][17] (in Japanese). Results showed that deflecting the tight span by a leaf-spring could smoothen the chain drive transmission. Using energy considerations, Ryabov 1968 [18] discussed the effective weight of the span to

included in the calculation of meshing impulse, and showed it to be equivalent to the weight of 1.67 links. Fawcett and Nicol 1977 [19] carried out experimental studies of the driven sprocket response to impact loading between rollers and sprockets, and showed that the impulsive loading could be significantly reduced by appropriate lubrication. Nicol and Fawcett 1977 [20] introduced a guiding device and showed theoretical and experimental studies of how this device could reduce the undesired effects of impact from meshing. Conwell et al. 1992 [21] designed an machine for measuring impact forces and link tension. Results showed an increased impact intensity at higher sprocket speeds and increased axial tension of the chain [22, 23]. Including the chain span transverse vibration in the study of impact intensity was first done by Wang et al. 1992 [24]. They carried out theoretical modeling of the meshing impulse, and by numerical simulation showed that through a sprocket speed range, the transverse chain vibration may greatly affect the impact intensity. The study [24] was expanded by Liu et al. 1997 [25] to include also the longitudinal chain vibration, and the coupling to the driven sprocket. Numerical simulation of the linear model-equations subjected to impulse forcing showed that the impact intensity varies greatly around system natural frequencies. It was also shown that a model including dynamic coupling produced results in agreement with experimental measurements of impact noise. Ryabov and Kryukov 1997 [26] formulated a set of coupled linear equations for the discrete connected chain links, and through a sequence of numerical simulations obtained graphs for the steady-state impact intensity under varied system parameters. Zheng et al. 2001 [27] presented an acoustical model relating the sound pressure from meshing with the dynamic response of the rollers only, reporting that the rollers had experimentally been observed to be the main source of noise. Using finite element modeling and numerical simulation they produced results in agreement with existing experimental measurements. Further experimental and finite-element investigations of noise in motor-cycle chain drives were carried out by Zheng et al. 2002 [28]. These showed that the generated noise is highest for rollers meshing with the smallest sprocket, and that noise can be reduced significantly by adding damping-material to the sprockets in the drive [29]. With a multi-body dynamics approach, Schiehlen and Seifried 2004 [30] presented three approaches for modeling the impact dynamics. Wang et al. 2013 [31] presented a study showing that a modified tooth profile could reduce the meshing impact in chain drives. A common motivation for the above studies has been noise reduction, and the reduction of impact intensity, in order to extend the service time of a roller chain drive.

Load distribution concerns the engagement of a loaded chain wrapped on a sprocket, with *distribution* referring to the distribution of sprocket tooth load, and distribution of chain link tension. Binder 1956 [10] presented a the geometric progression load distribution (GPLD) analysis to determine the tension in the roller chain links.

This method is based on the following assumptions: Mechanical clearances are not present, chain pitch is exactly equal to sprocket pitch, friction is neglected, the pressure angle is constant, chain and sprocket are considered as rigid bodies, the angular velocity of the sprocket is constant, the driving strand angle is unaffected by the driver position, and the line of sprocket tooth reaction is on the line of the tooth pressure angle. The result is analytical expressions for the progressive reduction of link tension from the tight to the slack span side. Marshek 1979 [32] introduced a spring-model analysis which considered flexibility of the chain and tooth, and by formulating a set of coupled equations for the link forces, with the free span axial forces acting boundary values, and assuming the rollers to be bedded, determined the link force distribution. Ryabov 1980 [33] studied the engagement of worn chain with a sprocket, in order to estimate the maximun permissible wear of a chain. In a later study, elastic deformation of the chain was also included [34]. Naji and Marshek 1983 [35] studied the load distribution using GPLD, and compared results obtained with a spring model. Results showed that for a large selection of steel chain and sprocket combinations, the elastic properties do not have an affect on the load distribution. In a following experimental study, effects of lubrication, misalignment, sprocket speed and slack span load was investigated. Results were compared to the analytical results obtained using the GPLD, and showed very good agreement. Lubrication, minor misalignment and variations of sprocket speed did not have a noticable effect on load distribution [36]. To further investigate the effects of sprocket flexibility, Eldiwany and Marshek 1989 [37] conducted experimental studies of load distributions of a steel chain wrapped on polymer sprockets. Naji and Marshek 1989 [38] extended the GPLD method to include the effect of the pitch difference between the sprocket teeth and roller chain, the frictional forces between the rollers and the sprocket teeth, and the centrifugal forces on the chain caused by rotation of the sprocket. Results showed that wear elongation of a chain causes an increased load level on the sprocket teeth. Kim and Johnson 1992 [39] modified the GPLD method to include a more accurate description of the tooth profile, according to the ANSI standard. Their theoretical results compared very well with existing experimental results [40]. Simulation studies of load distribution including two spans and two sprockets were presented by Troedsson and Vedmar 1999 [41] and [42]. A common motivation to the above studies has been to develop theoretical models of the load distribution, which compared well with experimental results. The development of the GPLD model has been successful in this. With good theoretical models, accurate predictions for the influence of wear and exact sprocket tooth geometry can be applied when deriving recommendations for the maximum allowable chain wear. Accurate theoretical load-distribution models can also be utilized in the development of improved geometric designs of the sprocket tooth.

System dynamics concerns the response of sprockets and/or spans when the interaction between these are taken into account. This does not necessarily imply a dynamic coupling, but the analysis of chain or sprocket response under loading which seem typical of roller chain drives. Mahalingam 1957 [43] showed that a varying axial tension in a (decoupled) chain span coming from polygonal action could be modeled as a string subjected to parametric excitation, and that varying axial tension of a (decoupled) span acting as a linear spring connected to the driven sprocket cause direct excitation of sprocket angular vibrations [44]. With simple theoretical models Nicol and Fawcett 1977 [45] reviews the types of vibration present in roller chain drives. Turnbull et al. 1977 [46] carried out experimental studies to investigate the dynamics of the driven sprocket under operating conditions dominated by dynamic effects, as opposed to the motion predicted by purely kinematic analysis. Fawcett and Nicol 1980 [47] also carried out experimental studies, which included measurements of the driven sprocket angular acceleration under constant operating conditions, and made comparisons with simple theoretical models. Wang and Mote 1987 [48] presented a comprehensive model of a belt drive with the endpoints subjected to impulsive displacements coming from the butt weld connecting the ends of a continuos span. Stability was examined of a single decoupled span. In a later study by Wang 1992 [49], the belt-drive model was re-introduced as a generic model for a timing chain drive, and stability of a decoupled span was investigated. The model consists of ten coupled non-linear ordinary- and partial differential equations, for the sprocket center positions, and angular displacements, as well as span longitudinal and transverse displacements. Ryabov 1971 [50] presented (empirical) formulas for the longitudinal wave propagation speed for different axial tensions. Ariaratnam and Asokanthan 1987 [51] reworked the study of Mahalingam [43], and in both these studies the argumentation is as follows: First, assume the span to be rigid, and calculate the tooth periodic variation of the driven sprocket angular motion from the kinematic analysis of the resulting the four-bar mechanism. Secondly, assume the span to be flexible, and calculate the resulting tension variation of the span from the (now prescribed) motion of the sprockets. While not completely obvious in their presentation, this is the argumentation that demonstrates how a (decoupled) chain span can be modeled as a string subjected to parametric excitation. The contradiction between the first and second assumption stands out to this author as significant, and it has motivated the development of more coherent model of the coupled motion of the chain spans and the driven sprocket. Choi and Johnson 1993 [52] presented results of coupled span and sprocket motion obtained by numerical simulation, and also carried out a study where a tensioner sprocket was included [53]. Lodge and Burgess 2002 [54] studied the transmission efficiency in roller chain drives, and the selection of chain and sprocket size for minimizing power loss [55]. A common motivation to the above studies is to minimize undesired vibration of the chain drive components coming from their dynamic interaction.

Full system simulations concerns the formulation of models aimed at the numerical simulation of the full coupled motion of roller chain drives components, where each link is included as separate degrees of freedom, and the interaction between the sprocket tooth and the rollers rely on a detailed modeling of the sprocket geometry. Troedsson and Vedmar 2001 [56] formulated a dynamic model for the coupled motion of a chain drive with two sprockets and two spans. Pedersen et al. 2004 [57] developed a multi-body simulation model for the analysis of roller chain drives in large marine diesel engines, and refined the modeling strategy for the roller-sprocket contact and an updated sprocket tooth geometry [58].

Axially moving materials concerns the study of string-, beam- and belt like structures traveling at a non-zero velocity between boundaries. This is a very large and active field, with publications added on a weekly basis. Here are presented the main references, which gives the best insight into the subject, in relation to the study of chain span dynamics. Axially moving materials belong to the class of gyroscopic systems, due to the presence of Coriolis forces. Thurman and Mote 1969 [59] used Hamiltons principle to derive the non-linear equations of motion for an axially moving string, and the influence of of transport velocity and non-linearity on the natural frequencies were analyzed, along with examples of the spatial modal distributions [60]. Meirovitch 1974 [61] analyzed the eigenvalue problem of gyroscopic systems, and carried out a modal analysis of discrete gyroscopic systems [62]. Based on these studies, Wickert and Mote 1990 [63] presented the exact modal solution for continuos systems, as well as energy studies, and studies of the forced and free response around super- and sub critical velocities [64, 65], respectively. The above studies demonstrate that the characteristics of an axially moving string is velocity dependent natural frequencies, the presence of a critical speed where the string axial tension reduces to zero, and complex-valued eigenfunctions, which are utilized by casting the system in a first order form. Mockensturm et al. 1996 [66] showed that the complex eigenfunctions were a superior basis compared to the eigenfunctions for stationary strings, when predicting parametric instability. Parker and Lin 2001 [6] analyzed the stability boundaries and non-linear response of axially moving strings subjected to multi-frequency parametric excitation. For experimental studies, the analytical and experimental work on parametric instability in belt drives by Michon et al. 2008 [67] and [68] could be of special interest to similar studies for roller chain drives. A main difference between chain and belt drive dynamics is that belt drives wrapped on pulleys have different contact zones, where there is sliding or adhesion, as opposed to chain drives, where there is no noticable relative motion between the rollers and sprockets. The models are therefore not directly comparable, but the studies of belt may continue to provide valuable input to the field of roller chain drives.

Reviews on the subjects related to the study of roller chain drives are presented here. Mote 1972 [69] introduces axially moving material research as problems considering the lateral response, vibration or stability of long slender members in which mass is continuously transported. Examples of such systems are magnetic and paper tapes, moving bands and belts, chain drives, moving strings, textile and fiberglass fibers, bandsaws, pipes containing flowing fluids, hydroelectric power plant conduits, oil lines, and fuel lines. Ulsoy et al. 1978 [70] reviews the principle developments related to band saw vibration and stability research. Fawcett 1981 [71] reviews papers relating to the general problem of axially moving materials, and papers relating to belt- and chain drives. Wickert and Mote 1988 [72] reviews the literature on the vibration and dynamic stability, and present fundamental modeling issues and research conclusions, excluding pipes conveying fluids. Wang and Liu 1991 [73] reviews research on the noise and vibration of chain drive systems, including noise source identification, load analysis, kinematic analysis, dynamic and vibration analysis, and noise and vibration controls. Rahnejat 2000 [74] reviews research on multi-body dynamics. Chen 2005 [75] considers research on the analysis and control of transverse vibrations of axially moving strings in a comprehensive review including 242 references. In another review, the latest progress on the nonlinear dynamics for transverse motion of axially moving strings is considered by Chen et al. [76]. Marynowski and Kapitaniak 2014 [77] reviews research on axially moving continua, including string- and beam like systems, elastic and viscoelastic plates.

1.2 Contribution of this work

The original contributions of this work, in relation to the existing research, can be outlined as follows: In [P1] is presented a formal and self contained analysis of the roller chain drive modeled as a four-bar mechanism. The kinematic analysis is general and offers both exact and approximate solutions for the motion of all four-bar members and the determination of both seating and release configurations. Presented are also novel approximate results for the phase between the seating and release events, as well as approximate analytical expressions for the driven sprocket angular motion, taking the discontinuous characteristics into account, as opposed to the existing approximate analysis [12], which was based on a Fourier expansion. The early kinematic studies were limited to specific cases of span lengths and shaft center distances, but the analysis carried out in this work is general. This work supplements the existing general kinematic analysis, specifically [13], which was incomplete, and not presented in a form that allowed for the use or reproduction of the presented results. Furthermore, the influence of the pitch fraction, which is a main design parameter, has been discussed, and shown to be less significant than has been stated previously for chain drives where the sprockets have a moderate or

high number of teeth.

As a completely novel contribution, the kinematic analysis is extended in [P2] to include both spans in a chain drive with two sprockets with the connecting spans tensioned to form straight lines. This type of analysis has not been undertaken previously; in all the existing studies, only the tight span connecting two sprockets has been considered. A method for calculating the total length of chain wrapping around two sprockets is given, and results show that the wrapping length varies during one tooth period, which is a novel contribution to the effects of polygonal action. The method allows for the exact calculation of sprocket center positions for a given chain length, which is not trivial, due to sprockets effectively forming polygons.

As a contribution to the study of string dynamics, in [P2] is presented the analysis of a string supported by moving boundaries, with endpoint displacements prescribed from a non-constant position. This models how a chain span has a variable length, and by assuming the length to be a first order vibration, it is shown that the effect of this is a second order effect in the equation of motion and boundary conditions for the axially moving string, which is an original contribution.

In [P2] is presented a novel contribution in both roller chain drive modeling, and (approximate) analysis. The prime goal of this work is to analyze the coupled dynamics of transverse span vibrations and driven sprocket angular vibrations. Existing models of roller chain drive dynamics did either not include the dynamic coupling at all [43, 51], or included the dynamic using models derived for belt drives [49] which suffered from being to complex to handle analytically. The analysis [49] did not take advantage of the kinematic coupling between the spans connected across a sprocket, where there is no slipping and relative motion between the sprockets and chain. This feature of roller chain drives introduced in this work allowed for the formulation of the coupling of span and sprocket motions. The perturbation analysis of the presented model identifies cases of internal and external resonance, thereby providing new insight into critical operating conditions in real chain drives. Example results show that compliance of the driven sprocket increases the frequency range where a chain span subjected to parametric excitation has a vibratory response, which is also a significant and novel result.

Finally, in this thesis, comparison is made between results of the kinematic analysis and multi-body simulation results, which is also a novel contribution to the study of chain drive kinematics.

1.3 Structure of this thesis

There are two accepted ways to write a PhD thesis at the Technical University of Denmark. One accepted form is to present a self contained thesis in which the author presents all the work done throughout the PhD-study. Another option is to publish scientific papers during the PhD-study, and then summarize the contributions of these papers in the thesis. The present thesis is of the second form, i.e. article based and thus containing a summarizing part and an article part.

The summarizing part attempts to balance the mathematical and theoretical nature of the publications, and at the cost of mathematical rigor, the emphasis is directed towards several themes, intended to: Provide a thorough motivation for the work carried out. Introduce the existing published research on the subject. Place the published work in this context. Present the relevant background information on real roller chain drives, and their applications in marine propulsion engines. Initiate readers which are not experts in this field to the characteristics of roller drives. Point out critical aspects of the research, which can motivate further studies. Give an overview of the work presented in the article publications. Make an emphasis of the engineering perspective, and application of the obtained results. Provide recommendations for the direction of future research.

After a review on the existing literature presented in this chapter, the next chapters introduce and summarize the kinematic and dynamic modeling and analysis of the roller chain drive. The full details and stringent treatment of the kinematic and dynamic contributions are given mainly in publications [P1, P2].

2 Classic kinematic analysis

This chapter summarizes the kinematic analysis of a roller chain drive modeled as a four-bar mechanism [P1]. The purpose of the presentation here is to provide insight into the motion of the chain drive components, as this forms the basis for interpretation of simulation and measurement results, and lays the foundation for the analysis of the chain drive dynamics. Due to sprockets forming polygons, the chain span and the driven sprocket is subjected to a characteristic loading which is important to understand when analyzing the chain drive dynamics.

In this analysis, the exact kinematic motion of the chain span components is determined, i.e. the position of the span endpoints as well as angular position, velocity and acceleration of the driven sprocket during one tooth-period of the driver sprocket. From these one can predict e.g. the positions of all the chain rollers in the span, assuming dynamic effects to be negligible. Kinematic analysis neglects deformation and dynamics effects, although these are of course are important, and in real operating chain drives, not negligible. However, the results presented here will still be useful for understanding measurement results obtained e.g. when the chain drive is subjected to slow turning of the driver, which is relevant for verifying both the numerical modeling of chain drive geometry and constraints, as well as experimental results. In both experimental and numerical simulation, a natural first step is to monitor the sensor output at the simplest possible operating conditions, which is the quasi-static motion of the drive operating at low angular velocities, for which results should be comparable with the kinematic predictions.

Furthermore, the kinematic analysis is intended to help the designer make the optimal choices of the chain drive parameters relating directly to the kinematics: Shaft center distance, sprocket radii, and number of teeth on the sprockets. As can

be expected, the effects of polygonal action are minimized by choosing sprockets which have short pitch lengths, and sprockets with a large radii, and operating at low angular velocities, as this ensures a smoother operation of the chain drive. In praxis, these choices are limited for the designer by concerns such as limited space for the drive, sprocket torque transmitting capabilities, specific gear ratios, shaft center requirements and torque transmitting capabilities. Thus, the kinematic analysis may aid the designer to make optimal choices under the given limiting circumstances.

This chapter is titled classic kinematic analysis, and this refers to the analysis considering only the tight span connecting two spockets, with the drive modeled using the equivalent four-bar mechanism. If the chain drive consists of only two sprockets there will also be a slack chain span connecting the two sprockets opposite of the tight span, but this is traditionally not considered in this type of analysis. In case there are more than two sprockets in the drive, there will be not be a slack span opposite to the tight span, and the analysis covers the transfer of torque between two neighboring sprockets connected to rotate in the same direction in a larger chain drive system.

In the following, approximate results for the motion of the driven sprocket are also presented. Simple approximate expressions for the seating and release configurations are given, and these are used for obtaining the first analytical expression for the phase between rollers seating and releasing. The exact and approximate results are compared and shown to be in very good agreement for practical chain drives. These approximate results ease the calculation of the motion of the driven sprocket, and may aid designers to quickly evaluate designs and estimate chain drive loads. The obtained results include the discontinuous properties of the driven sprocket motion.

In Figure 2.1 is shown the typical design for roller chains applied in marine diesel engines. The chain element in contact with the sprocket is the chain roller. Friction occurs due to relative motion among the chain elements, which is necessary for the continued motion of the drive. Therefore, lubrication is important in order to ensure a high efficiency and minimize wear between the pin and bushings, which causes chain elongation during the coarse of operation. The ANSI standard roller chain sprocket geometry is shown in Figure 2.2. The curves at the bottom of the tooth form is called the seating curve, while the curves next to the seating curve are called the working curves. New chains have an over length error, and the over length error increases in the course of operation, due to wear between the pin and the bushing.

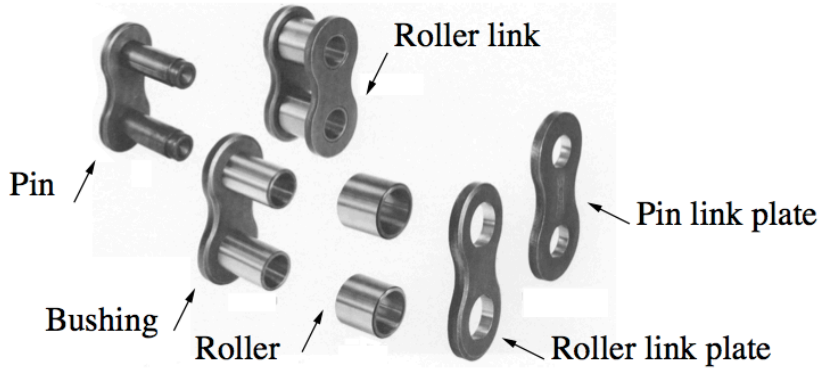

Figure 2.1: Roller chain components, Tsubaki chain (figure from [58]).

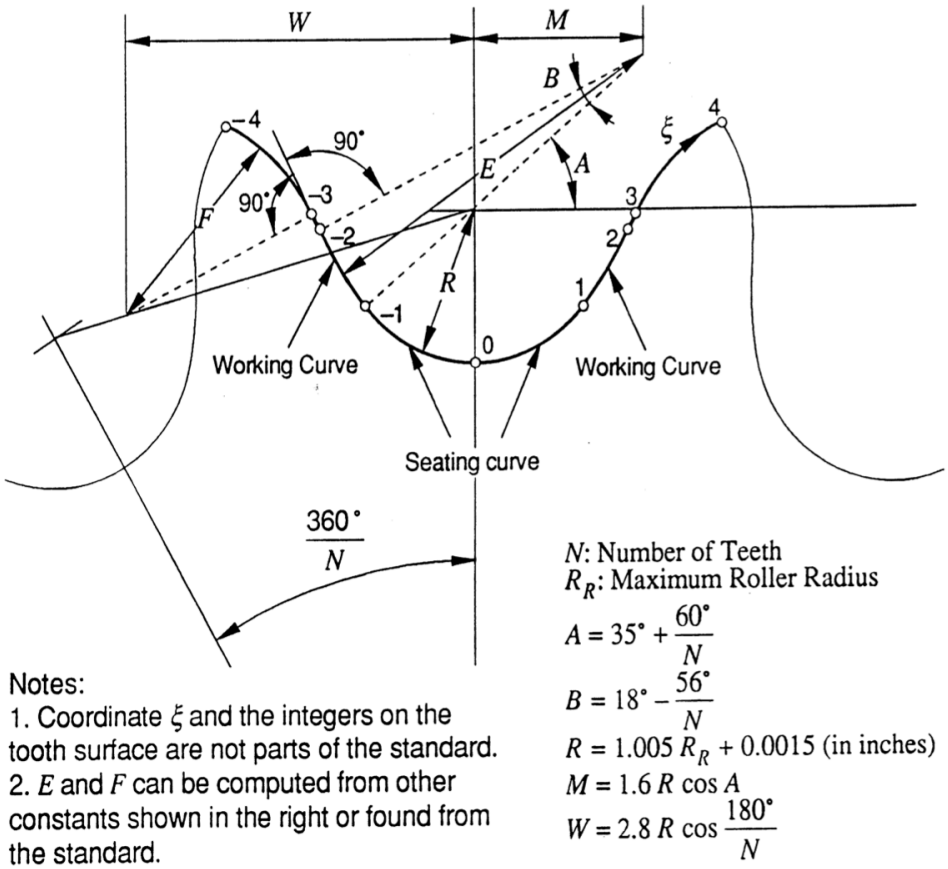

Figure 2.2: ANSI standard sprocket geometry (figure from [39]).

2.1 Exact kinematic analysis

In the kinematic analysis of the roller chain drive modeled as a four-bar mechanism, friction, mass, elasticity, tolerances, clearances and manufacturing inaccuracies of the drive components are ignored. It is assumed that the span is tensioned to form a straight line, and chain rollers are positioned exactly at the center of the seating curves. Results therefore describe the motion of ideal chain drives operating at non-resonant conditions and very low speeds.

Figure 2.3 shows sketch of a chain span meshing with a sprocket. Rollers are shown as small circles, thereby marking the chain as a connection of rigid links. The chain moves from left to right and the roller S_N will be removed from the free span as the sprocket rotates clockwise around point C. Shown in the sketch is the exact moment where roller B_1 gets in contact with the sprocket and thereby define the new endpoint for the span.

Several geometric properties are defined from Figure 2.3. The pitch, p, is the distance between two chain rollers and also the length of the sides of the pitch polygon, witch is formed by connecting the centers of the sprocket seating curves. Half the angle between two seating curve centers is referred to as the pitch angle α. The pitch polygon has inscribed circle radius r and the circle drawn out by the centers of the seating curves on the sprockets is referred to as the pitch circle and has radius R. By formula, these variables are given by, respectively,

$$\alpha = \frac{\pi}{m}, \quad r = \frac{p}{2\tan\alpha}, \quad R = \frac{p}{2\sin\alpha}, \tag{2.1}$$

where m is the number of teeth on the sprocket.

It is seen from Fig. 2.3 that the length and endpoint positions of the free span varies discontinuously as the sprocket rotate clockwise around C. Rotation of the sprocket causes a vertical movement of the span endpoint between values r and R, and a horizontal movement between positions B_1 and B_2. The angle between the chain span $S_N B_1$ and the line CB_1 varies during rotation of the sprocket, and therefore a constant driving torque will not be transmitted evenly to the chain. Vectors $\mathbf{u}_1$ and $\mathbf{u}_2$ indicate the sprocket velocities at rollers B_1 and B_2, respectively. These velocities differ in direction and this cause an impact between the roller B_1 and the sprocket. Collectively, these effects are referred to as polygonal action, their magnitude decrease as the number of sprocket teeth increase, but remains finite and, a characteristic for roller chain drives.

Figure 2.4 shows the kinematic model in the coordinate system used throughout the analysis. The driving sprocket constraining the motion is centered at C and

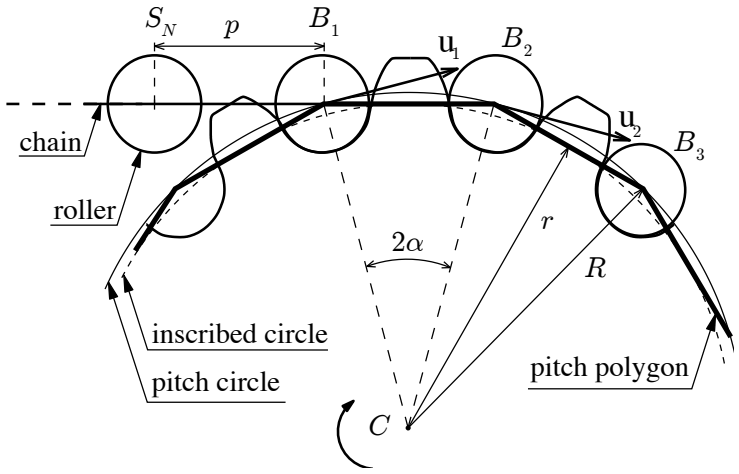

Figure 2.3: Sprocket meshing with chain

the driven sprocket at O. Subscripts c and o are used to refer to those sprockets, e.g. α_o and R_c. Both sprockets are drawn as pitch polygons, connected by a line A_1B_1 representing the tight chain span.

When the chain drive consists of only two sprockets there will be a slack chain span connecting the two sprockets opposite of the tight span, and this will not be considered in the present analysis. In case there are more than two sprockets there will be no slack span between sprockets O and C and the analysis presented here covers the transfer of torque between two neighboring sprockets in a larger chain drive system.

The origin of the fixed Cartesian XY-coordinate system is coincident with the center O of the driven sprocket. It is orientated such that the X-axis is parallel with the tangent T_oT_c common to the two inscribed circles, so that the coordinates (x_c, y_c) of C is:

$$x_c = |T_oT_c| = (N + 1 + f)p, \quad f \in [0,\ 1[, \quad N \in \mathbb{N}, \quad y_c = r_o - r_c, \tag{2.2}$$

thereby defining the integer number of pitches N plus a fraction of pitch lengths f. For a wide range of typical chain drives lines OA_1 and CB_1, make small variations around the vertical direction and the slope of the span make small variations around the horizontal direction, while OC remain fixed. The smallness in variations makes the kinematic model suitable for approximate analysis.

When the roller chain drive is in operation, chain links will recurrently enter and leave the chain span and consequently the span length varies discontinuously with sprocket angular rotation, c.f. Fig. 2.4. The driving sprocket constrain the motion, and as it rotates the angle $2\alpha_c$ in clockwise direction, one tooth period passes and

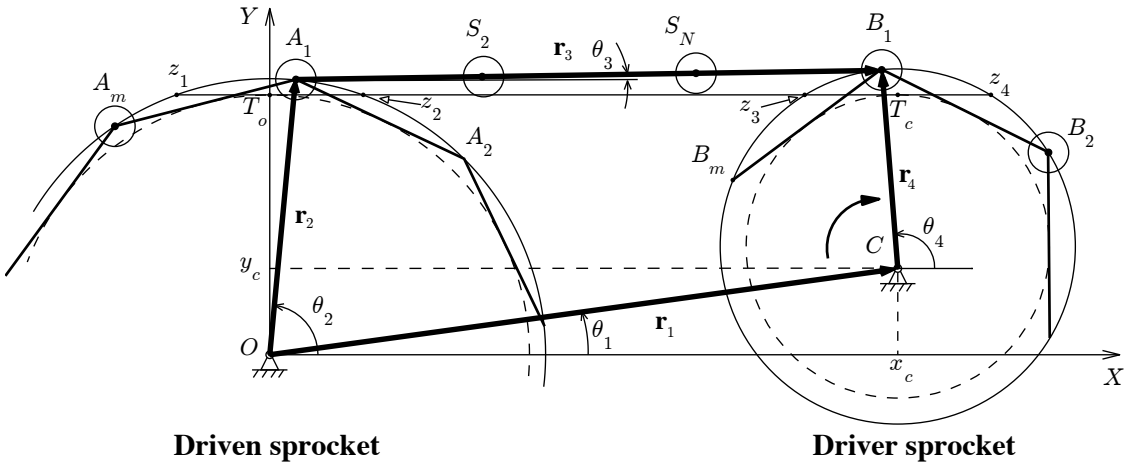

Figure 2.4: Chain drive kinematically modeled as a four-bar mechanism

two events occurs: Roller A_1 loses contact with the driven sprocket and is released into the free span, thereby *in*creasing the span length by one pitch. Similarly, roller S_N gets in contact with the driving sprocket, thereby *de*creasing the length of the span by one pitch. In the general case where $f \neq 0$ the span length $|A_1B_1|$ can be shown to vary between the two lengths given by

$$|A_1B_1| = (N + j)p,\ j = 1, 2,\ \text{for}\ f \neq 0. \tag{2.3}$$

Exactly how the length varies in time depends on the driver position, and requires the analysis of the four-bar mechanism $OABC$ in Figure 2.4. The vectors in the four-bar mechanism in Figure 2.4 are written in polar form as $\mathbf{r}_n = r_n e^{i\theta_n}$, $n = 1, 2, 3, 4$, where r_n is the length of the vector, θ_n the orientation measured positive counter clockwise from the X-axis, and the real and imaginary parts of the vector are parallel to the X- and Y-axis, respectively. The equations governing the position, velocity and acceleration of the four-bar mechanism members are

$$\mathbf{r}_2 + \mathbf{r}_3 = \mathbf{r}_1 + \mathbf{r}_4, \tag{2.4}$$

$$i\omega_2\mathbf{r}_2 + i\omega_3\mathbf{r}_3 - i\omega_4\mathbf{r}_4 = \mathbf{0} \tag{2.5}$$

$$(i\alpha_2 - \omega_2^2)\mathbf{r}_2 + (i\alpha_3 - \omega_3^2)\mathbf{r}_3 - (i\alpha_4 - \omega_4^2)\mathbf{r}_4 = \mathbf{0}. \tag{2.6}$$

where $\omega_n = d\theta_n/dt$, $\alpha_n = d\omega_n/dt$, $n = 2, 3, 4$, and

$$r_1 = \sqrt{x_c^2 + y_c^2},\ r_2 = R_o,\ r_3 = L + hp,\ r_4 = R_c,\ L \equiv (N + 1)p. \tag{2.7}$$

The span length $r_3 = |A_1B_1|$ is introduced here as L, and a step function h, for which the definition requires the determination of the seating and release configurations.

2.1.1 Position analysis

The configuration of the four-bar mechanism for which a roller is just *seated* on the driver sprocket is shown in Figure 2.5. Variables related to the *seating* and *release* of a roller are subscripted s and r, respectively. The two solutions for θ_{4s} can be

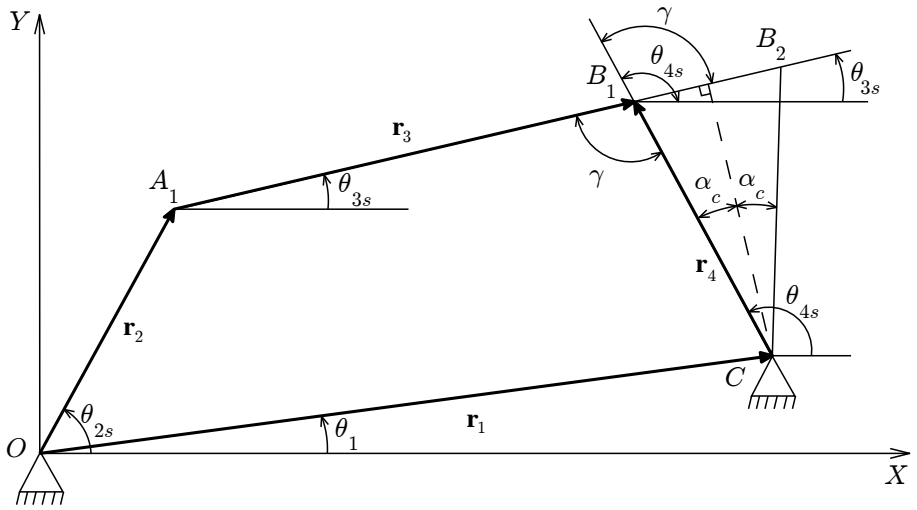

Figure 2.5: Equivalent four-bar mechanism at the instant where a roller seats on the driver sprocket C.

shown to be

$$\theta_{4s} = 2\arctan(\tau_{1,2}), \quad \theta_{3s} = \theta_{4s} - \gamma, \quad \gamma = \pi/2 + \alpha_c \tag{2.8}$$

$$\theta_{2s} = \arctan\Big(\frac{r_1\sin\theta_1 + r_4\sin\theta_{4s} - r_3\sin\theta_{3s}}{r_1\cos\theta_1 + r_4\cos\theta_{4s} - r_3\cos\theta_{3s}}\Big). \tag{2.9}$$

where

$$\tau_{1,2} = \frac{-B_s \pm \sqrt{B_s^2 - C_s^2 + A_s^2}}{C_s - A_s}. \tag{2.10}$$

and

$$\begin{aligned} A_s &= 2r_1r_4\cos\theta_1 - 2r_1r_3(\cos\theta_1\cos\gamma - \sin\theta_1\sin\gamma),\\ B_s &= 2r_1r_4\sin\theta_1 - 2r_1r_3(\cos\theta_1\sin\gamma + \sin\theta_1\cos\gamma),\\ C_s &= r_1^2 + r_4^2 + r_3^2 - r_2^2 - 2r_4r_3\cos\gamma. \end{aligned} \tag{2.11}$$

where all lengths r_n are given by (2.7) with $h = 0$. There are two solutions sets, corresponding to the two values of τ in (2.10). These correspond to configurations where the sprockets are connected by the span to rotate either in the same or opposite directions. The two solutions for θ_{2s} are of opposite sign, and the solution-set where $\theta_{2s} > 0$ is the one for which both sprockets rotate in the same direction.

The configuration for which a roller is released from the driven sprocket can be determined following an approach similar to the determination of the seating configration [P1]. When the seating and release configurations are determined, the function h varies according to

$$h = h(\theta_4) = \begin{cases} 0 & \text{for } \theta_{4s} \geq \theta_4 \geq \theta_{4r} \\ 1 & \text{for } \theta_{4r} \geq \theta_4 \geq \theta_{4s} + 2\alpha_c \end{cases} \tag{2.12}$$

Note that the angle θ_4 decrease, as the driver rotates in clockwise direction. With h determined, the span length varies according to $r_3 = L + hp$, cf. (2.7). The angles θ_{4s} and θ_{4r} are cumbersome to determine exactly, but simple and rather accurate approximations are determined in the approximate analysis.

Determining the driven sprocket angular position θ_2 and the span angle θ_3 as a function of θ_4 follows steps similar to the ones carried out for the seating and release configurations, i.e. factorization of coefficients A, B and C from (2.4), and the solution for θ_2 given by $\arctan(\tau_{1,2})$, where $\tau_{1,2}$ are polynomial roots. The result is the *input-output* relation $\theta_4 = f(\theta_2)$, i.e. the driven sprocket angular position as a function of the driver sprocket angular position [P1].

The kinematic motion of the chain drive is tooth-periodic, i.e. the position of the four-bar members repeat when the driver angle advances by $2\alpha_c$, the angle between two consecutive teeth. During one period a roller will have been released into, and another one removed, from the span.

2.1.2 Angular velocity and acceleration

The angular velocity of the driven sprocket ω_2 generally varies with time, even if the driver sprocket rotates at constant angular velocity ω_4. From (2.5) one finds

$$\omega_2 = \omega_4 \, \frac{r_4}{r_2} \, \frac{\sin(\theta_4 - \theta_3)}{\sin(\theta_2 - \theta_3)}. \tag{2.13}$$

Note here, that the driver angular velocity may vary, i.e. $\omega_4 = \omega_4(t)$. The angular acceleration α_2 of the driven sprocket depends both on the driver sprocket angular acceleration α_4 and the sprocket angular velocities ω_2 and ω_4, and from (2.6) one finds

$$\alpha_2 = \alpha_4 \, \frac{\omega_2}{\omega_4} + \frac{\omega_4^2 r_4 \cos(\theta_4 - \theta_3) - \omega_2^2 r_2 \cos(\theta_2 - \theta_3) - \omega_3^2 r_3}{r_2 \sin(\theta_2 - \theta_3)}, \tag{2.14}$$

With the above analysis, the exact angular motion of the driven sprocket has been determined as a function of the driver angular motion. The exact seating and release configurations have been determined, and the span length variation is thereby given.

2.2 Approximate analysis

Presented here are approximate formulas for seating and release configurations, as well as angular position, velocity and acceleration of the driven sprocket. In the analysis above, exact solutions were obtained from coupled nonlinear algebraic equations, e.g. (2.4) split into real and imaginary parts, with θ_n, $n = 2, 3, 4$ being dependent variables of the resulting trigonometric functions. To obtain simple approximate solutions, which are also accurate, the trigonometric functions are expressed using carefully chosen Taylor expansions, e.g. the seating angle θ_{4s} is obtained through a Taylor expansion around $\pi/2 + \alpha_c$.

All parameters are nondimensionalized to reduce the number of variables and make the order of magnitude of the various terms easily comparable. All lengths are nondimensionalized by L, and nondimensional parameters are identified by over-bars,

$$\bar{R}_c = \frac{R_c}{L}, \quad \bar{R}_o = \frac{R_o}{L}, \quad \bar{r}_c = \frac{r_c}{L}, \quad \bar{r}_o = \frac{r_o}{L}, \quad \bar{p} = \frac{p}{L}, \tag{2.15}$$

from which it follows that $\bar{x}_c = 1 + f\bar{p}$ and $\bar{y}_c = \bar{r}_o - \bar{r}_c$.

2.2.1 Seating and release configurations

The algebra required to obtain the approximations is comprehensive, and only the results needs to be summarized here. For the seating configuration, the approximate solution for the angular positions of the four-bar members are approximately

$$\theta_{4s} \approx \frac{\pi}{2} + \alpha_c + \bar{p}\alpha_o f(f-1), \tag{2.16}$$

$$\theta_{3s} \approx \bar{p}\alpha_o f(f-1), \tag{2.17}$$

$$\theta_{2s} \approx \pi/2 + \alpha_o(1-2f). \tag{2.18}$$

Similarly for the release configurations,

$$\theta_{2r} \approx \pi/2 - \alpha_o - \bar{p}\alpha_c f(f-1), \tag{2.19}$$

$$\theta_{3r} \approx -\bar{p}\alpha_c f(f-1), \tag{2.20}$$

$$\theta_{4r} \approx \pi/2 - \alpha_c(1-2f), \tag{2.21}$$

For real chain drives both the non-dimensional pitch length $\bar{p}$ and the pitch angle α_o will be small. Therefore the terms in (2.16)-(2.21) containing products $\bar{p}\alpha_o$ and $\bar{p}\alpha_c$ will be small corrections to the remaining terms. Impact has not been the object of investigation of this work, but in (2.16) it is shown that the seating position θ_{4s} is close to point z_3 in Fig. 2.4, as is often assumed in studies of impact and

noise [52, 27]. In Fig. 2.3 the relative velocity between a seating roller and the driver sprocket $\mathbf{u}_1 - \mathbf{u}_2$, is therefore practically independent of f. Assuming the span is a straight line, the main design factor affecting the relative velocity, besides the angular velocity of the driver, is therefore the number of teeth on the driver sprocket (the pitch angle), and the sprocket radius. Comparison between the exact and approximate seating and release configurations show a very good agreement [P1].

The excitation of the chain drive coming from the polygonal effect depends on the phase between the seating and release of the rollers. There has previously not existed analytical expressions for the phase, but with the approximate expression it is possible to introduce this:

$$\psi = \theta_{4s} - \theta_{4r} \approx 2\alpha_c(1 - f), \tag{2.22}$$

where the approximation have been obtained using Eq. (2.21) and Eq. (2.16), in which the small term $\bar{p}\alpha_o$ have been assumed vanishing. This result show how there is a very simple relation between the pitch fraction f and the phase between seating and release of the rollers.

2.2.2 Driven sprocket angular motion

For the driven sprocket, approximate analytical expressions for angular position, velocity and acceleration have been obtained. Needless to say, to evaluate the driven sprocket motion, the driver sprocket motion must be given, i.e. θ_4, ω_4 and α_3 are known functions of time. The approximate angular position, velocity and acceleration of the driven sprocket is then, respectively:

$$\theta_2 \approx \frac{\pi}{2} + \frac{\bar{p}(f-h)(1+\frac{1}{2}\bar{p}(f+h)) - \bar{R}_c(1+f\bar{p})(\theta_4 - \pi/2)}{\bar{R}_o\bar{R}_c(\theta_4 - \pi/2) - \bar{R}_o(1+f\bar{p})}, \tag{2.23}$$

$$\omega_2 \approx \omega_4 \frac{\bar{R}_c(1-(\theta_4 - \pi/2)^2)}{\bar{R}_o(1-(\theta_2 - \pi/2)^2)}, \tag{2.24}$$

$$\alpha_2 \approx \alpha_4 \frac{\omega_2}{\omega_4} + \omega_2^2(\theta_2 - \pi/2) - \omega_4^2 \frac{R_c}{R_o}(\theta_4 - \pi/2). \tag{2.25}$$

The seating and release event are taken into account in the expression for θ_2 by the discontinuous jump of the function h, which varies discontinuously with θ_4 according to Eq. (2.12). Consequently, the span endpoints position shifts and the angles θ_2 and θ_4 jumps discontinuously making the driven sprocket angular velocity and acceleration, non-smooth and discontinuous, respectively.

2.3 Example results

Three different chain drive configurations are used to illustrate the above analytical results, with properties as listed in Table 3.1. For each of the configurations, the

	n_c	n_o	N
Coarse	6	9	4
Medium	12	18	11
Fine	21	63	34

Table 2.1: Configurations

pitch fraction is chosen to be $f = \{0,\ 0.5,\ 0.75\}$. Minimum and maximum variation of the driven sprocket velocity occurs for $f = 0$ and $f = 0.5$, and $f = 0.75$ have been chosen to illustrate the general case. A constant angular velocity of $\omega_4 = 100$ rpm ≈ 10 rad/s for the driver has been used when calculating the driven sprocket angular velocity and acceleration.

Figure 2.6 shows the exact and approximate results for the coarse, medium and fine configurations in columns C, M and F, respectively. The horizontal axis shows the angular position of the driver normalized so that $[0, 1]$ correspond to one tooth period, starting when a roller seats on the driver.

Angular position of the driven sprocket is shown in Figure 2.6(a-b-c). There is seen to be very good agreement between exact and approximate results, especially for the medium and fine configurations, which are of most practical importance. The phase ψ between rollers being seated ($\triangledown$) and released ($\triangle$) is shown with a double arrow in Figure 2.6(a). Since the horizontal axis shows one tooth period, the phase between seating and release is simply $\psi = 1 - f$, as shown in (2.22).

The velocity ratio between the driven and driver sprocket varies during one tooth period and is shown in Fig. 2.6(d-e-f). All three graphs shows excellent quantitative and qualitative agreement between exact and approximate results. For the coarse, medium and fine configurations the variation of the velocity ratio is seen to be on the first, second and third decimal point, respectively. This demonstrates how the magnitude of the velocity variation decreases rapidly as the number of teeth is increased.

In Fig. 2.6(d-e) it is seen that the velocity ratio variation decreases and smoothens when $f = 0$, compared to $f = 0.5$. However, as the tooth ratio n_c/n_o decreases (smaller than about 1/3), the effect of changing f becomes less significant. This can be seen in Fig. 2.6(f), where the curves for $f = 0$ and $f = 0.5$ are practically

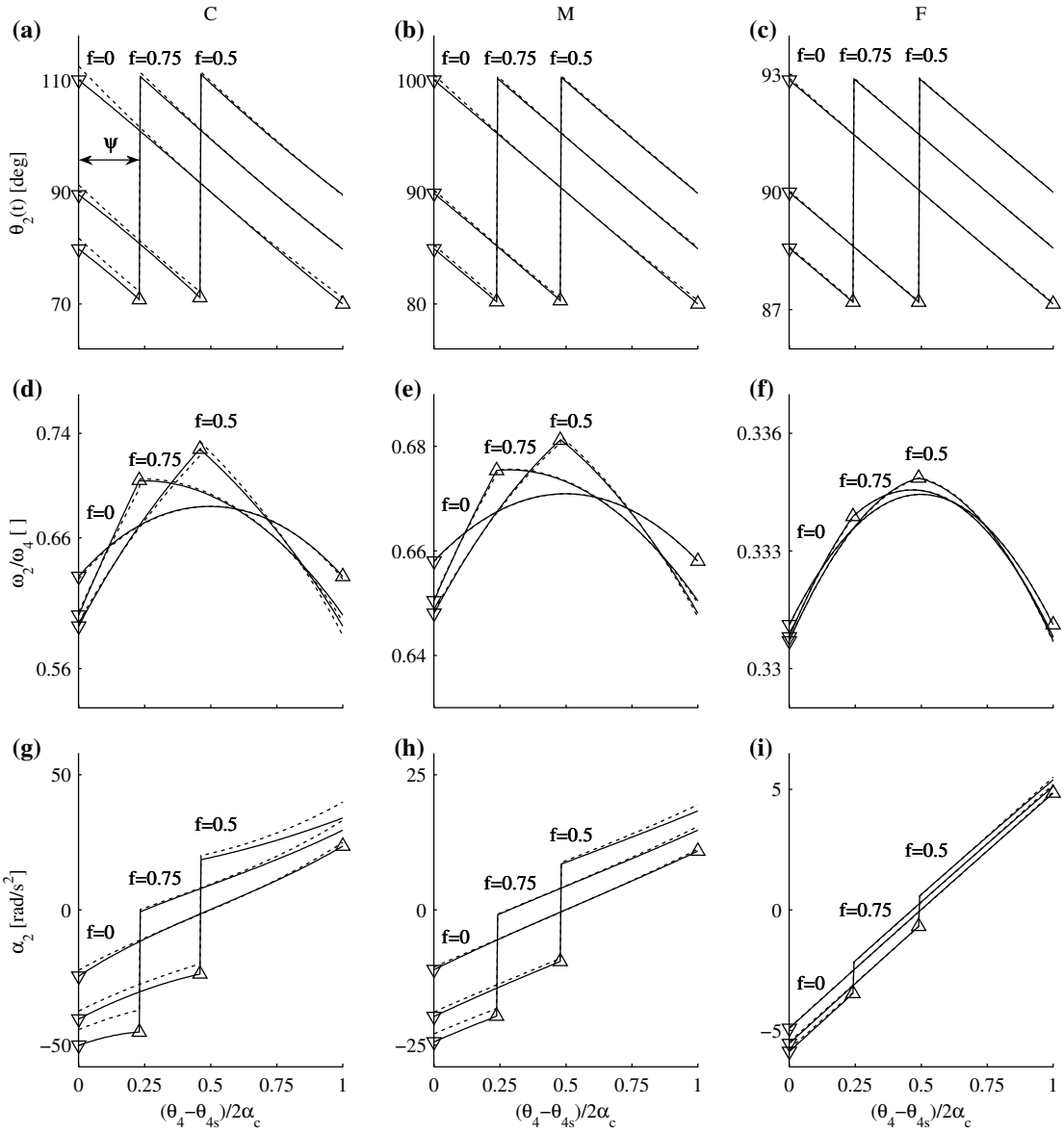

Figure 2.6: Exact (–) and approximate (--) angular *position*, *velocity* and *acceleration* (first, second and third row, respectively) of the driven sprocket for one tooth period, for the *coarse*, *medium* and *fine* chain drive configuration (first, second and third column, respectively). A roller seating on the driver sprocket is indicated by $\triangledown$, and the release of a roller from the driven sprocket is indicated by $\triangle$.

identical. Lastly, the velocity ratio will only be constant in the special case $n_c = n_o$ and $f = 0$, as can be seen from Eq. (2.24).

The driven sprocket angular acceleration in Figures 2.6(g-h-i) shows good quantitative and qualitative agreement between exact and approximate results. In the results presented here the driver rotates with constant angular velocity, and despite that, two sudden jumps in angular acceleration occurs when $f \neq 0$, whereas for $f = 0$ the acceleration only jumps at the end of the interval. The magnitude of a discontinuous jump occurring when a roller is seated or released decrease rapidly as the number of teeth is increased on the driver- and driven sprocket, respectively. Thus, the discontinuous jumps are most prominent for sprockets with few teeth.

For a driver rotating with constant angular velocity the time between seating and release will be given by $\psi = (1 - f)T$, where T is the tooth period. Seating and release will only happen simultaneously if $f = 0$. Only in the special case where $f = 0$ and $n_c = n_o$ will the angular velocity and acceleration of the driven- and driver sprockets be equal.

In studies of string and roller chain drive dynamics it is often assumed that polygonal action leads to a parametric excitation described by time harmonic variation of span tension or velocity. However, the driven sprocket acceleration in Fig. 2.6(g-h-i) is shown to be non-smooth and this could be taken into consideration when modeling chain drive loads.

The error has been calculated between the approximate and exact results for the driven sprocket angular position, velocity and acceleration as the normalized root mean square deviation. Approximation errors for the driven sprocket angular position $\tilde{\theta}_2$ are less than 0.5 %, and decreasing when the chain span becomes longer and the number of teeth on the sprockets increase, as expected. Similarly for the approximation of the driven sprocket angular velocity $\tilde{\omega}_2$, where errors are less than 0.1 %. The approximation errors for the driven sprocket angular acceleration $\tilde{\alpha}_2$ are less than 10 % for $n, N > 12$ and reduce to a level of about 5 % [P1].

2.4 Comparison with multi-body simulation

To give another illustration of the motion of the chain span, the exact kinematic predictions of roller span motion is shown together with the results of multi-body simulation of a simple roller chain drive. The multi-body dynamics simulations are carried out using the program described in [57, 58]. In the multi-body model the mass of the chain is assumed to be lumped at the roller locations, and springs and dampers with constant stiffness and damping coefficients model the chain links.

Clearances between pin and bushing are neglected as well as the rotational inertia of the rollers about their centre of gravity. Tooth geometry in the program used to produce the results presented here is Type II per ASA B29.1-1950. Since the purpose is merely illustration, details of all the program input parameters are not presented here, but given in Appendix A.1 as the program input file, which allows for the full reproduction of the presented results with the program SIMCH.

The simulation is carried out with a constant driver speed of 10 rpm for the configuration M in Table 3.1 with a chain consisting of 40 links, where $f = 0.43$ is chosen to achieve a positive pretension of both spans. In Figure 2.7 is shown the result of the kinematic analysis together with the results of multi-body simulation. The figure shows the curves traced by the rollers of the tight span connecting two sprockets and bears resemblance to a phase plane, i.e. the results obtained by multi-body simulation shows the trace of the roller center coordinates as they move in time, and similarly for the trace of the roller centers as predicted by the kinematic analysis, where the span moves as a straight line connecting the two rotating sprockets.

Knowing that the kinematic analysis predicts the roller trace of the span moves as a straight line, the simulation results can be interpreted as a superposition of rigid motion of a string with moving endpoints, with an overlay of harmonic vibrations of the span at the first mode. In this way, the kinematic analysis provides a valuable tool for interpreting simulation results. Furthermore, the kinematic analysis helps to illustrate what type of results can be expected in the laboratory if e.g. an accelerometer were to be mounted on a chain link to follow the path of the chain; in this case the accelerometer will output measurements showing a contribution at the tooth frequency which is not due to dynamic span vibration, but the kinematic motion of the chain. Also, a motion sensor mounted to measure the transverse motion of the chain span at e.g. the span midpoint will measure a clear contribution at the tooth frequency, not due to span vibration, but due to the kinematic motion of the span coming from the effects of polygonal action.

2.5 Further remarks

The kinematic analysis of the roller chain drive modeled as a four-bar mechanism has been thoroughly investigated. This is meant to aid the interpretation of results of simulation and experimental measurements, and provide an understanding of the characteristic loading of the chain drive components and the influence of the main design parameters. Attention has been directed at deriving kinematic predictions of the driven sprocket angular motion, and it was originally the intention to compare

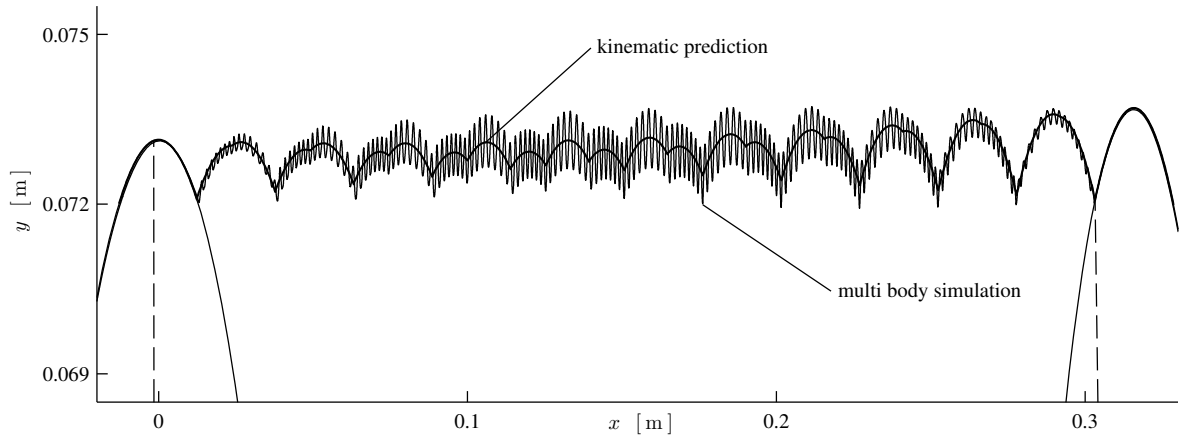

Figure 2.7: Shown are the curves traced out by the chain roller centers at they move in time when the driver sprocket rotates. The results of multi-body simulation and the kinematic predictions based on the present analysis are indicated in the figure. Broken lines are drawn from the sprocket centers to the roller constituting the span endpoint at the instant where a roller seats on the driver sprocket.

these predictions with the results of multi-body simulation. However, when doing so it becomes apparent that the response of the driven sprocket is sensitive to the parameters relating to the dynamics of the sprocket, i.e. inertia, rotational damping, flexibility coming from the connected chain spans, and loading of the driven sprocket. Therefore, the direct similarity to the kinematic predictions is unlikely in the general case, and has therefore not been pursued.

3 Closed system kinematics

It is common to the published kinematic studies that the analysis only considers the tight span transferring the torque between two sprockets (rotating in the same direction). In this chapter, a kinematic analysis is introduced which attempts to also include the slack span. There are several motivations for this: First, there exists no exact analytical predictions of how the shaft center distance can be chosen to achieve a specific pretension of the chain, let alone the shaft center distance that results in tight spans for a given chain length. Second, the development of kinematic analysis to consider more than just one span may prove useful in the design of real chain drives, which often includes drivers with the chain transmitting torque to more than one sprocket. Third, the analysis may reveal new phenomena related to the effects of polygonal action, which are both of practical and academic interest.

Results of the analysis [P2] demonstrates that the total wrapping length of the chain varies periodically with the tooth frequency. This leads to a prediction of a tooth-periodic variation of the axial tension in the chain spans. It also demonstrates that a real chain drive must include compliant components for a tensioned chain to wrap tightly around rotating sprockets, as the sprockets are effectively eccentric. The fact that the wrapping length varies with the tooth frequency in effect renders this analysis approximate. This is due to an assumption made in the analysis: Only the slack span can deform. In a real chain drive the deformation would be distributed to all the links of the chain. However, it is not readily apparant how to perform an analysis which takes this into account, and this is left for future work.

The kinematic analysis presented is for two sprockets with arbitrary number of teeth and center distance, where the sprockets are modeled as polygons, and the chain

spans are pretensioned to form straight lines. The method allows for determination of the shaft center distance for which a chain with a given number of links wraps tightly around two sprockets. Results are exact when the total wrapping length equals an integer number of chain links, since in this case, the chain is not deformed. It is of practical relevance because real chains have a high axial stiffness, and the axial span tension is therefore sensitive to the sprocket center positions. The effect of a variable wrapping length has been observed for real chains, but has not previously been treated theoretically.

3.1 Wrap length determination

Here is presented an outline of the analysis. The approach relies on modeling the chain drive as a four-bar mechanism: By letting the upper span and the two sprockets move as constrained by the four-bar mechanism, the lower span length is "measured" as the distance between the seating curve centers which constitutes the lower span endpoints at the driver and driven sprocket. These lower span endpoint positions are determined by considering which of the sprocket seating curves are within the angular position intervals of the seating and release configurations. These intervals are

$$\theta_a \in [\theta_{as} - 2\alpha_c,\ \theta_{as}], \tag{3.1}$$

$$\phi_a \in [\phi_{ar},\ \phi_{ar} + 2\alpha_o], \tag{3.2}$$

$$\theta_b \in [\theta'_{br} + \pi + \beta,\ \theta'_{br} + \pi + \beta + 2\alpha_c], \tag{3.3}$$

$$\phi_b \in [\phi'_{bs} + \pi + \beta - 2\alpha_o,\ \phi'_{bs} + \pi + \beta], \tag{3.4}$$

where the angular position of the sprockets to the rollers constituting the current span endpoint for the tight span a are given by θ_a and ϕ_a, for the the driver and driven sprockets, respectively. Seating and release angles θ_{as}, ϕ_{ar} for the upper span a are determined by analysis of the four-bar mechanism $OABC$ in the X, Y coordinate system shown in Figure 3.1. Similarly, for the lower span for the lower span b the angular positions of the sprockets to the rollers constituting the current span endpoint of the span b are given by θ'_b, ϕ'_b, which are determined in the X', Y' coordinate system by analysis of the four-bar mechanism $CDEO$. The angles $2\alpha_c$ and $2\alpha_o$ is the angle between two consecutive teeth on the driver and driven sprocket, respectively, and the angle between the two coordinate systems is $\pi + \beta$, where β is given by

$$\beta = 2 \arccos\big(x_c/|OC|\big). \tag{3.5}$$

Subscripts o, c and a, b are used to relate variables specific to sprockets O, C and spans a, b respectively, e.g. α_o and θ_b. It is convenient to consider one period of the

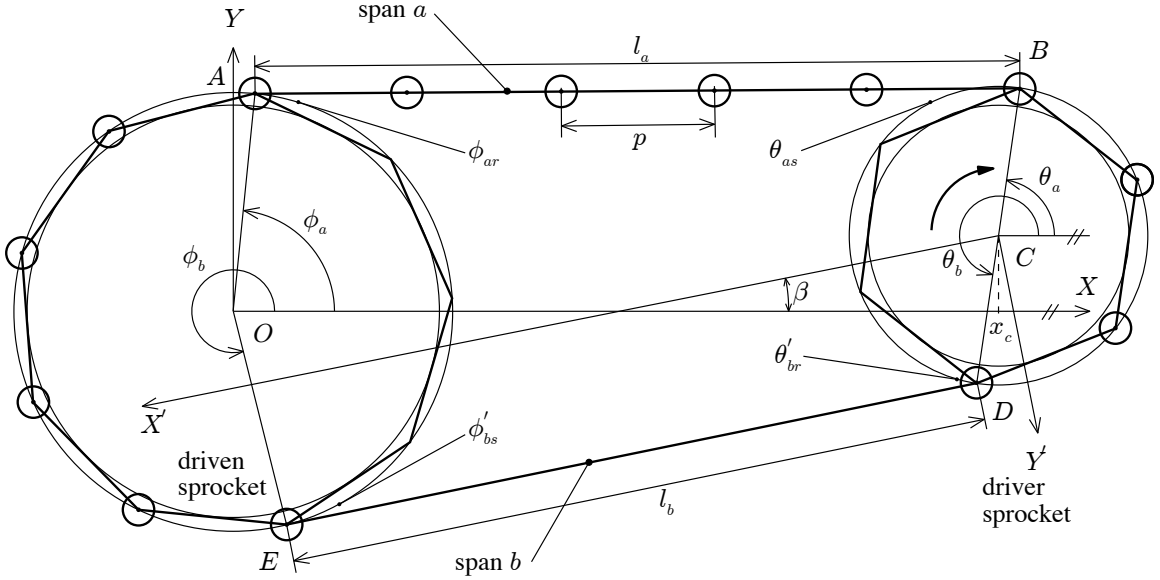

Figure 3.1: Kinematic model of a chain drive consisting of two sprockets connected by tight spans a and b of instantaneous length l_a and l_b, respectively. The driver sprocket C rotates counter-clockwise.

angular motion to start from θ_{as}, the configuration where a roller from the span a seats on the driver sprocket. As demonstrated in chapter 2 the upper span length varies according to

$$l_a = (N + 1 + h)p, \quad h = \begin{cases} 0 & \text{for } \theta_{as} \geq \theta_a \geq \theta_{ar}, \\ 1 & \text{for } \theta_{ar} \geq \theta_a \geq \theta_{as} + 2\alpha_c. \end{cases} \tag{3.6}$$

Note that θ and ϕ decrease as the sprockets rotates in clockwise direction. Expressing the angels to span b in terms of the angles to span a and integer increments of 2α gives

$$\theta_b = \theta_a + 2\alpha_c \hat{n}_c, \tag{3.7}$$

$$\phi_b = \phi_a + 2\alpha_o \check{n}_o - 2h\alpha_o, \tag{3.8}$$

where the function h ensures that ϕ_b decrease continuously, as ϕ_a jumps discontinuously when a roller is released from the driven sprocket at ϕ_{ar}. In (3.7)-(3.8) the total number of sprocket seating curves has been split into being either free or occupied by a chain roller, i.e.

$$n = \check{n} + \hat{n}, \quad \check{n}, \hat{n} \in \mathbb{N}, \tag{3.9}$$

where the number of seating curves with a roller seated is $\check{n}$ and the number of seating curves with no roller seated is $\hat{n}$. Substituting (3.7) into (3.3) gives the

number of free seating curves on the driver sprocket:

$$\frac{\theta'_{br} - \theta_a + \pi + \beta}{2\alpha_c} \leq \hat{n}_c \leq \frac{\theta'_{br} - \theta_a + \pi + \beta}{2\alpha_c} + 1. \tag{3.10}$$

Similarly, by substituting (3.8) into (3.4) the number of rollers seated on the driven sprocket can be determined from

$$\frac{\phi'_{bs} - \phi_a + \pi + \beta}{2\alpha_c} - 1 + h \leq \check{n}_o \leq \frac{\phi'_{bs} - \phi_a + \pi + \beta}{2\alpha_c} + h. \tag{3.11}$$

With $\hat{n}_c$ determined from (3.10), the contact angle to the lower span at the driver sprocket can be determined from (3.7). The contact angle to the lower span at the driven sprocket can be determined from (3.8) with $\check{n}_o$ determined from (3.11) and h given in (3.6). The total wrapping length of the chain is then

$$L = l_a + l_b + (\check{n}_c + \check{n}_o)p, \tag{3.12}$$

with l_a given by (3.6), $\check{n}_c$ by (3.9) and the lower span length calculated from

$$l_b = \sqrt{(x_c + R_c \cos\theta_b - R_o \cos\phi_b)^2 + (y_c + R_c \sin\theta_b - R_o \sin\phi_b)^2}. \tag{3.13}$$

The total length L of the chain wrapping around both sprockets was determined by assuming that only span b could deform. To improve the quantitative estimate of the wrapping length variation, the deformation of the other chain drive components could be included, i.e. the deformation of the both spans, and the link-deformation of chains wrapped on sprockets [35, 38, 39]. The above analysis serves as an initial investigation of this effect of polygonal action, which has not been treated previously. However, the kinematic configuration of all the chain drive components determined when the wrapping length equals an integer number of chain pitches is exact. It is also useful for initializing e.g. multi-body simulations of roller chain drives.

One drawback of the above analysis, which may provide an indication of a more elegant approach, is that the analysis does not make any advantages of symmetry, which in fact is not present when the two four-bar mechanisms $OABC$ and $CDEO$ are not analyzed in the same coordinate system. The analysis of the $CDEO$ four-bar mechanism is made in the X', Y' coordinate system, and results are then "transferred" to the X, Y coordinate system using by the angle between the two coordinate systems $\pi + \beta$. It is possible that an analysis which used a coordinate system where the the abscissa connected the two sprocket centers could prove more advantageous.

3.2 Example results of wrapping length variation

To illustrate the results of the above wrapping length variation, twelve different chain drive configurations are introduced. These specify the full and exact geometric configurations of roller chain drives with two sprockets modeled as polygons, and connected to have two tight spans. Besides illustrating the above analytical results with examples, these configurations are also intended as benchmark configurations. Either these can be used for comparison with experimental results, or for the initializing of numerical simulations.

Properties and ID of the configurations are listed in Table 3.1. For a given pitch length p, number of teeth n_c, n_o, span length given by N and pitch fraction f, the sprocket center positions can be found from (2.2). The tight span length l_a can be determined from (3.6), and the total number of links in the chain is given by M. Calculated values for the minimum, mean and maximum wrapping length obtained from (3.12) are presented, all nondimensionalized with the pitch p. Configuration C_1 has been subject to experimental measurements of "angular displacement error" [11] as well as kinematic studies of driven sprocket angular motion [P1].

Table 3.1: Chain drive configurations

ID	n_c	n_o	N	M	f	$L_{\min}/p$	L_{mean}/p	$L_{\max}/p$
A_1	6	12	4	20	0.3325	20.0020	20.0200	20.0411
A_2			8	28	0.4066	28.0027	28.0162	28.0329
A_3			16	44	0.4516	44.0046	44.0130	44.0236
B_1	12	12	8	31	0.5015	31.0030	31.0032	31.0034
B_2			16	46	0.0024	46.0048	46.0048	46.0048
B_3			24	63	0.5032	63.0064	63.0065	63.0066
C_1	12	18	11	40	0.4302	40.0040	40.0091	40.0149
C_2			22	62	0.4655	62.0066	62.0100	62.0138
C_3			33	84	0.4786	84.0085	84.0110	84.0138
D_1	24	32	16	63	0.4106	63.0064	63.0079	63.0094
D_2			24	79	0.4408	79.0080	79.0095	79.0112
D_3			32	95	0.4569	95.0097	95.0111	95.0126

Note from Table 3.1, that if both chain spans are to be in tension for a given configuration, the pitch fraction f cannot be chosen freely.

Figure 3.2 shows how the wrapping length varies during one tooth period for the configurations in Table 3.1. In general, the magnitude of the wrapping length

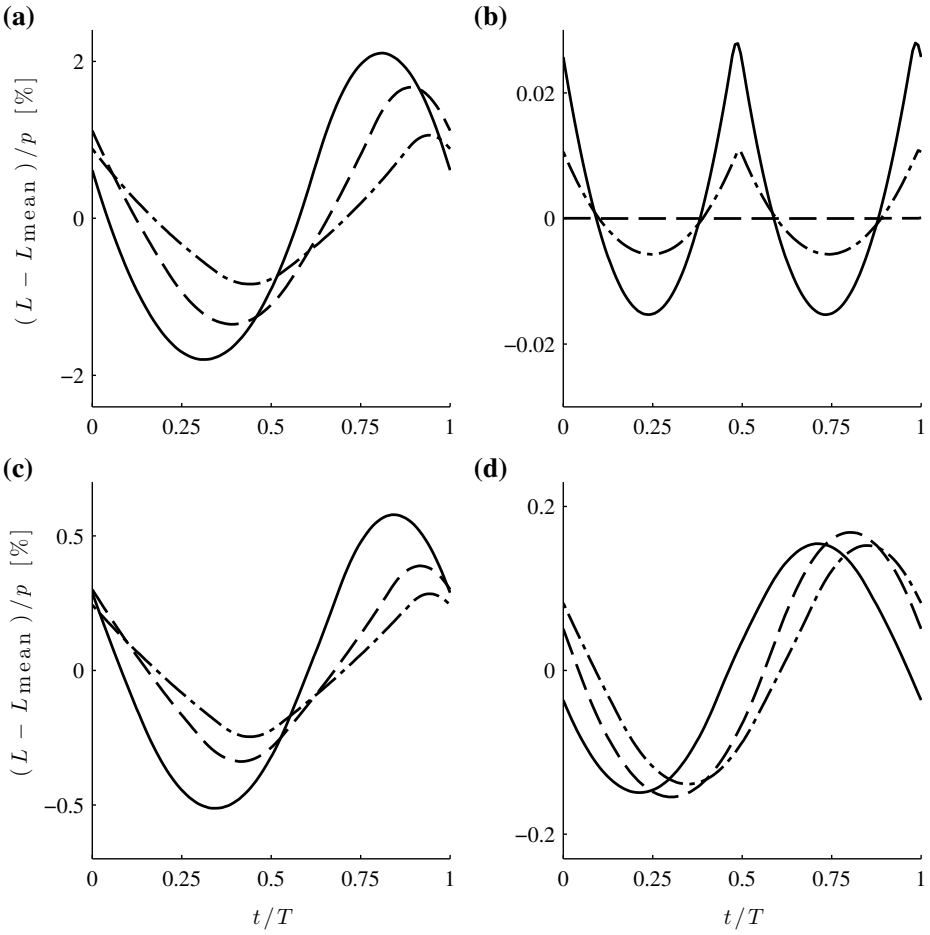

Figure 3.2: Chain wrapping length variation $L - L_{\text{mean}}$ normalized by pitch p for one tooth period. Configurations A-D are shown in figures (a)-(d), respectively. The line types $-$, $--$ and $-\cdot-$ identify the, short, medium and long span lengths, respectively.

variation is seen to decrease as the number of sprocket teeth and span length is increased. For the special configuration B where $n_c/n_o = 1$, it is seen from Figure 3.2(b) that the length variation decreases significantly, and vanishes completely for configuration B_2, where the number of links M equals an even number and $f \simeq 0$. Except for configurations B, the wrapping length variation resembles a harmonic function, albeit the variations are not completely symmetric.

3.3 Comparison with multi-body simulation

A comparison between the analytical predictions of the wrapping length variation and results obtained from multi-body simulation is shown in Figure 3.3. The Figure shows the wrapping length variation L normalized by the chain pitch p for two tooth periods. Simulation results are obtained for the configuration C_1 at

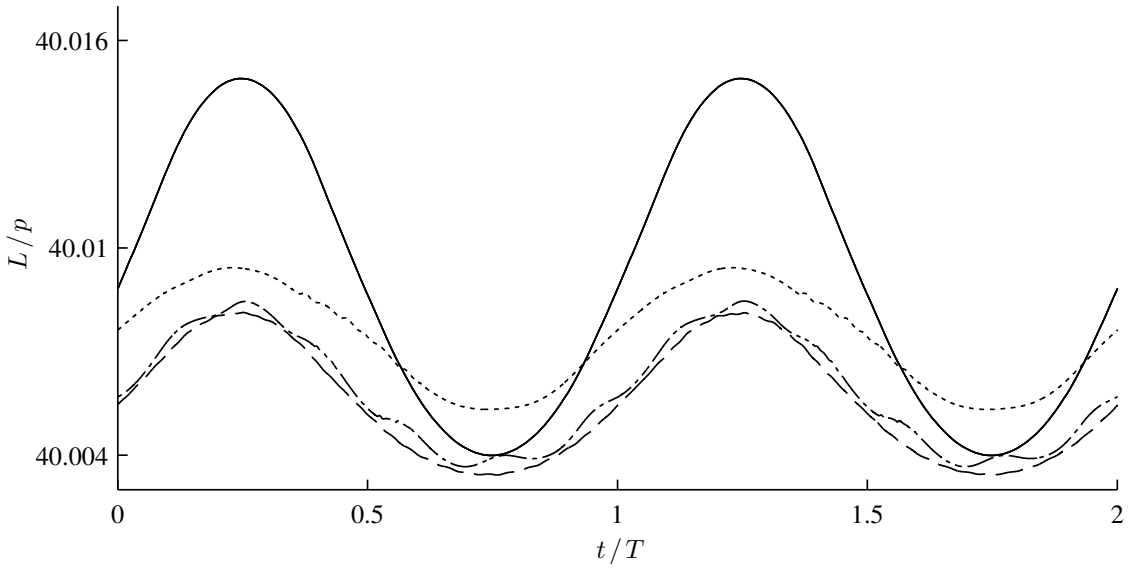

Figure 3.3: Chain wrapping length variation L normalized by pitch p for two tooth periods for configuration C_1 in Table 3.1. The full line is the kinematic prediction. Broken lines $--$, $-\cdot-$ and $\cdots$ lines are results obtain from multi-body simulation, with a driver speed of 10, 100 and 300 rpm, respectively.

10, 100 and 300 rpm. Input parameters for the simulation is given in Appendix A.1, albeit the driver frequency has been set to the said values, and the sampling frequency has been chosen appropriately. There is excellent qualitative agreement between the analytical predictions and the numerical results, with all graphs bearing resemblance to harmonic functions and . Quantitatively, the kinematic prediction of the minimum wrapping length is also excellent. The wrapping length variation amplitude is about a factor of two larger than the results obtained with multi-body simulation. One contribution to this could be that the sprockets are compliant in the multi-body model, which means that the chain rollers can be indented into to the tooth, thereby reducing the effective sprocket radius slightly. At the chosen driver speeds, the chain spans has no significant vibratory response, and it seen that the simulation results obtained at 10, 100 and 300 rpm are nearly identical, which supports the hypothesis that the effect of wrapping length variation should not be limited to drives operating at low speeds.

3.4 Further remarks

A time-varying wrapping length demonstrates that a chain drive with tight spans must generally include compliant components to function. During installation of real chain drives, i.e. when the drive is stationary and unloaded, the span tension will depend on the angular position of the driver sprocket. During operation the

axial force is then expected to vary periodically with the tooth frequency. The effect appears here for chain drives with only two sprockets, but is also expected for chain drive configurations with more sprockets and spans, and should also not be limited to low-speed chain drives. We hypothesize that multiple sprockets can be positioned to either attenuate or amplify the effect of a variable wrapping length. If this is the case, careful positioning of e.g. a tensioner sprocket could possibly neutralize the effect of a variable wrapping length, and allow for a constant span tension even for chain drive configurations where the sprockets have few teeth.

4 Dynamics

This chapter summarizes the efforts on modeling and analyzing the coupled angular motion of the sprockets and the transverse vibration of the chain spans. The chain spans are modeled as axially moving uniform strings subjected to parametric excitation coming from the driven- and driver sprocket angular vibration and transverse excitation coming from moving boundaries. All the chain spans are in tension and this provide elastic coupling across the sprockets. Fundamental to the analysis is the introduction of an assumed stationary operating state where the chain spans operate at a nominal mean axial tension, and the input power balances the output power, to ensures that there is no overall acceleration of the drive. The presented model allows for the study of the coupled sprocket and span motion which is analyzed through perturbation methods. Before introducing the analysis effort presented in [P2], some information is given on roller chain drives and marine propulsion engines, which form the background for some important aspects of the mathematical modeling.

4.1 Modeling background

The mathematical modeling relates directly to the presented kinematic analysis at several points: The chain spans are supported by moving boundaries c.f. Figure 2.7. The span length changes c.f. Eq's. (2.7) and (2.12) or (3.6). The effect of a tooth-periodic wrapping-length variation is included c.f. Figure 3.3.

Chain drives applied in low-speed marine propulsion engines are powered directly by the crankshaft. An example of a chain drive layout is shown in Figure 4.1, which is a four cylinder test engine, model 4T50MX. In the figure the silhouette

of a person is included to provide a sense of scale. When the chain drive only requires a small fraction of the power generated by the engine, and the inertia of the drive is small compared to the full engine system, the dynamics of the chain drive can be assumed not to affect the crankshaft motion, i.e. the chain drive is kinematically forced. This is relevant in combustion engines where the chain drive powers auxiliary equipment using only a small fraction of the power required at the main output. For example with ship propulsion engines, the chain drive powering the hydraulic pumps is driven directly by the crankshaft, and consumes only about 1% of the power required for driving the propulsion propeller.

A combustion engine generates distinct pulses for each cylinder ignition, and therefore the angular velocity of the crankshaft is not constant. The engine crankshaft motion can be predicted through modeling and simulation by the engineers designing engines. Results of such engine simulations for the 4T50MX engine are shown in Figure 4.2, which show the angular displacement during one revolution of the crankshaft at the nominal speeds of 50, 80 and 110 rpm. In marine propulsion engines there is no clutch or gearbox between the crankshaft and propeller, and the maximum continuos rating of the engine is about 110 rpm.

In the mathematical modeling the angular displacements of the driver sprocket will be assumed given, i.e. θ_2^* is introduced, and this refers to the type of engine angular displacement shown in 4.2. As a reminder to the reader coming from the kinematic analysis, it is emphasized that while the kinematic analysis considered e.g. the driven sprocket angular *position, velocity* and *acceleration*, the dependent variables of the dynamic analysis are now the angular *displacements*. The displacements can be thought of as motion added to the nominal steady-state operation of the chain drive components.

4.2 Chain drive design praxis

Selection of chains, sprockets and chain-drive layout can be done by following directions provided by the chain drive manufactures, e.g. Tsubaki, Timken, Link-Belt, Renold, and Diamond Chain Company. The content of these directions is given a short review here. The design should take into account factors such as: Power rating, number of sprocket teeth, multiple strands, types of driven load (smooth load, moderate shock, heavy shock), types of input power (internal combustion engine w. hydraulic drive, electric motor drive, internal combustion engine with mechanical drive), arrangement, and lubrication (manual, drip, slinger disc, pump). Chain manufactures also provide tools for measuring the chain elongation. The typical data provided for a specific chain type, besides the geometric properties, are

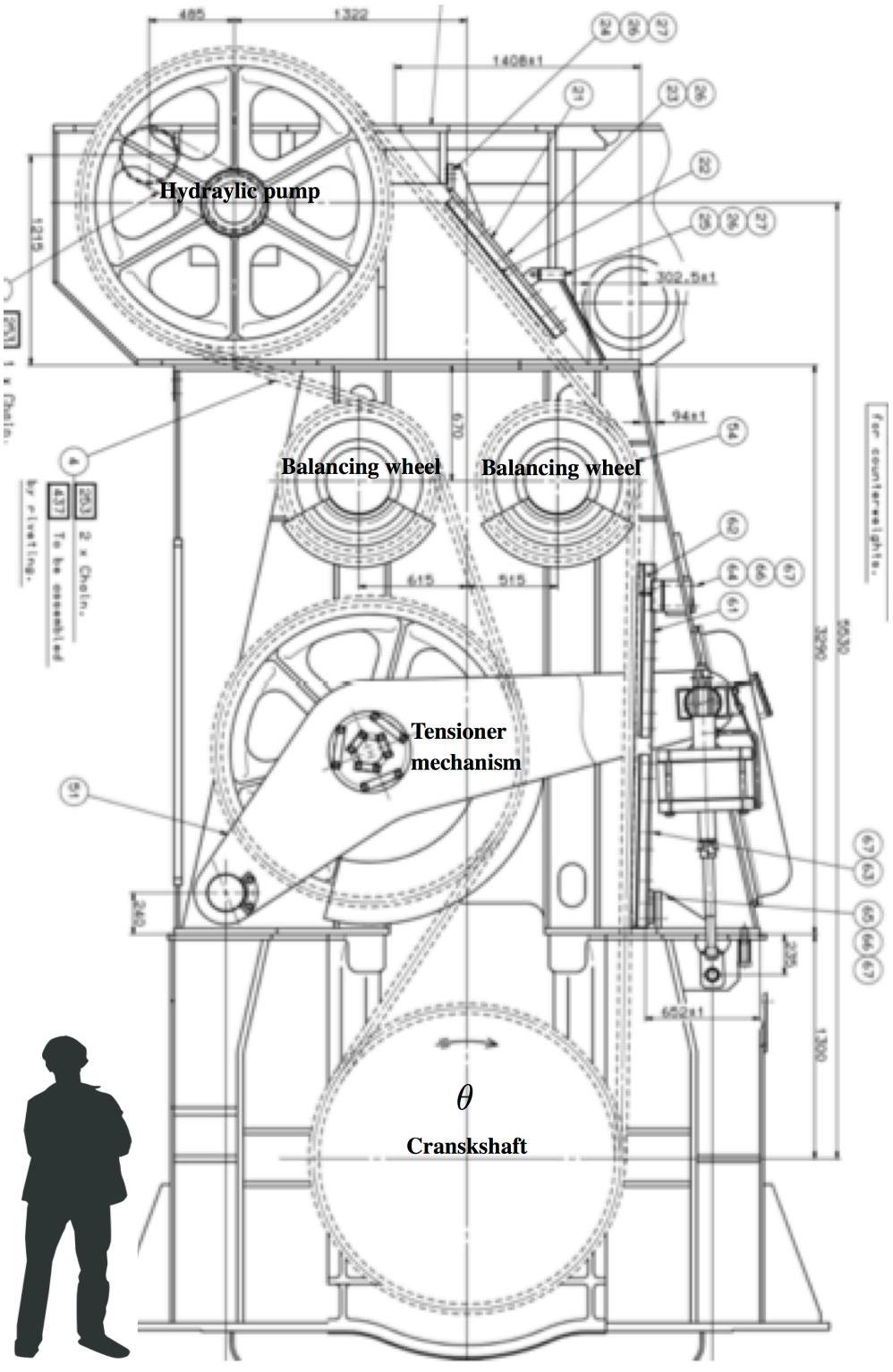

Figure 4.1: Four-stroke MAN Diesel engine, model 4TMX50, with roller chain drive powering the hydraulic pump. Seen in this illustration are also the tensioner mechanism which is adjusted to ensure the desired pretension, the balancing wheels which counter-act the horizontal excitation from the pistons, and guide bars, which in some designs are mounted along the spans to limit transverse vibration.

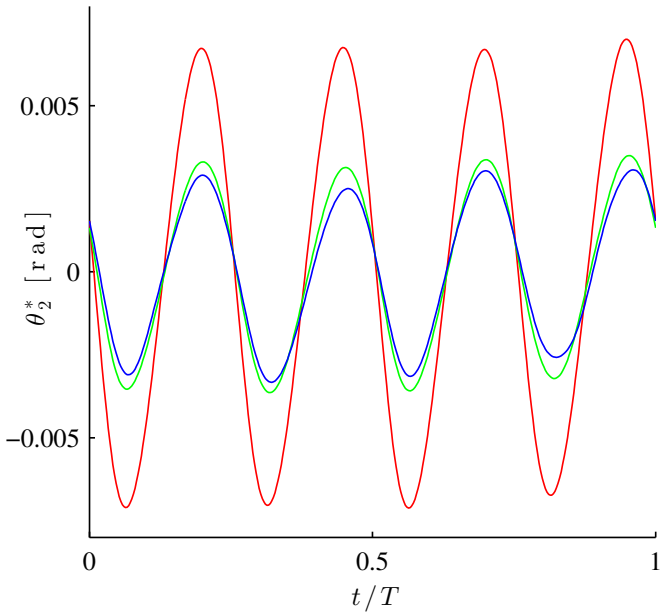

Figure 4.2: Crankshaft angular displacements θ_2^* for a four-stroke marine diesel engine model 4TMX50 at 50, 80 and 110 rpm in *red, green* and *blue* lines, respectively. These results are obtained by engine designers from numerical models (GTORSI).

values for: Minimum ultimate tensile strength, average tensile strength, maximum allowable load, and approximate weight per unit length. The design guides does not consider dynamic phenonema, and usually assumes that one span remains slack.

4.3 Critical chain drive parameter values

When comparing the sources that has been available to this project, it becomes clear that specifically the axial stiffness, as understood in the context of vibration and dynamics, EA with SI unit [N], is not readily available to the engineer through the data provided by chain manufactures. Three examples are provided to make this point clear: A) The *specific stiffness* given for a Tsubaki steel chain with pitch 1" is s' = 5600 [kNm/m], according to the data sheet "ChainCharacteristics.xls" provided by MAN Diesel A/S. B) The *average tensile strength* given for a Tsubaki RS80 steel chain with pitch 1" is 17640 [lb], or 78.4 [kNm/m], according to the data sheet provided for the RS80 chain by Tsubaki. C) The *axial stiffness* EA given for a timing chain of unspecified pitch length is 404.9 [kNm/m], according to the research paper [49]. As can be seen from the three examples, the three values differs by three orders of magnitude. However, it may be that the data provided does not represent the same physical quantity (although they are provided with the same unit) but in that case it should be clarified how to obtain correct values for the

axial stiffness EA. Lastly, it appears from the available data that the maximum allowable load of roller chains is much lower than the axial stiffness, and in that case it is a reasonable assumption that the transverse wave speed is much lower than the axial wave speed.

Choosing appropriate values for the axial stiffness EA in the work carried out on multi-body simulation of roller chain drives [57, 58] was also subject to dispute, and it is recommended that future choices of axial stiffness should preferably be based on experimental measurements. In fact, based on a thorough review of the simulation results, it is concluded by this author, that the manual for the multi-body simulation program SIMCH is in error: For the chain axial stiffness, it states that the input should be the chain axial stiffness for one meter chain, but this leads to wrong results, and the correct input value should be the link stiffness.

As mentioned in the introduction and illustrated in Figure 1.1, the properties of the chain are in fact not uniform, and the propagation of especially longitudinal waves through a periodic structure is known to be non-trivial at certain frequencies, with band-gaps being one phenomena known to this type of structures. For the experimental investigations of roller chain drive dynamics, it is therefore recommended to initialize experiments by investigating the wave propagation properties of the roller chain. The only known experimental work on this topic was reported by Ryabov 1971 [50], where experimental results demonstrated that the longitudinal wave speed depends on the axial tension of the chain, but approaches a constant value as the axial tension is increased (for uniform rods and strings the longitudinal wave speed is independent of the axial tension). The results were obtained for three specific Soviet chain types, and it is suggested that the subject is investigated further.

4.4 Modeling chain drive dynamics

A simple model consisting of two sprockets is considered, with gravity ignored. The local coordinate systems and definitions of displacements are shown in Figure 4.3. The dependent variables $U, \tilde{U}, \hat{W}, \hat{\tilde{W}}$ and θ_1 are the displacements measured at a steady state of operation, i.e. the particular solution of the forced response, calculated when the mean of the input torque M_2 equals the mean of the output torque M_1.

The angular displacement of the driving sprocket is assumed to be given, i.e. θ_2^* is a known function of time. Prescribed external forcing included in the multiple scales analysis is identified throughout the analysis by a star $(\,)^*$. Assuming the initial total span (pre)tension $P_{\text{tot}} = P_{\text{pre}} + \tilde{P}_{\text{pre}}$ at zero external load and zero angular

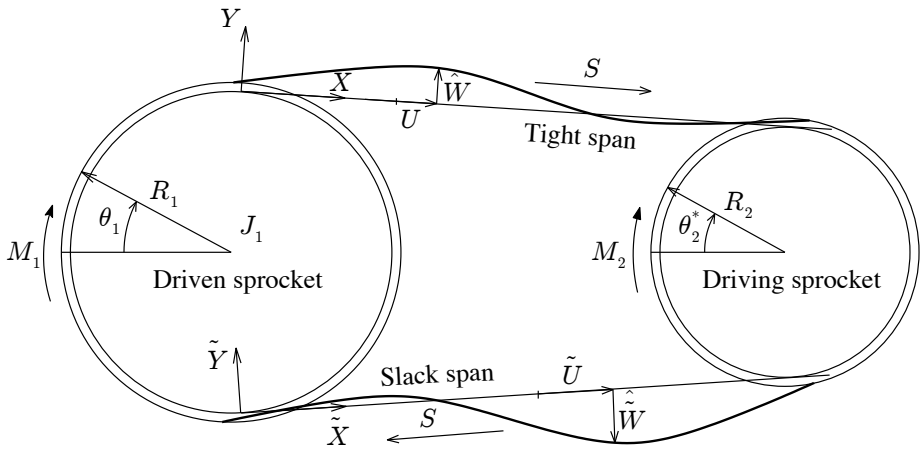

Figure 4.3: Mechanical model of a chain drive system with two sprockets

velocity to be known, as well as the nominal span velocity S and input torque $\hat{M}_2$, the longitudinal forces at steady state operation are, for the tight and slack spans

$$P_0 = \tfrac{1}{2}(P_{\text{tot}} + \hat{M}_1/R_1), \tag{4.1}$$

$$\tilde{P}_0 = \tfrac{1}{2}(P_{\text{tot}} - \hat{M}_1/R_1). \tag{4.2}$$

The output torque $\hat{M}_1$ is modeled as comprised of a constant (brake) load $\hat{f}_1$, rotational viscous damping $\hat{d}_1$, and a time dependent torque $\hat{M}_1^*(t)$, where t is time

$$\hat{M}_1 = \hat{d}_1 S/R_1 + R_1\hat{f}_1 + \hat{M}_1^*. \tag{4.3}$$

For $\hat{M}_1^* = 0$ Eq's (4.1)-(4.2) and (4.3) demonstrate how the nominal tension, and thereby the natural frequencies of the chain spans, varies with initial pretension, operating speed, and constant external load. Centrifugal forces are not included in this model, which could be relevant for high-speed roller chain drives. It is also noted that chain wear corresponds to a reduction of P_{tot}.

4.4.1 Governing equations

It is only the intention here to give an overview of the central equations. The full derivation of the coupled equations of motion and their approximate solution is given in [P2]. The roller chain is modeled as a uniform axially moving string supported by moving boundaries, as illustrated in Figure 4.4. The coordinate system X, Y is inertial, and the amount of string material within the boundaries varies. To take this into account it is necessary to allow the position from which the span endpoint displacements are prescribed from to be functions of time; $X_1(T)$ and $X_2(T)$ models

this. Between the seating and release events, the distance $X_2(T) - X_1(T)$ equals the span length, and the boundaries move in the positive x-direction at nominal speed $S \geq 0$. Longitudinal and transverse displacements of the string are denoted by $U(X,T)$ and $\hat{W}(X,T)$, respectively, while out of plane motion is not considered.

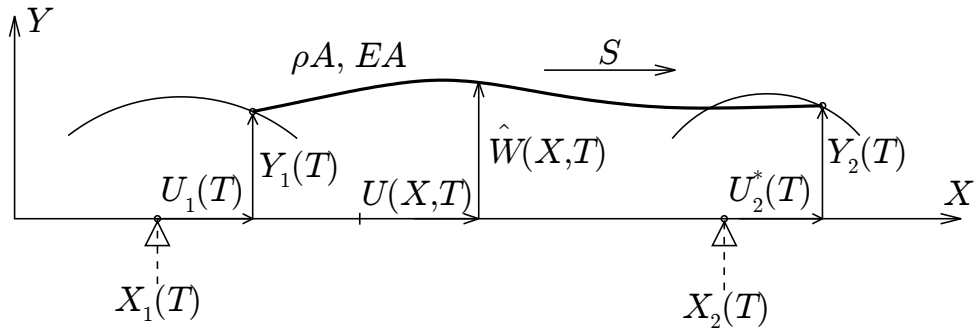

Figure 4.4: Axially moving chain span supported by moving boundaries

The equation of motion for the transverse motion of the tight span becomes

$$w_{,tt} + 2s w_{,xt} - (\alpha\gamma - s^2) w_{,xx} - \varepsilon\alpha\Big(u_2^* - u_1 + \tfrac{1}{2}\int_0^1 w_{,x}^2\, dx\Big) w_{,xx} \\ = -y_{1,tt}\,(1-x) - y_{2,tt}\,x - 2s(y_{2,t} - y_{1,t}) + O(\varepsilon^2), \quad (4.4)$$

where $y_1(t), y_2(t)$ is the prescribed transverse displacement of the span endpoints, as it can be prescribed by the kinematic motion of the span endpoints seated on the sprockets. The terms u_2^*, u_1, and the integral term cause parametric excitation of the axially moving string. The transverse vibration of the span is coupled to the driven sprocket displacements u_1, and parametrically forced by u_2^*, which is prescribed by the driver angular displacements. All displacements have been made dimensionless by the shaft center distance l. Time T is made dimensionless by the natural frequency of string of length l subjected to axial tension P_t, and dimensionless parameters have been introduced as

$$t = \sqrt{\frac{P_t}{\rho A l^2}}\,T, \quad s = \frac{S}{\sqrt{\frac{P_t}{\rho A}}}, \quad \alpha = \frac{EA}{P_t}, \quad \gamma = \frac{P_0}{EA}, \quad (4.5)$$

The boundary positions has been assumed to move in the axial and transverse direction by a small amount $O(\varepsilon)$, and it is shown that this leads to a second order effect in the equation of motion and boundary conditions for transverse vibrations of the chain span,

$$w(0,t) = 0 + O(\varepsilon^2), \quad w(1,t) = 0 + O(\varepsilon^2). \quad (4.6)$$

Deriving the equation of motion for the driven sprocket and establishing the stationary operating state relies on the assumption that longitudinal waves propagate instantly, compared to the time scale of wave propagation for the lower transverse modes. With this assumption the axial strain is constant along the chain span length, i.e. only time dependent. With this the approximate solution for the longitudinal displacements can be shown to be

$$u(x,t) = u_1(t) + e(t)\big(x - x_1(t)\big) - \tfrac{1}{2}\int_{x_1(t)}^{x} \hat{w}_{,x}^2\, dx, \tag{4.7}$$

where $e(t)$ is the axial dynamic strain

$$e(t) = u_2^* - u_1 + \tfrac{1}{2}\int_0^1 w_{,x}^2\, dx + O(\varepsilon^2). \tag{4.8}$$

Here $e(t)$ is termed the *dynamic* strain, as there is also a *constant* strain component $e_0 = P_0/EA$ coming from the mean axial load of the chain operating at the assumed stationary state where P_0 is given by (4.1). The equation of motion for the driven sprocket is derived using Newton's second law. Therefore the forces acting on the body are specified directly, as opposed to being derived through energy considerations. The axial force contains both the constant and dynamic part of the axial strain, and can be shown to be:

$$N(t) = \alpha\big(e(t) + \gamma\big) - s^2, \tag{4.9}$$

where the first term relates to the dynamic strain component, the second to the constant strain component, and s^2 accounts for the reduction of axial tension due to the non-dimensional axial transport velocity, which may ultimately cause the axial tension to vanish at the so called critical transport velocity. To establish the stationary state for the driven sprocket, it is assumed that the axial forces due to the *constant* strain components of both spans balance the constant part of the output torque (4.3). With this, the equation of motion for the driven sprocket can be shown to be

$$Ju_{1,tt} + du_{1,t} + 2\alpha u_1 = 2\alpha u_2^* + \frac{\alpha}{2}\int_0^1 (w_{,x}^2 - \tilde{w}_{,x}^2)\,dx + M_1^*(t). \tag{4.10}$$

This is an inhomogeneous ordinary second order differential equation for the driven sprocket displacements u_1 at the pitch circle, measured from steady state operating conditions. The equation is nonlinearly coupled to the upper and lower span transverse displacements w and $\tilde{w}$. On the left hand side the terms are inertia, damping and stiffness, respectively. Stiffness 2α comes from the axial stiffness of the two chain spans. The span endpoint axial displacement u_2^* is given directly by the kinematic forcing from the driver sprocket angular displacement θ_2^*.

4.4.2 Modeling transverse excitation

The span endpoint positions y_1, y_2 follows curves which resemble a cycloid, as chain rollers successively act as the span endpoints when the sprockets rotate, e.g. the span endpoint recurrently moves between points B_1 and B_2 in Figure 2.3. At the instant where a roller enters (or leaves) the chain span, the projections of the nominal tangential velocity in the y-direction changes discontinuously, cf. $\mathbf{u}_1 - \mathbf{u}_2$ in Figure 2.3. Therefore, the endpoint transverse velocities are non-smooth in time, and the span endpoint accelerations jumps discontinuously in time, which leads to impulsive loading of the chain spans from meshing. To represent the impulsive loading at the span endpoints, the acceleration jumps are modeled using Dirac pulse trains,

$$y_{1,tt} = \sum_{j=-\infty}^{\infty} Q_1 \delta(t - j\tau_o), \quad y_{2,tt} = \sum_{j=-\infty}^{\infty} Q_2 \delta(t - (\psi + j)\tau_o), \tag{4.11}$$

where τ_o is the non-dimensional tooth period. The Dirac pulses of the two endpoint accelerations are separated in time by the phase ψ given by (2.22), which depends on the shaft center distance, specifically the pitch fraction f defined by (2.2). Assuming the span to remain straight, the relative velocities between two neighboring rollers at the instant of seating and release, respectively, are given by

$$Q_1 = 2s \sin \alpha_1 = \frac{sp}{R_1}, \quad Q_2 = 2s \sin \alpha_2 = \frac{sp}{R_2}, \tag{4.12}$$

where α_1, α_2 are the pitch angles, R_1, R_2 are the pitch circle radius, p is the pitch length, and it has been used that $R_1 = p/(2 \sin \alpha_1)$ and $R_2 = p/(2 \sin \alpha_2)$. It is seen from (4.12) that increased sprocket radius, shorter pitch length and lower velocities reduce the endpoint acceleration discontinuities. The discontinuous accelerations are assumed to be dominating.

The forcing coming from meshing is tooth-periodic, and in the analysis expanded as Fourier series. Since the impulsive excitation acting at both span ends is represented by Fourier series with harmonic terms of the same frequencies, the forcing can be reduced to one expansion, where the coefficients become the addition of the two components from either span end. Thus, two impacts at either span end is represented by a single Fourier series expansion with harmonic terms that are multiples of the tooth frequency.

4.5 Approximate analysis

The vibrations of the chain spans and the driven sprocket are governed by coupled non-linear partial differential equations for the spans (4.4) (with an equivalent

equation for the slack span), and the ordinary differential equation for the driven sprocket (4.10). To reduce the partial differential equations for the spans to ordinary differential equations, a Galerkin expansion of the m'th and n'th mode is employed of the tight and slack span, respectively, using test functions for stationary uniform strings. The resulting equations neglects the Coriolis terms $2sw_{,xt}$, since these require either the use of complex mode shapes for axially moving strings, or an even+odd two-mode expansions of stationary strings. Following the Galerkin expansion, the result is a system of three coupled non-linear second order differential equations, where ξ_m and $\tilde{\xi}_n$ are the modal amplitudes of the spans, and u_1 is the angular displacement of the driven sprocket:

$$\xi_{m,tt} + 2\mu_m \xi_{m,t} + \omega_m^2 \xi_m + \alpha_m \big(u_2^* - u_1 + p_o^*(t)\big)\xi_m + \kappa_m \xi_m^3 = \sum_{j=-\infty}^{\infty} k_m e^{ij\Omega_o t}, \quad (4.13)$$

$$\tilde{\xi}_{n,tt} + 2\tilde{\mu}_n \tilde{\xi}_{n,t} + \tilde{\omega}_n^2 \tilde{\xi}_m + \tilde{\alpha}_n \big(u_1 - u_2^* + p_o^*(t)\big)\tilde{\xi}_n + \tilde{\kappa}_n \tilde{\xi}_n^3 = \sum_{j=-\infty}^{\infty} \tilde{k}_n e^{ij\Omega_o t + \phi}, \quad (4.14)$$

$$u_{1,tt} + 2\mu_\theta u_{1,t} + \omega_\theta^2 u_1 + \eta_n \tilde{\xi}_n^2 - \eta_m \xi_m^2 = \omega_\theta^2 u_2^* + M_1^* J^{-1}, \quad (4.15)$$

To analyze the dynamics of this system the Method of Multiple Scales is employed. It is a perturbation method which relies on the sorting of terms into orders of magnitude, and the results and solution procedure depends on this ordering. To analyze possible resonance conditions, the following terms are assumed small: linear viscous damping terms with μ, parametric coupling terms in the parenthesis, squared and cubic non-linearities, and the external forcing of the chain spans from impact loading, which is represented by Fourier expansions. The terms p_0^* model the variable wrapping length introduced in chapter 3.

So far, the parametric excitation $p_o^*(t)$, the kinematic forcing of the driver sprocket $u_2^*(t)$ and the external excitation of the driven sprocket $M_1^*(t)$ has been assumed to have a zero mean, but otherwise arbitrary. Each of them is assumed to be mono-frequency harmonic,

$$p_o^* = p_0 \cos(\Omega_0 T_0), \quad (4.16)$$

$$M_1^*/J = p_1 \cos(\Omega_1 T_0), \quad (4.17)$$

$$u_2^* = p_2 \cos(\Omega_2 T_0), \quad (4.18)$$

From the perturbation analysis, a set of resonance conditions can be deducted which are all of practical relevance. For the tight span with natural frequency ω_m,

resonant excitation occurs under the following conditions

External resonance from meshing: $j\Omega_0 \approx \omega_m$,
Parametric resonance from driver or meshing: $\Omega_2 \approx 2\omega_m$ and/or $\Omega_0 \approx 2\omega_m$,
Internal two-to-one sprocket-span resonance: $\omega_\theta \approx 2\omega_m$.

Similarly for the slack span with natural frequency $\tilde{\omega}_n$:

External resonance from meshing: $j\Omega_0 \approx \tilde{\omega}_n$,
Parametric resonance from driver or meshing: $\Omega_2 \approx 2\tilde{\omega}_n$ and/or $\Omega_0 \approx 2\tilde{\omega}_n$,
Internal two-to-one sprocket-span resonance: $\omega_\theta \approx 2\tilde{\omega}_n$.

For the driven sprocket with natural frequency ω_θ:

External resonance from sprocket excitations: $\Omega_2 \approx \omega_\theta$ and/or $\Omega_1 \approx \omega_\theta$,
Internal two-to-one span-sprocket resonance: $2\tilde{\omega}_n \approx \omega_\theta$ and/or $2\omega_m \approx \omega_\theta$.

Clearly, a multitude of resonance - and combined resonance cases exists, which involves one, two or all three degrees of freedom. These are all of practical relevance, and identify (less desirable) dynamic phenomenas which may occur in roller chain drives.

Note that for e.g. the tight span motion, primary parametric and external resonance coming from polygonal action (p_0 and k_m terms in (4.13)) cannot exist simultaneously, since primary parametric resonance requires $\Omega_0 \approx \omega_m$, in which case the external forcing is has frequency $j\Omega_0 \approx j2\omega_m$, i.e. non-resonant. Primary parametric resonance of both spans simultaneously is possible in real chain drives when there is no torque on the driven sprocket, as in the case of a guide or coupler sprocket; under these conditions the natural frequency of the two spans will be nearly identical, and coupling could occur across the driven sprocket if it is compliant.

Out of the above possible resonance cases, three examples have been considered which are of practical interest, but also demonstrate how the motions (de)couple in this model; primary parametric resonance of the tight span, external resonance of the driven sprocket, and lastly, those two cases combined, i.e. primary parametric resonance of the tight span along with internal resonance of the driven sprocket.

4.5.1 Primary parametric resonance of the tight span

The example demonstrates how decoupled transverse vibration of a single chain span, coming from a harmonic variation of axial tension leading to parametric resonance, could be realized in a real roller chain drive. Primary parametric resonance of the tight span (4.13) is considered, with excitation coming the driver sprocket, i.e. p_2. There are no other external or internal resonances, and the tight and slack span are detuned such that ω_m is away from $\tilde{\omega}_n$.

For the external forcing coming from p_2, the nearness to primary parametric resonance of the tight span is quantified by a detuning parameter σ_2, such that

$$\Omega_2 = 2\omega_m + \varepsilon\sigma_2, \tag{4.19}$$

The response is shown to be similar an isolated parametrically excited axially moving string, see e.g. Figure 1.3. The slack span and the driven sprocket has a respons that effectively goes to zero. The tight span has a trivial solution

$$a = 0, \quad \cos(\psi_2) = \frac{2\sigma_2\omega_m}{\alpha_m p_2}, \tag{4.20}$$

that is, a solution exists for which the span does not vibrate, but there exists also a non-trivial solution:

$$a^2 = \frac{4\omega_m}{3\kappa_m}\left(\sigma_2 \pm \sqrt{\left(\frac{\alpha_m p_2}{2\omega_m}\right)^2 - 4\mu_m^2}\right), \quad \tan\psi_2 = \frac{2\mu_m}{\frac{4\omega_m a^2}{3\kappa_m} - \sigma_2}, \tag{4.21}$$

where a is the amplitude of the span response.

The direct external excitation of the driven sprocket is given by the term $\omega_\theta^2 u_2^*$ in (4.15), and specified by $p_2\cos\Omega_2$ in (4.18), is assumed to be non-resonant and of order $O(\varepsilon)$, where $\varepsilon \ll 1$. This in effect renders the driven sprocket with a zero vibratory response, i.e. the driven sprocket is not compliant to the driver sprocket excitation. For this to hold in the case where the external excitation of the driven sprocket coming from p_2 is *not* weak, but $O(1)$, the frequencies Ω_2 and ω_θ should be so far apart that the driven sprocket forced response given by $\omega_\theta^2 p_2/(\omega_\theta^2 - \Omega_2^2)\cos(\Omega_2 T_0)$ becomes $O(\varepsilon)$. The example demonstrates how the span vibrations and sprocket response decouple from the remaining system, when the excitation is weak and non-resonant.

4.5.2 Primary external resonance of driven sprocket

During normal operation of a real chain drive, the nominal (angular) velocity varies according to the desired operating conditions. As the excitation from the driver is often period with the driver nominal angular velocity, cf. Figure 4.2, it is relevant to examine the case where the external excitation is near-resonant to the driven sprocket, $\Omega_2 \approx \omega_\theta$. The other direct and parametric excitations are assumed non-resonant. To describe the nearness of external resonance, a detuning parameter σ_θ is by

$$\omega_\theta = \Omega_2 + \varepsilon\sigma_\theta. \tag{4.22}$$

For the driven sprocket response there exists no trivial solution, and the stationary amplitude v and phase ψ_θ can be shown to be

$$v = \frac{1}{2}\frac{\omega_\theta p_2}{\sqrt{\mu_\theta^2 + (\omega_\theta - \Omega_2)^2}}, \quad \tan\psi_\theta = \frac{-\mu_\theta}{\omega_\theta - \Omega_2}. \tag{4.23}$$

The results demonstrate that for near-resonant excitation of the driven sprocket there will be no transverse vibrations of the spans, if the excitation frequency is not near primary parametric resonance of the spans. However, this is under the assumption that the parametric excitation of the chain spans is small compared to the linear axial stiffness of the chain spans in (4.13)-(4.14), which might not be fulfilled under large resonant vibrations of the driven sprocket. However, in real chain drives, the ratio between linear axial stiffness and parametric excitation can be decreased by increasing the pretension P_{tot}, which may also move the natural frequencies of the span away from critical excitation frequencies. Note from (4.23) that in the present model, rotational damping of the driven sprocket is the only mechanism which will limit the response of the driven sprocket subjected to resonant excitation.

This case indicates that for a real roller chain drive in operation, passing a natural frequency of the driven sprocket does not lead to transverse span vibrations if the excitation is not near parametric resonance of the spans, and that rotational damping of the driven sprocket may reduce the resonant response.

4.5.3 Combined parametric and internal resonance between span and sprocket

The first example analyzed the span response when the driven sprocket is not compliant, i.e. the driver excitation let to a vibratory response of the chain span only. The second example demonstrated near resonant excitation of the driver sprocket, where the driver excitation only caused a vibratory response of the driven sprocket. Here is analyzed the case where the driver excitation may cause a vibratory response of both the driven sprocket and the chain span. This is both of practical interest, and novel to the study of the dynamics of axially moving strings.

Thus we consider primary parametric excitation of the tight span $\Omega_2 \approx 2\omega_m$ combined with internal two-to-one resonance between span and the driven sprocket $\omega_\theta \approx 2\omega_m$. All remaining excitations are assumed non-resonant, and the two spans are detuned by loading of the driven sprocket, such that ω_m is away from $\tilde{\omega}_n$. To describe the nearness to primary parametric resonance we introduce the detuning parameter σ_2 defined by (4.19).

$$\Omega_2 = 2\omega_m + \varepsilon\sigma_2. \tag{4.24}$$

Similarly, to describe the nearness to internal resonance we introduce the detuning σ_θ defined by

$$\omega_\theta = 2\omega_m + \varepsilon\sigma_\theta. \tag{4.25}$$

The equations governing stationary amplitudes:

$$0 = -\mu_m a - \Lambda_1 a v \sin\psi_1 - f_1 a \sin\psi_2, \tag{4.26}$$

$$0 = -\mu_\theta v + \Lambda_2 a^2 \sin\psi_1 - f_2 \sin(\psi_2 - \psi_1), \tag{4.27}$$

$$\tfrac{1}{2} a\sigma_2 = \Lambda_0 a^3 + \Lambda_1 a v \cos\psi_1 + f_1 a \cos\psi_2, \tag{4.28}$$

$$v(\sigma_2 - \sigma_\theta) = \Lambda_2 a^2 \cos\psi_1 + f_2 \cos(\psi_2 - \psi_1). \tag{4.29}$$

There is a trivial solution given by,

$$a = 0, \quad v^2 = \frac{f_2^2}{\mu_\theta^2 + (\sigma_2 - \sigma_\theta)^2}, \quad \tan(\psi_2 - \psi_1) = \frac{\mu_\theta}{\sigma_\theta - \sigma_2}, \tag{4.30}$$

Representing pure rotational motion of the driven sprocket without transverse vibrations of the upper span, as examined in section 4.5.2. As for non-trivial solutions $a \neq 0$, corresponding to coupled motions of the driven sprocket and the tight span, the algebraic set of nonlinear equations (4.26)-(4.29) are not readily solved for a and v; instead a numerical solution is obtained.

4.6 Example results of the dynamic analysis

To illustrate results of the above three resonance cases, the solutions are obtained for a specific chain drive, using again configuration C_1 in Table 3.1 with pitch $p = 0.0254$ m, and mass, stiffness, damping and loading parameter values as listed in Table 4.1. The first mode of the tight span is considered, i.e. ξ_m in (4.13), with $m = 1$. With a stationary angular velocity of the driver of 400 rpm there will then be internal resonance between the tight span and the driven sprocket.

Table 4.1: Dynamic parameters

P_{tot}	1000	N
EA	0.56e6	N
ρA	2.61	kg/m
$\hat{J}_1$	0.6	kg m^2
$\hat{f}_1$	200	N
$\hat{d}_1$	1.1	Nms/rad
θ_2^*	0.005	rad
μ_θ	0.02	
μ_m	0.02	

4.6.1 Parametric resonance of the tight span

Here we present an example of the results derived in section 4.5.1 for the response of the tight span under primary parametric excitation. The analysis demonstrated that the tight span transverse motion decouples, because the driven sprocket is non-compliant. The solution for the steady state span vibration amplitude a given by (4.21) is shown in Figure 4.5 along with numerical solutions shown with circles $\circ$. Broken and full lines identifies stable and unstable solution states, respectively.

The resonance peak near $\Omega_2/\omega_m = 2$ bends to the right due to nonlinear hardening coming from increased axial tension at large amplitudes, represented by the cubic nonlinearity in the model. Increased parametric excitation amplitude p_2 and decreased damping μ_m widens the resonance peak. It is seen that as the upper branch bends to the right, there are two co-existing stable solutions; one with zero amplitude and another with a large amplitude. Since this is a non-linear response, the solution to which the system converges depends on the initial conditions, which for the numerical solutions were chosen at random, to demonstrate the presence of coexisting solution branches.

In real chain drives, adjusting the span tension to change the natural frequency of the span can be used as an approach to ensure that the the span does not operate near the critical excitation frequencies.

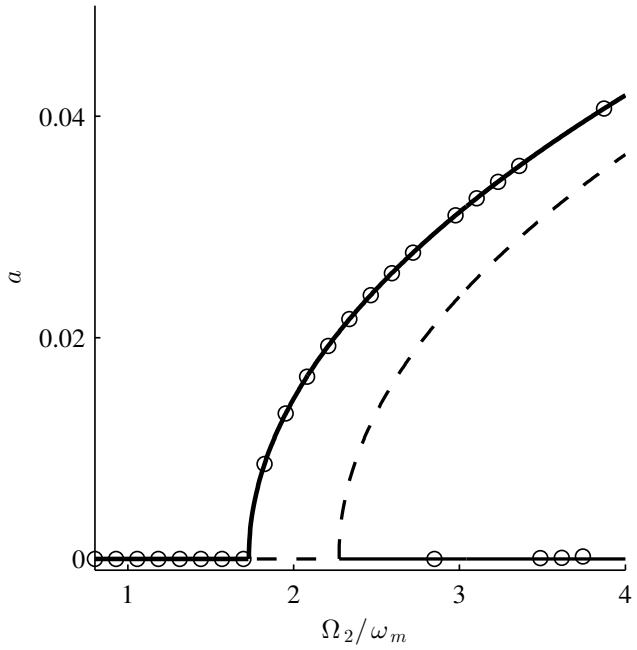

Figure 4.5: The tight span transverse vibration amplitude a at primary parametric resonance according to perturbation results (4.21) (solid lines stable, dashed line unstable), and numerical solution of the modulation equations (circles).

4.6.2 Resonant excitation of driven sprocket

The solution for the driven sprocket steady state amplitude v given by (4.23) is shown in Figure 4.6 for the resonant excitation of the driven sprocket, as analyzed in section 4.5.2. Near $\Omega_2/\omega_\theta = 1$ there is a clearly defined maximum amplitude. The analysis showed that increased damping reduces the height of the resonance peak.

In this example the sprocket motion decouples since the spans are tensioned to prevent transverse vibration. Therefore, the response is essentially linear, and the numerical solution confirms there is only a single, independent of initial conditions. The analysis presupposes that the parametric excitation amplitude of the spans is small compared to the span linear stiffness, and the solution is only a good approximation when these conditions are fulfilled; they could be violated during large resonant vibration amplitudes of the driven sprocket, which should therefore still be avoided in real roller chain drives.

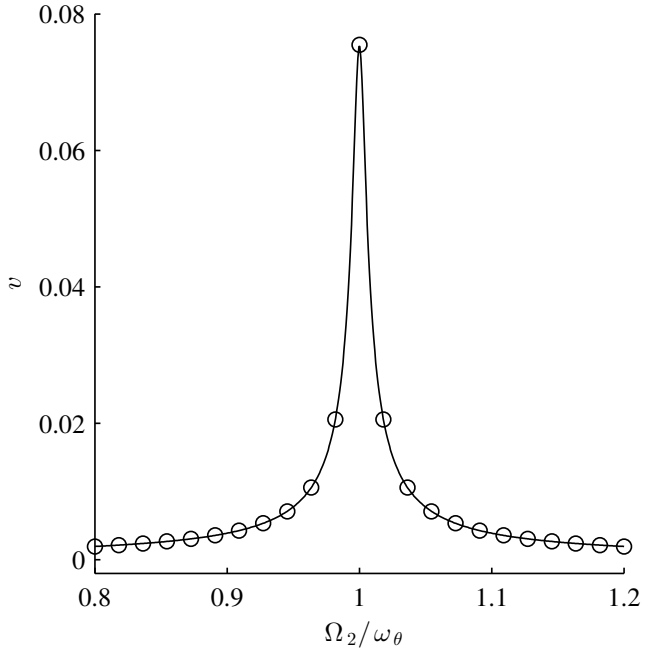

Figure 4.6: The driven sprocket angular vibration amplitude v at resonant direct external excitation according to the perturbation results (4.23) (solid line), and numerical solutions of the modulation equations (circles).

4.6.3 Combined parametric resonance and internal resonance

The combination of internal resonance and parametric resonance was investigated in section 4.5.3. The solution for the span and sprocket steady state response is obtained through numerical integration of the modulation equations. Results for the stationary amplitudes a of the span and v of the driven sprocket are shown in Figures 4.7 and 4.8, respectively. In these figures exact parametric resonance occurs for $\sigma_2 = 0$, and exact internal resonance occurs on the line running diagonally across the graphs where $\sigma_\theta = \sigma_2$.

Figure 4.7(a) shows three projections of the span vibration amplitude for three values of the detuning of internal resonance σ_θ, as indicated by bold lines in Figure 4.7(b). First, note the qualitative and quantitative similarity between the bended resonance peak in the response of the decoupled span motion in Figure 4.5 and the response drawn with solid bold lines for $\sigma_\theta/\omega_m = -1.9$ in Figure 4.7(a) and at the edge of Figure 4.7(b). For $\sigma_\theta/\omega_m = -1.9$ the amplitude a is zero until $\sigma_2/\omega_m > -0.3$. For $\sigma_2/\omega_m > 0.5$ the stationary amplitude jumps between two solution states. This is similar to what is shown in Figure 4.5, where the span motion was decoupled, and it also appears from Figure 4.7 that for $\sigma_2/\omega_m > 0.5$ there are two coexisting solutions between which the response jumps between depending on the initial conditions.

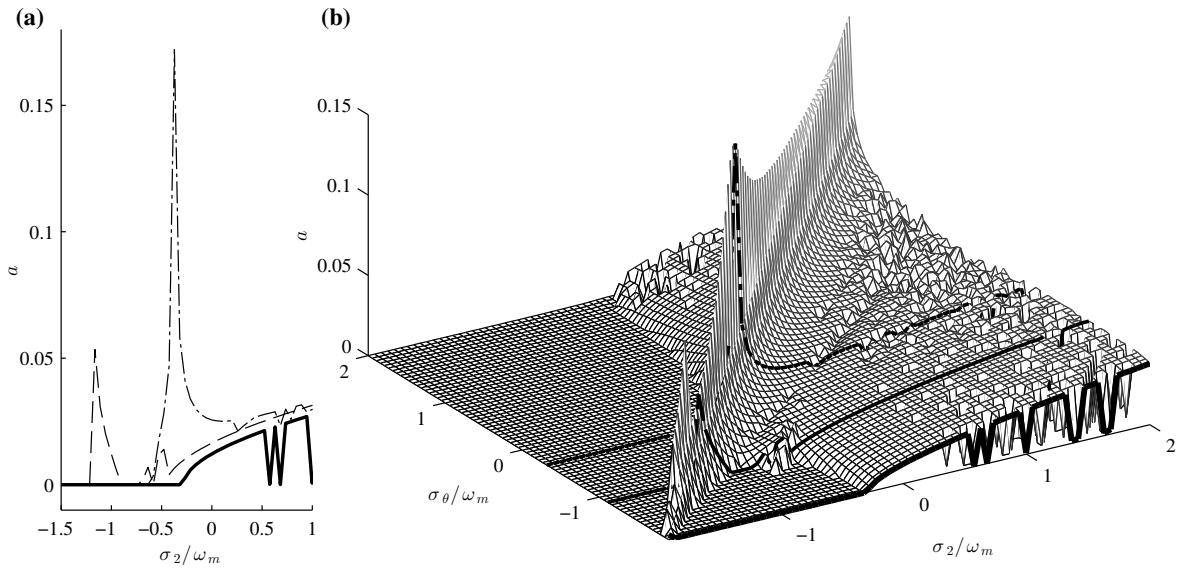

Figure 4.7: Tight span transverse vibration amplitude a under combined primary parametric resonance and internal resonance obtained by integration of the modulation equations. In (a) cross sections of (b) for values $\sigma_\theta/\omega_m \simeq [-1.9,\ -1.1,\ -0.3]$ are shown with lines $[-,\ --,\ -\cdot-]$, respectively.

Secondly, it is seen Figure 4.7 that there is a large upright amplitude peak running diagonally across Figure 4.7(b) near exact internal resonance $\sigma_\theta = \sigma_2$. As $\sigma_\theta/\omega_m = \sigma_m/\omega_m$ increase from below to approach zero, the upright resonant peak combines with the bended resonance peak and the amplitude reaches maximum for $\sigma_\theta/\omega_m = \sigma_m/\omega_m \simeq -0.3$. The upright peak is present for values of σ_2/ω_m much lower than zero, and the upright and bended resonance peaks are separated for $\sigma_\theta/\omega_m < -1.1$. This indicate that when the driven sprocket is compliant, chain span vibrations excited by parametric excitation can occur for much lower values of σ_2/ω_m than when the span is decoupled, which is a significant and novel result. In real chain drives, this means that span transverse vibration can be excited at frequencies lower than parametric resonance when the driven sprocket has a vibratory response.

Figure 4.8(a) shows three projections of the driven sprocket amplitude for three values of the detuning of parametric resonance σ_2 indicated with bold lines in Figure 4.8(b). We observe a qualitative and partly quantitative similarity to the upright resonance peak in the response of driven sprocket motion in Figure 4.6 and the cross sections in Figure 4.8(a). The maximum value of v is observed for $\sigma_2/\omega_m \simeq -0.5$.

For all the presented examples it is noted that the response is obtained using a perturbation method assuming near-resonance. Thus, predictions will be most accurate near $\sigma_\theta = \sigma_m = 0$.

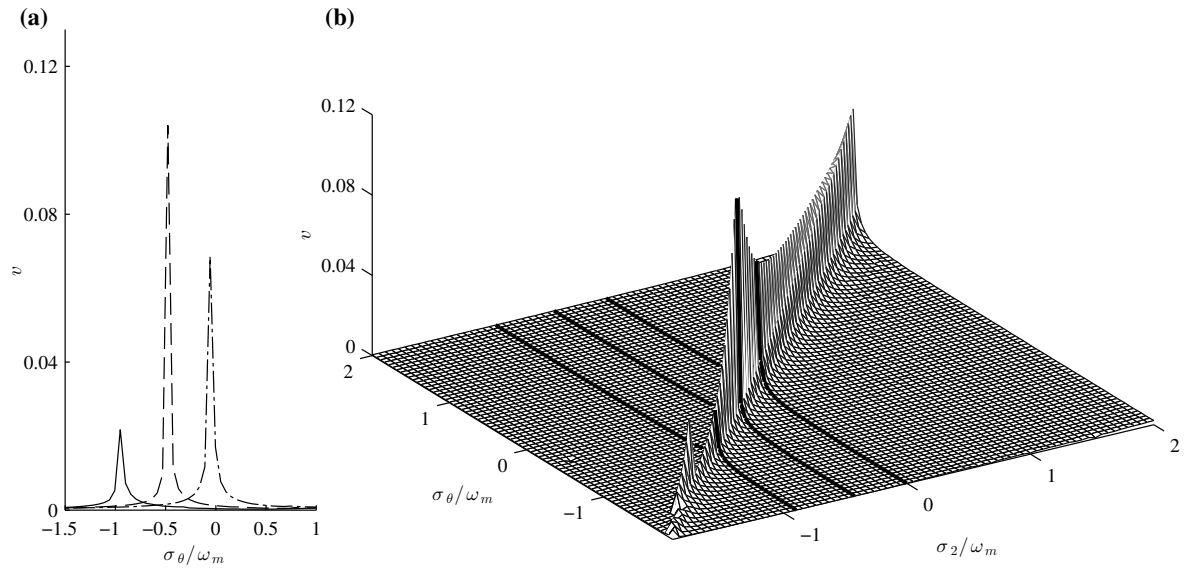

Figure 4.8: Driven sprocket angular vibration amplitude v under combined parametric and internal resonance obtained by integration of the modulation equations. In (a) cross sections of (b) for values $\sigma_2/\omega_m \simeq [-0.9,\ -0.5,\ 0]$ are shown with lines $[-,\ --,\ -\cdot-]$, respectively.

4.7 Further remarks

There are several points at which the approximate analysis could be improved and extended. To to obtain a better quantitative agreement with numerical solutions of the full model equations, more accurate test functions for the Galerkin expansion could be applied, as introduced in [P4]. Different choices for the ordering of magnitude, i.e. assignment of smallness to specific terms, could be changed to yield more even more results for the coupled dynamics of the system. Also, more than one mode could be considered for each span. However, the main contribution of this work is the model given by the three coupled equations for the two spans and the driven sprocket, and the approximate analysis demonstrating that solutions of the coupled equations can be obtained in a systematic manner.

5 Conclusion

5.1 Summary and discussion

The work comprising this thesis is focused on developing analytical predictions for the properties of roller chain drives which are relevant to the engineering community. It is focused on two separate subjects: Kinematics and dynamics. Besides theoretical analysis the work effort has been focused on mathematical modeling and these results are also considered to be important contributions to the field.

Kinematic analysis based on the analysis of the chain drive modeled as a four bar mechanism have been considered, with the main points being:

- A chain drive is modeled as a four-bar mechanism. Equations governing position, velocity and acceleration are derived, conveniently nondimensionalized, and solved exactly and approximately.
- Seating and release configurations are determined, and simple approximate expressions including only the dominant design parameters are derived.
- The instantaneous span length is determined, and its discontinuous variation with time is given a simple formulation.
- An approximate expression for the phase between chain roller seating and release is determined, giving insight into the time intervals between the discontinuous accelerations of the driven sprocket.
- Example results are presented for coarse, medium and fine chain drive configurations, showing very good agreement between exact and approximate results.

- Comparison is made between multi-body simulation and the results of kinematic analysis. It is demonstrated how the kinematic analysis is useful for aiding the interpreting both simulation results and experimental measurements.

The closed form approximate results provide insight into the effects of changing design parameters, and allows for a convenient estimation of the chain drive kinematics. The study treats only the case where the span connects the sprockets such that they rotate in the same direction. However, it is expected that spans connecting the two sprockets as the inner tangent could be treated following a similar approach.

An extension of the kinematic analysis considering only one chain span connecting two sprockets is introduced. The approach is based on the analysis of the four-bar mechanism, and is aimed at determining the wrapping length of a chain when the chain spans are tensioned to form straight lines connecting the driver and driven sprocket. The main points of these results are:

- A kinematic model of a two-sprocket roller chain drive with straight spans was presented, along with a procedure for calculating the total chain wrapping length.
- Results demonstrated that the total wrapping length of the chain generally varies periodically with the tooth frequency.
- Twelve exact chain drive configurations where presented, which may serve as bench-mark configurations for numerical models.
- The chain wrapping length was shown to be constant for a configuration where both sprockets have the same number of teeth and the chain consists of an even number of chain links.
- Comparison was between the kinematic prediction of a variable wrapping length and multi-body simulations. The results showed excellent qualitative agreement, and good quantitative agreement.
- Based on the kinematic analysis, it is predicted that there will generally be a tooth period variation of axial tension in real chain drives.

The kinematic analysis considering the chain wrapping tightly around the sprockets is a new field in the study of chain drive kinematics, and although the analysis presented here is approximate, it demonstrates an important phenonema, and could motivate further research.

Dynamic modeling and approximate analysis of a simple roller chain drive is undertaken, and the main points are:

- Equations of motion for the chain spans is derived, treating the problem of an axially moving string supported by moving boundaries. It is demonstrated that a first order variable string length leads to a second order effect.
- A new dynamic model of the coupled motion of the tight chain spans transverse vibration and the driven sprocket angular displacement is derived. The model introduces, and assumes, a steady operation state from which displacements are measured.
- The dynamic model provides insight into resonance conditions and amplitude responses, and is analyzed approximately using a mode shape expansion and perturbation analysis.
- Three example results of the dynamic analysis are presented, illustrating the conditions where the motions of the span and sprockets decouple. Results for a case of combined internal and parametric resonance showed that large span vibrations can occur due to compliance of the driven sprocket.
- Though the model is simple, it provides useful insight into the coupled dynamics of chain drives, and may aid the design and interpretation of numerical and experimental results.

The approximate analysis of the dynamic model could be improved by exact mode shapes for axially moving strings. However, these are complex and it would increase the extend of the required algebra. It is also expected that this would only lead to quantitatively better predictions, and not significant qualitative differences. Furthermore, the approximate analysis could be extended or modified by assuming a different ordering of magnitude of the excitations etc., and it is expected that this could be done successfully with the method of multiple scales employed here.

5.2 Suggestions for future work

For the kinematic analysis, there are several tasks that could be undertaken in direct extension of this work: Analysis of the kinematics of two sprockets connected to make the sprockets rotate in opposite directions. Further research of the varying wrapping length variation: Development of a new analysis approach, and positioning of sprockets in chain drives with more than two sprockets to either attenuate of amplify the effect of a varying wrapping length.

It is expected that the dynamic model introduced here could be extended to include roller chain drives with more than two sprockets, as e.g. the chain drive in Figure 4.1. Due to the systematic structure of multiple scales analysis presented [P2], where the modulation equations decouple for non-resonant excitation, it is expected that the dynamics of chain drives with more than two sprockets could be analyzed using a similar modeling and analysis approach. In the analysis presented here the coupled motion of transverse span vibrations happens across a single degree of freedom oscillator, which is the driven sprocket with a given natural frequency. For a larger chain drive with more sprockets, this would correspond to modal excitation near the natural frequencies of the coupled rotational motion of the sprockets, with the spans acting as linear springs.

Lastly, it is expected that the greatest outcome of further research in the field of roller chain drives could be obtained through experimental work, in comparison with the theoretical results presented here, and the simulation results that can be obtained from the multi-body simulation program. As mentioned in section 4.3 the experimental investigations should first give careful consideration to the correct determination of the parameter values for roller chains that can be applied to obtain correct theoretical results using uniform string models for the chain. Specifically the longitudinal wave speed of roller chains. The correct axial stiffness of the roller chain is important in both the predictions of the natural frequencies of transverse span vibration, and the natural frequencies of the sprockets connected to the chain spans acting as linear springs.

Following the experimental determination of the correct parameter values to assign to the theoretical models, the analytical predictions of this study could be tested in an experimental setup of chain drive with two sprockets. Ideally, the experiment should be designed such that the driven sprocket damping, loading and inertia can easily be modified, the sprockets and chain type can easily be interchanged, and angular excitation can be applied to the driver sprocket, e.g. to mimic the excitation coming from combustion engines.

Bibliography

[P1] N. Fuglede and J. J. Thomsen. Kinematics of roller chain drives - exact and approximate analysis. *Submitted for Journal Publication*, 2014.

[P2] N. Fuglede and J. J. Thomsen. Kinematic and dynamic modeling and approximate analysis of a roller chain drives. *Submitted for Journal Publication*, 2014.

[P3] N. Fuglede and J. J. Thomsen. Roller chain drive vibration analysis based on a string model with boundaries moving non-smoothly. In *3rd International Conference on Vibro Impact Systems and Systems with Non-smooth Interactions*, 22-26/7/2013, Leinsweiler, Germany.

[P4] N. Fuglede and J. J. Thomsen. Vibrations of axially moving strings with in-plane oscillating supports. In *1st International Colloquium on Time-periodic Systems, Current trends in theory and application*, 27-30/8/2012, Frankfurt, Germany.

[P5] N. Fuglede and J. J. Thomsen. Roller chain drive analysis: simplified modeling and analysis of the dynamic effects of meshing. In *7th European Nonlinear Dynamics Conference*, 24-29/7/2011, Rome, Italy.

[6] R. G. Parker and Y. Lin. Parametric instability of axially moving media subjected to multifrequency tension and speed fluctuations. *Journal of Applied Mechanics*, 68(1):49–57, 2001.

[7] G. M. Bartlett. Roller chain drives in theory and practice. *Product Engineering*, 2(4):253–255, 1931.

[8] R. A. Morrison. Polygonal action in chain drives. *Machine Design*, 24(9): 155–159, 1952.

[9] E. I. Radzimovsky. Eliminating pulsations in chain drives. *Product Engineering*, 26(7):153–157, 1955.

[10] R. C. Binder. *Mechanics of the Roller Chain Drive: Based on Mathematical Studies by RC Binder*. Prentice-Hall, 1956.

[11] G. Bouillon and G. V. Tordion. On polygonal action in roller chain drives. *Journal of Engineering for Industry*, 87(2):243–250, 1965.

[12] S. R. Turnbull and J. N. Fawcett. Approximate kinematic analysis of the roller chain drive. *Proceedings of the Fourth World Congress on Theory of Machines and Mechanisms*, pages 907–911, 1975.

[13] C. K. Chen and F. Freudenstein. Toward a more exact kinematics of roller chain drives. *Journal of Mechanisms Transmissions and Automation in Design*, 110(3):269–275, 1988.

[14] R. Binder and W. Covert. Impact between chain roller and sprocket in chain drive. *Franklin Institute – Journal*, 245(4):319–329, 1948.

[15] F. R. Archibald. Energy losses in chain-belt problem. *Mechanical Engineering*, 68(2):139–142, 1946.

[16] M. Okoshi and K. Uehara. Study on the uneveness of transmission by roller chain (1st report). *Journal of the Japan Society for Precision Engineering*, 25 (9):425–431, 1959.

[17] M. Okoshi and K. Uehara. Study on the uneveness of transmission by roller chain (4th report). *Journal of the Japan Society for Precision Engineering*, 25 (9):545–551, 1959.

[18] G. K. Ryabov. Inertia effects of impact loading in chain drives. *Russian Engineering Journal*, 48(8):17–19, 1968.

[19] J. N. Fawcett and S. W. Nicol. The influence of lubrication on tooth-roller impacts in chain drives. *Proceedings of the Institution of Mechanical Engineers*, 191(21):271–275, 1977.

[20] S. W. Nicol and J. N. Fawcett. Reduction of noise and vibration in roller chain drives. *Proceedings of the Institution of Mechanical Engineers*, 191(39):363–370, 1977.

[21] J. C. Conwell, G. E. Johnson, and S. W. Peterson. Experimental investigation of the impact force that occurs when a roller seats on the sprocket during normal operation of a roller chain drive. In *International Power Transmission and Gearing Conference*, volume 43-2, pages 717–721, 1992.

[22] J. C. Conwell and G. E. Johnson. Design, construction and instrumentation of a machine to measure tension and impact forces in roller chain drives. *Mechanism and Machine Theory*, 31(4):525–531, 1996.

[23] J. C. Conwell and G. E. Johnson. Experimental investigation of link tension and roller-sprocket impact in roller chain drives. *Mechanism and Machine Theory*, 31(4):533–544, 1996.

[24] K. W. Wang, S. P. Liu, S. I. Hayek, and F. H. K. Chen. On the impact intensity of vibrating axially moving roller chains. *Journal of Vibration and Acoustics*, 114(3):397–403, 1992.

[25] S. P. Liu, K. W. Wang, S. I. Hayek, M. W. Trethewey, and F. H. K. Chen. A global-local integrated study of roller chain meshing dynamics. *Journal of Sound and Vibration*, 203(1):41–62, 1997.

[26] G. K. Ryabov and A. V. Kryukov. Shock loads in chain transmissions. *Russian Engineering Research*, 17(6):15, 1997.

[27] H. Zheng, Y. Y. Wang, G. R. Liu, K. Y. Lam, K. P. Quek, T. Ito, and Y. Noguchi. Efficient modelling and prediction of meshing noise from chain drives. *Journal of Sound and Vibration*, 245(1):133–150, 2001.

[28] H. Zheng, Y. Wang, K. P. Quek, G. R. Liu, Y. Noguchi, and K. Lam. Investigation of meshing noise of roller chain drives for motorcycles. *Noise Control Engineering Journal*, 50(1):5–11, 2002.

[29] H. Zheng, Y. Y. Wang, and K. P. Quek. A refined numerical simulation on dynamic behavior of roller chain drives. *Shock and Vibration*, 11(5-6):573–584, 2004.

[30] W. Schiehlen and R. Seifried. Three approaches for elastodynamic contact in multibody systems. *Multibody System Dynamics*, 12(1):1–16, 2004.

[31] Y. Wang, D. Ji, and K. Zhan. Modified sprocket tooth profile of roller chain drives. *Mechanism and Machine Theory*, 70:380–393, 2013.

[32] K. M. Marshek. On the analyses of sprocket load distribution. *Mechanism and Machine Theory*, 14(2):135–139, 1979.

[33] G. K. Ryabov. The engagement of a worn chain with a sprocket. *Russian Engineering Journal*, 60(4):31–34, 1980.

[34] Y. S. Zeltser and G. K. Ryabov. Increasing the life of drive roller chains. *Soviet Engineering Research*, 2(7):27–29, 1982.

[35] M. R. Naji and K. M. Marshek. Analysis of sprocket load distribution. *Mechanism and Machine Theory*, 18(5):349–356, 1983.

[36] B. H. Eldiwany and K. M. Marshek. Experimental load distributions for double pitch steel roller chains on steel sprockets. *Mechanism and Machine Theory*, 19(6):449–457, 1984.

[37] B. H. Eldiwany and K. M. Marshek. Experimental load distributions for double pitch steel roller chains on polymer sprockets. *Mechanism and Machine Theory*, 24(5):335–349, 1989.

[38] M. R. Naji and K. M. Marshek. Effects of the pitch difference on the load ditribution of a roller chain drive. *Mechanism and Machine Theory*, 24(5): 351–362, 1989.

[39] M. S. Kim and G. E. Johnson. Mechanics of roller chain-sprocket contact: a general modelling stragegy. *American Society of Mechanical Engineers, Design Engineering Division (Publication) DE*, 43(2):689–695, 1992.

[40] M. S. Kim and G. E. Johnson. Mechanics of roller chain-sprocket contact: observations about the contact phenomena and load distribution. *American Society of Mechanical Engineers, Design Engineering Division (Publication) DE*, 43(2):697–702, 1992.

[41] I. Troedsson and L. Vedmar. A method to determine the static load distribution in a chain drive. *Journal of Mechanical Design*, 121(3):402–408, 1999.

[42] I. Troedsson and L. Vedmar. A method to determine the dynamic load distribution in a chain drive. *Proceedings of the Institution of Mechanical Engineers, Part C: Journal of Mechanical Engineering Science*, 215(5):569–579, 2001.

[43] S. Mahalingam. Transverse vibrations of power transmission chains. *British Journal of Applied Physics*, 8(4):145–148, 1957.

[44] S. Mahalingam. Polygonal action in chain drives. *Journal of The Franklin Institute*, 265(1):23–28, 1958.

[45] S. W. Nicol and J. N. Fawcett. Vibrational characteristics of roller chain drives. *Engineering*, 217(1):30–32, 1977.

[46] S. R. Turnbull, S. W. Nicol, and J. N. Fawcett. Experimental investigation of the dynamic behavior of a roller chain drive. *British Library Archive - ASME Papers*, (77), 1977.

[47] J. N. Fawcett and S. W. Nicol. Vibration of a roller chain drive operating at constant speed and load. *Proceedings of the Institution of Mechanical Engineers*, 194:97–101, 1980.

[48] K. W. Wang and C. D. Mote, Jr. Band wheel system vibration under impulsive boundary excitation. *Journal of Sound and Vibration*, 115(2):203–216, 1987.

[49] K. W. Wang. On the stability of chain drive systems under periodic sprocket oscillations. *Journal of Vibration and Acoustics*, 114(1):119–126, 1992.

[50] G. K. Ryabov. Propagation of an elastic wave in transmission chains. *Russian Engineering Journal*, 51(7):20–21, 1971.

[51] S. T. Ariaratnam and S. F. Asokanthan. Dynamic stability of chain drives. *Journal of Mechanisms Transmissions and Automation in Design*, 109(3): 412–418, 1987.

[52] W. Choi and G. E. Johnson. Vibration of roller chain drives at low, medium and high operating speeds. *American Society of Mechanical Engineers, Design Engineering Division*, 63:29–40, 1993.

[53] W. Choi and G. E. Johnson. Transverse vibrations of a roller chain drive with a tensioner. *American Society of Mechanical Engineers, Design Engineering Division*, 63:19–28, 1993.

[54] C. J. Lodge and S. C. Burgess. A model of the tension and transmission efficiency of a bush roller chain. *Proceedings of the Institution of Mechanical Engineers, Part C: Journal of Mechanical Engineering Science*, 216(4):385–394, 2002.

[55] Lodge and Burgess. An investigation into the selection of optimum chain and sprocket size. *Journal of Engineering Design*, 15(6):563–580, 2004.

[56] I. Troedsson and L. Vedmar. A dynamic analysis of the oscillations in a chain drive. *Journal of Mechanical Design*, 123(3):395–401, 2001.

[57] S. L. Pedersen, J. M. Hansen, and J. A. C. Ambrosio. A roller chain drive model including contact with guide-bars. *Multibody System Dynamics*, 12(3): 285–301, 2004.

[58] S. L. Pedersen. Model of contact between rollers and sprockets in chain-drive systems. *Archive of Applied Mechanics*, 74(7):489–508, 2005.

[59] A. L. Thurman and C. D. Mote, Jr. Free periodic nonlinear oscillation of an axially moving strip. *Journal of Applied Mechanics*, 36(1):83–91, 1969.

[60] C. D. Mote, Jr. and A. L. Thurman. Oscillation modes of an axially moving material. *Journal of Applied Mechanics*, 38(1):279–280, 1971.

[61] L. Meirovitch. A new method of solution of the eigenvalue problem for gyroscopic systems. *AIAA Journal*, 12(10):1337–1342, 1974.

[62] L. Meirovitch. Modal analysis for response of linear gyroscopic systems. *Journal of Applied Mechanics*, 42(2):446–450, 1975.

[63] J. A. Wickert and C. D. Mote, Jr. Classical vibration analysis of axially moving continua. *Journal of Applied Mechanics*, 57(3):738–744, 1990.

[64] J. A. Wickert and C. D. Mote, Jr. On the energetics of axially moving continua. *Journal of the Acoustical Society of America*, 85(3):1365–1368, 1989.

[65] J. A. Wickert. Nonlinear vibration of a traveling tensioned beam. *International Journal of Non-Linear Mechanics*, 27(3):503–517, 1992.

[66] E. M. Mockensturm, N. C. Perkins, and A. G. Ulsoy. Stability and limit cycles of parametrically excited, axially moving strings. *Journal of Vibration and Acoustics*, 118(3):346–351, 1996.

[67] G. Michon, L. Manin, R. G. Parker, and R. Dufour. Duffing oscillator with parametric excitation: Analytical and experimental investigation on a belt-pulley system. *Journal of Computational and Nonlinear Dynamics*, 3(3), 2008.

[68] G. Michon, L. Manin, D. Remond, R. Dufour, and R. G. Parker. Parametric instability of an axially moving belt subjected to multifrequency excitations: Experiments and analytical validation. *Journal of Applied Mechanics*, 75(4), 2008.

[69] C. D. Mote, Jr. Dynamic stability of axially moving materials. *The Shock and Vibration Digest*, 4(4):2–11, 1972.

[70] A. G. Ulsoy, C. D. Mote, Jr., and R. Szymni. Principal developments in band saw vibration and stability research. *Holz als Roh- und Werkstoff*, 36(7): 273–280, 1978.

[71] J. N. Fawcett. Chain and belt drives, a review. *Shock and Vibration Information Center, The Shock and Vibration Digest*, 13(5):5–12, 1981.

[72] J. A. Wickert and C. D. Mote, Jr. Current research on the vibration and stability of axially-moving materials. *The Shock and Vibration Digest*, 20(5): 3–13, 1988.

[73] K. W. Wang and S. P. Liu. On the noise and vibration of chain drive systems. *The Shock and Vibration Digest*, 23(4):8–13, 1991.

[74] H. Rahnejat. Multi-body dynamics: historical evolution and application. *Proceedings of the Institution of Mechanical Engineers Part C-Journal of Mechanical Engineering Science*, 214(1):149–173, 2000.

[75] L.-Q. Chen. Analysis and control of transverse vibrations of axially moving strings. *Applied Mechanics Review*, 58(2):91–116, 2005.

[76] L. Q. Chen, W. Zhang, and J. W. Zu. Nonlinear dynamics for transverse motion of axially moving strings. *Chaos Solitons & Fractals*, 40(1):78–90, 2009.

[77] K. Marynowski and T. Kapitaniak. Dynamics of axially moving continua. *International Journal of Mechanical Sciences*, 81:26–41, 2014.

P1 Publication 1

The following manuscript [P1] has been submitted for journal publication. It contains a thorough and complete derivation of the exact and approximate kinematics of the roller chain drive analyzed as a four-bar mechanism.

Kinematics of Roller Chain Drives - Exact and Approximate Analysis

Niels Fuglede, Jon Juel Thomsen[1,]

Department of Mechanical Engineering, Technical University of Denmark, Building 404, DK-2800, Lyngby, Denmark

Abstract

An exact and approximate kinematic analysis of a roller chain drive modeled as a four-bar mechanism is presented. The span connects the sprockets such that they rotate in the same direction, and the sprocket size, number of teeth, and shaft center distance can be arbitrary. The driven sprocket angular position, velocity and acceleration, as well as span length, is calculated and their (discontinuous) variation with driver angular position and main design parameters is illustrated. Kinematic predictions for the chain span motion are compared to results of multibody simulation, and there is seen to be very good agreement. All together this gives new insights into the characteristics of chain drive kinematics and the influence of main design parameters.

Keywords: Roller chain, chain drives, kinematics, four-bar mechanism, multibody simulation

[1]Corresponding author: jjt@mek.dtu.dk

1. Introduction

Roller chain drives are widely used machine elements due to high energy efficiency and timing capabilities. Research topics include kinematics, chain span dynamics, load distributions, coupled sprocket and span dynamics, alternative design, multibody dynamics, roller impact and noise emission. A literature survey of noise and vibration was given by Wang and Liu [1]. Belt drives is a related research area and a survey including also this was given by Fawcett [2]. Also relevant for chain span dynamics are the studies of axially moving materials, surveyed by Chen [3].

The discrete nature of a chains introduce several effects, collectively known as polygonal action. Some of these effects are less desirable, e.g. the uneven transfer of torques between the sprockets and impact between chain rollers and sprockets. Polygonal action is inherent of chain drives, because a chain wrapped around sprockets form polygons rather than circles.

In chain drive kinematics, mass and elasticity are neglected and usually also tolerances and manufacturing inaccuracies of the drive components. Results therefore describe the motion of ideal chain drives operating at non-resonant conditions and very low speeds. The main object of investigation is often the velocity of the driven sprocket, and parameters of main concern are shaft center distance and tooth ratio. A detailed kinematic analysis reveals the characteristic loading of the chain drive and may aid the interpretation of simulation- and measurement results.

Early studies of the kinematics includes the work by Bartlett [4], who observed that sprockets could be modeled as polygons. He derived an expression for the minimum and maximum variation of the angular velocity ratio. He also noted that these are obtained when sprockets are positioned

such that the length of the driving span equals an integer number of pitch lengths, or an odd number of half pitches, respectively. In the work by Morrison [5] the kinematic motion of the chain drive is recognized to happen through a series of four-bar mechanisms. An expression for the shaft center distance giving the smallest velocity ratio variation was given. It was then shown how shaft center distance influence the angular acceleration of the driven sprocket, and thereby the chain drive loads.

A full monograph was written by Binder [6] on roller chain drives containing treatments of many subjects relevant for chain drive designers, including standard tooth geometry, static loading, velocity variations as well as friction and wear. The dynamics of the driven sprocket was considered by Mahalingam [7], who expressed the tension variation of the chain span due to polygonal action using the first harmonic term of a Fourier approximation. With this approximation, the driven sprocket is subjected to mono-frequency forced vibration and high-frequency components originating from impact loading and discontinuity are unaccounted for. The periodic fluctuations of driven sprocket velocity was studied by Bouillon and Tordion [8] both numerically and experimentally. An approximate analysis, also of the driven sprocket velocity, was made by Turnbull and Fawcett [9], who expressed the driven sprocket velocity as a series expansion, and illustrated the influence of the number of expansion terms for different centre distances and tooth ratios. A general kinematic analysis was presented by Chen and Freudenstein [10], where the shaft center distance could be arbitrary. The configuration of the chain drive where a roller seats on the driver sprocket was determined. The kinematic analysis also highlighted the discontinuous variation of span length, angular velocity- and acceleration ratios. Standards for design and dimensions of roller chains and sprockets are maintained by

organizations such as ANSI, BS and DIN.

Numerical analysis of roller chain drive systems has been developed using a multibody modeling approach by Pedersen et al. [11], which can take into account non-linear dynamic coupling, exact tooth geometry and impact phenonema [12]. A general methodology for planar models of multibody chain drives has been suggested by Pereira et al. [13]. Models that can include joint clearances are presented by [14].

In this study we present an exact kinematic analysis of the motion of the chain span components, i.e. the position of the span endpoints as well as angular position, velocity and acceleration of the driven sprocket during one tooth-period of the driver sprocket. Approximate results for the motion of the driven sprocket are also derived, based on the exact results. Simple approximate expressions for the seating and release configurations are derived, and these are used for obtaining the first analytical expression for the phase between rollers seating and releasing. The exact and approximate results are compared and shown to be in very good agreement for practical chain drives. The approximate results significantly ease the calculation of the motion of the driven sprocket, and may aid designers to quickly evaluate designs and estimate chain drive loads. The obtained results include the discontinuous properties of the driven sprocket motion, as opposed to the existing approximate analysis [9]. Comparison is made between kinematic predictions of the chain span path, and results multibody simulation. There is seen to be very good agreement and the kinematic analysis proves useful for interpreting the simulation results.

2. Exact kinematic analysis

The purpose of the analysis presentation is to make a clear illustration and derivation of the kinematic movement of the chain drive modeled as a four-bar mechanism. This presentation reworks and expands on results presented [10], but with motion coordinates better suited for approximate analysis. Attention is on presenting a self contained analysis, with complete results and clear derivations.

2.1. Kinematic model

The kinematic model defines how the chain drive elements and their dimensions are simplified as rigid components connected by perfect frictionless joints. The assumptions, geometry, coordinate system for the model, and the governing equations are presented in the following.

2.2. Assumptions

In the kinematic analysis the geometry of the chain and sprockets are assumed to be a perfect match, i.e. 1) sprocket pitch is equal to chain pitch, 2) the chain drive is without any mechanical clearances, and 3) a roller seated on the sprocket is positioned in the center of the sprocket seating curve. Neglecting dynamic effects introduce the following assumptions: 4) the span is perfectly straight, 5) chain and sprocket elements are rigid, and 6) the system is frictionless.

2.3. Basic geometry

Consider the sketch of a chain meshing with at sprocket in Fig. 1. Rollers are shown as small circles, thereby marking the chain as a connection of rigid links. The chain moves from left to right and the roller S_N will be removed

from the free span as the sprocket rotates clockwise around point C. Shown in the sketch is the exact moment where roller B_1 gets in contact with the sprocket and thereby define the new endpoint for the span.

Several geometric properties can be defined from Fig. 1. The pitch, p, is the distance between two chain rollers and also the length of the sides of the pitch polygon, witch is formed by connecting the centers of the sprocket seating curves. Half the angle between two seating curve centers is referred to as the pitch angle α. The pitch polygon has inscribed circle radius r and the circle drawn out by the centers of the seating curves on the sprockets is referred to as the pitch circle and has radius R. By formula, these variables are given by, respectively,

$$\alpha = \frac{\pi}{m}, \quad r = \frac{p}{2\tan\alpha}, \quad R = \frac{p}{2\sin\alpha}, \tag{1}$$

where m is the number of teeth on the sprocket.

It is seen from Fig. 1 that the length and endpoint positions of the free span varies discontinuously as the sprocket rotate clockwise around C. Rotation of the sprocket causes a vertical movement of the span endpoint between values r and R, and a horizontal movement between positions B_1 and B_2. The angle between the chain span $S_N B_1$ and the line CB_1 varies during rotation of the sprocket, and therefore a constant driving torque will not be transmitted evenly to the chain. Vectors $\mathbf{u}_1$ and $\mathbf{u}_2$ indicate the sprocket velocities at rollers B_1 and B_2, respectively. These velocities differ in direction and this cause an impact between the roller B_1 and the sprocket.

Collectively, these effects are referred to as polygonal action, their magnitude decrease as the number of sprocket teeth increase, but remains finite and, a characteristic for roller chain drives.

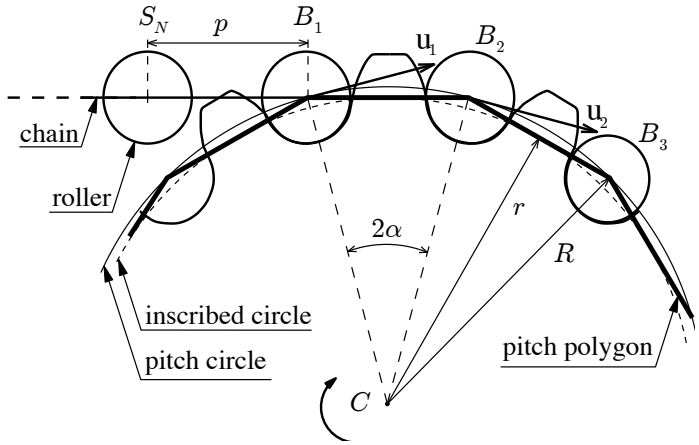

Figure 1: Sprocket meshing with chain

2.4. Coordinate system

Figure 2 shows the kinematic model in the coordinate system used throughout the analysis. The driving sprocket constraining the motion is centered at C and the driven sprocket at O. Subscripts c and o will be used to refer to those sprockets, e.g. α_o and R_c. Both sprockets are drawn as pitch polygons, connected by a line A_1B_1 representing the tight chain span. The main object of investigation is the tight span, since it transfers the torque from the driving sprocket to the driven sprocket.

When the chain drive consists of only two sprockets there will be a slack chain span connecting the two sprockets opposite of the tight span, and this will not be considered in the analysis. In case there are more than two sprockets there will be no slack span between sprockets O and C and the analysis presented here covers the transfer of torque between two neighboring sprockets in a larger chain drive system.

The origin of the fixed Cartesian XY-coordinate system is coincident with the center O of the driven sprocket. It is orientated such that the X-axis is parallel with the tangent T_oT_c common to the two inscribed circles,

so that the coordinates (x_c, y_c) of C is:

$$x_c = |T_o T_c|, \quad y_c = r_o - r_c. \tag{2}$$

For a wide range of typical chain drives lines OA_1 and CB_1, make small variations around the vertical direction and the slope of the span make small variations around the horizontal direction, while OC remain fixed. The smallness in variations makes the kinematic model suitable for approximate analysis.

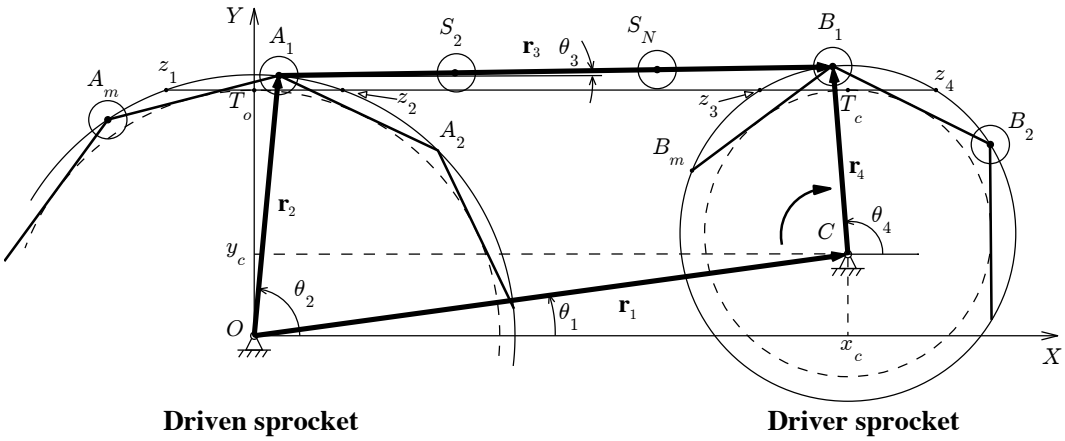

Figure 2: Chain drive kinematically modeled as a four-bar mechanism

2.5. Span length

When the roller chain drive is in operation, chain links will recurrently enter and leave the chain span and consequently the span length varies discontinuously with sprocket angular rotation, c.f. Fig. 2. The driving sprocket constrain the motion, and as it rotates the angle $2\alpha_c$ in clockwise direction, one tooth period passes and two events occurs: Roller A_1 loses contact with the driven sprocket and is released into the free span. It happens at the instant where the slope of $A_m A_1$ equals the slope of the span, and shifts the span endpoint from roller A_1 to A_m, thereby *in*creasing span

length by one pitch. Similarly, roller S_N gets in contact with the driving sprocket at the instant where the slope of $B_m B_1$ equals the slope of the span. This makes S_N the new span endpoint, thereby *de*creasing the length of the span by one pitch.

The length of the span and its dependency on design parameters is determined next. In Fig. 2, the common inner tangent $T_o T_c$ of the inscribed circles intersect the pitch circle of sprocket O in points z_1 and z_2. Similarly, the tangent intersects the pitch circle of sprocket C in points z_3 and z_4. The length $|z_1 z_2|$ equals one pitch, as do $|z_3 z_4|$. The span $A_1 B_1$ must equal an integral number of pitches and its length can be determined using the points z_1, z_2, z_3, and z_4. From Fig. 2 one finds that the chain span length $|A_1 B_1|$ fulfills

$$|z_2 z_3| \leq |A_1 B_1| \leq |z_1 z_4|, \tag{3}$$

where $|z_2 z_3| = |T_o T_c| - p$ and $|z_1 z_4| = |T_o T_c| + p$. Generally $|z_2 z_3|$ equals an integer number of pitches N plus a fraction of pitch lengths f, both defined from

$$|z_2 z_3| = (N + f)p, \quad f \in [0,\ 1[, \quad N \in \mathbb{N}. \tag{4}$$

In the chosen coordinate system the length of the common inner tangent $|T_o T_c|$ equals x_c; using (4) its length can be expressed as

$$x_c = |T_o T_c| = (N + 1 + f)p. \tag{5}$$

With this (3) can be written

$$(N + f)p \leq |A_1 B_1| \leq (N + 2 + f)p. \tag{6}$$

In the general case where $f \neq 0$ the span length $|A_1 B_1|$ fulfills the inequality (6) with two solutions,

$$|A_1 B_1| = (N + j)p,\ j = 1, 2,\ \text{for } f \neq 0. \tag{7}$$

The span length varies discontinuously between these two values when a roller is seated on the driver sprocket, and released from the driven sprocket, respectively.

In the special case where $f = 0$ the common inner tangent equals an integral number of pitches. Then inequality (6) has three solutions for the span length: $|A_1B_1| = (N + j)p,\ j = 0, 1, 2,$ for $f = 0$. However, these solutions exist simultaneously, and only in one instant, which is the specific configuration of the chain drive where $A_m A_1 B_m B_1$ align and coincide with points $z_1 z_2 z_3 z_4$, respectively, c.f. Fig. 2. Further rotation of the sprockets from this configuration will cause roller A_1 to be released from the driven sprocket, making A_n the new span endpoint. At the same time, roller S_N is seated on the driver sprocket, making B_m the new span endpoint. Thus, when $f = 0$, the release and seating of rollers happens simultaneously and the span length remains constant at

$$|A_1B_1| = (N + 1)p, \text{ for } f = 0. \tag{8}$$

With the above it has been determined how the chain span length generally shifts between two values, depending on the design parameters, i.e. the common inner tangent length $|T_oT_c|$, pitch length p, and pitch fraction f. How the length varies depends on the driver position, as will be determined in the following.

2.6. Governing vector equations

The vector equations presented here describe the position-, velocity- and acceleration relations for the kinematic model of the chain drive. For ease of notation, the vectors in the four-bar mechanism in Fig. 2 are written in polar form as $\mathbf{r}_n = r_n e^{i\theta_n}$, $n = 1, 2, 3, 4$, where r_n is the length of the vector,

θ_n the orientation measured positive counter clockwise from the X-axis, and the real and imaginary parts of the vector are parallel to the X- and Y-axis, respectively. The vectors in the four-bar mechanism are defined as

$$\mathbf{r}_1 = OC, \quad \mathbf{r}_2 = OA_1, \quad \mathbf{r}_3 = A_1B_1, \quad \mathbf{r}_4 = CB_1. \tag{9}$$

Sprocket centers do not move and therefore $\mathbf{r}_1$ is constant with time. From Fig. 2, the equation governing the position of link joint B_1 is

$$\mathbf{r}_2 + \mathbf{r}_3 = \mathbf{r}_1 + \mathbf{r}_4, \tag{10}$$

sometimes referred to as the closure- or four-bar equation. For $n = 2, 3, 4$, angular velocities and accelerations are introduced as $\omega_n = d\theta_n/dt$ and $\alpha_n = d\omega_n/dt$, respectively. Differentiating (10) with respect to time gives, since $dv_n/dt = 0$, the equation relating the velocities

$$i\omega_2\mathbf{r}_2 + i\omega_3\mathbf{r}_3 - i\omega_4\mathbf{r}_4 = \mathbf{0}. \tag{11}$$

Finally, differentiating (11) with respect to time gives the equation for the accelerations

$$(i\alpha_2 - \omega_2^2)\mathbf{r}_2 + (i\alpha_3 - \omega_3^2)\mathbf{r}_3 - (i\alpha_4 - \omega_4^2)\mathbf{r}_4 = \mathbf{0}. \tag{12}$$

The factor $i = \sqrt{-1}$ in the coefficient of a vector indicates a direction perpendicular to that vector, taken in clockwise direction. Equations (11) and (12) represent the velocity and acceleration vector diagrams, respectively [15].

As noted above, the span length shifts between two fixed values as rollers are seated and released from the sprockets. It is useful to express span length $r_3 = |A_1B_1|$ using the lower value of the span length, introduced here as L, and a step function h. The function h is unity when the span length assumes its upper value and zero otherwise. Vectors $\mathbf{r}_2$ and $\mathbf{r}_4$ have constant length

given by pitch circle radii and, $r_1 = |OC|$ can be determined from Fig. 2, thus

$$r_1 = \sqrt{x_c^2 + y_c^2},\ r_2 = R_o,\ r_3 = L + hp,\ r_4 = R_c,\ L \equiv (N+1)p \qquad (13)$$

A formal definition of the function $h = h(\theta_4)$ is given below using the seating and release configurations.

2.7. Introduction to position analysis

The configurations of the chain drive for which a roller is just *seated* on the driver sprocket and just *released* from the driven sprocket, are determined first. Between these two events, the span length remain constant. The angular position of the driven sprocket during the rotation of the driver sprocket is then determined in the subsequent *input-output* analysis.

Splitting (10) into real and imaginary parts gives the equations to be solved in order to determine the positions of the four-bar members:

$$r_2 \cos\theta_2 + r_3 \cos\theta_3 = r_1 \cos\theta_1 + r_4 \cos\theta_4, \qquad (14)$$

$$r_2 \sin\theta_2 + r_3 \sin\theta_3 = r_1 \sin\theta_1 + r_4 \sin\theta_4, \qquad (15)$$

which can also be derived directly from Fig. 2.

2.8. Configuration with roller just seated on driver sprocket

Figure 3(a) shows the four-bar mechanism OA_1B_1C in the exact configuration where roller B_1 seats on the driver sprocket C, making B_1 the new span endpoint. Figure 3(b) shows the configuration when a roller is just released from the driven sprocket. Variables related to the *seating* and *release* of a roller are subscripted s and r, respectively.

When determining the seating and release configurations, the span length in both cases attain its lower value. Therefore all lengths r_n are given by

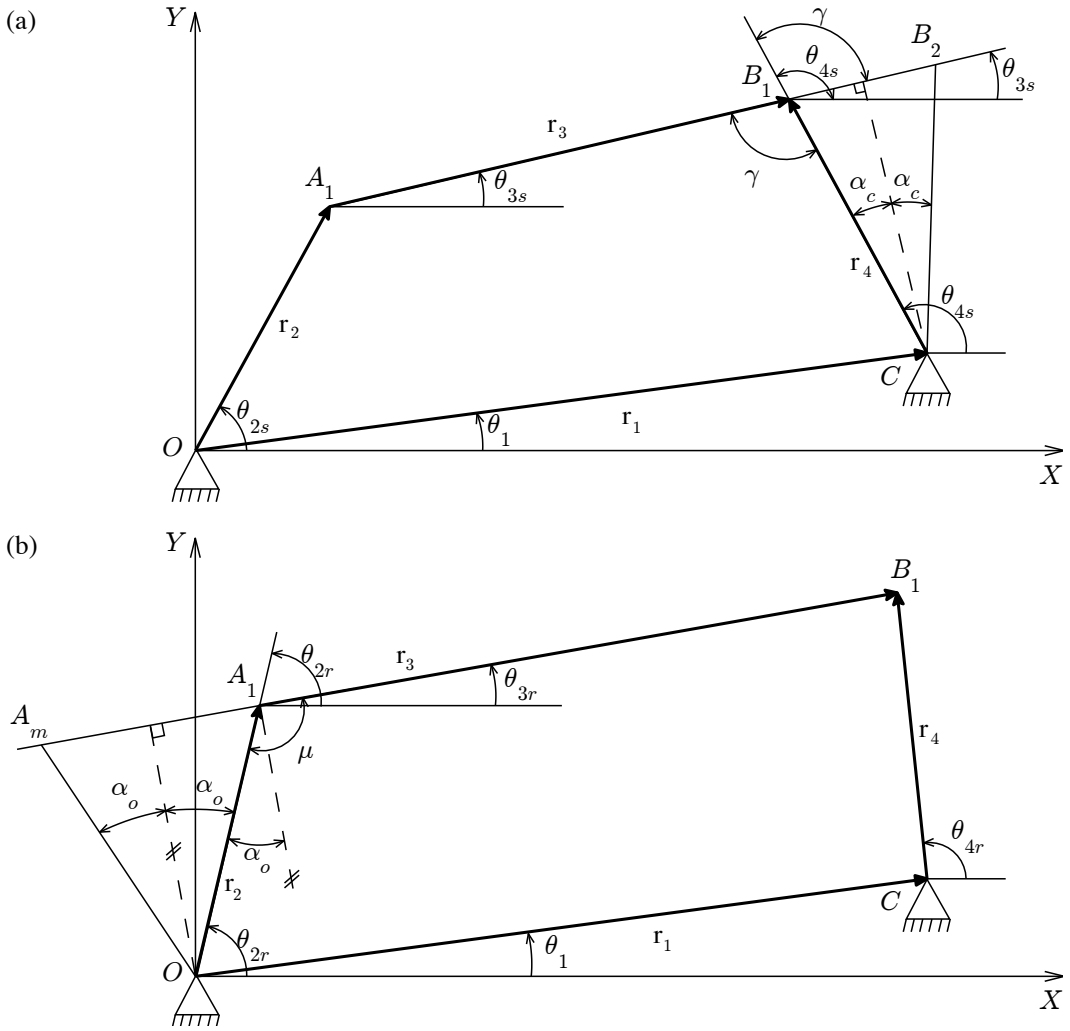

Figure 3: Equivalent four-bar mechanism when a roller (a) just seats on sprocket C, and (b) just releases from sprocket O.

(13) with $h = 0$. What then remains for the configuration to be determined are the angles θ_n, $n = 2, 3, 4$. At point B_1 in Fig. 3(a) it is seen that

$$\theta_{3s} = \theta_{4s} - \gamma, \tag{16}$$

where $\gamma = \pi/2 + \alpha_c$ is known, cf. (1). When θ_{3s} is expressed in terms of θ_{4s} and γ, there are two remaining unknowns to be determined from (14)-(15), namely θ_{2s} and θ_{4s}. To do this one can first square and add (14) and (15) to eliminate θ_{2s}. Expanding the squared terms, and also the trigonometric terms containing θ_{3s} using (16), e.g., $\sin\theta_{3s} = \sin\theta_{4s}\cos\gamma - \cos\theta_{4s}\sin\gamma$, gives

$$A_s\cos\theta_{4s} + B_s\sin\theta_{4s} + C_s = 0, \tag{17}$$

with coefficents

$$\begin{aligned} A_s &= 2r_1r_4\cos\theta_1 - 2r_1r_3(\cos\theta_1\cos\gamma - \sin\theta_1\sin\gamma), \\ B_s &= 2r_1r_4\sin\theta_1 - 2r_1r_3(\cos\theta_1\sin\gamma + \sin\theta_1\cos\gamma), \\ C_s &= r_1^2 + r_4^2 + r_3^2 - r_2^2 - 2r_4r_3\cos\gamma. \end{aligned} \tag{18}$$

Equations in the form of (17)-(18) will reappear in the following sections and it is therefore useful to present the solution in a general formulation. Consider the equation $A\cos\theta + B\sin\theta + C = 0$, from which θ is to be determined [16]. By introducing $\sin\theta = 2\tau/(1+\tau^2)$, $\cos\theta = (1-\tau^2)/(1+\tau^2)$, with $\tau = \tan(\theta/2)$, the equation can be written as a second order polynomial in τ, with solutions

$$\tau_{1,2} = \frac{-B \pm \sqrt{B^2 - C^2 + A^2}}{C - A}. \tag{19}$$

The two solutions for θ are then

$$\theta = 2\arctan(\tau_{1,2}). \tag{20}$$

Following this approach, the solution for θ_{4s} is given by (20) when the coefficients in (18) are substituted into (19). With θ_{4s} determined, the solution

for θ_{3s} is given by (16). Finally, θ_{2s} is determined by division of (15) with (14), leading to

$$\theta_{2s} = \arctan\Big(\frac{r_1 \sin\theta_1 + r_4 \sin\theta_{4s} - r_3 \sin\theta_{3s}}{r_1 \cos\theta_1 + r_4 \cos\theta_{4s} - r_3 \cos\theta_{3s}}\Big). \tag{21}$$

There are two solutions sets, corresponding to the two values of τ in (19). These correspond to configurations where the sprockets are connected by the span to rotate either in the same or opposite directions. The two solutions for θ_{2s} are of opposite sign, and the solution-set where $\theta_{2s} > 0$ is the one for which both sprockets rotate in the same direction.

2.9. Configuration with roller just released from the driven sprocket

Figure 3(b) shows the configuration where roller A_1 loses contact with the driven sprocket O and thereby enters the span, making A_n the new span endpoint. At this event θ_3 attains the value

$$\theta_{3r} = \mu + \theta_{2r} - \pi, \tag{22}$$

where $\mu = \pi/2 + \alpha_o$, the span length is at its lower value, and all lengths are given by (13) with $h = 0$. With θ_1 known and fixed, and θ_{3r} given by (22), θ_{2r} and θ_{4r} remain to be determined from (14)-(15). We do this by squaring and adding (14) and (15) to eliminate θ_{4r}, expanding the squared terms, substituting (22) for θ_{3r}, and expanding using trigonometric relations, e.g. $\cos\theta_{3r} = \cos\theta_{2r}\cos(\mu-\pi) - \sin\theta_{2r}\sin(\mu-\pi)$, and finds:

$$A_r \cos\theta_{2r} + B_r \sin\theta_{2r} + C_r = 0, \tag{23}$$

with coefficients,

$$\begin{aligned} A_r &= -2r_2r_1\cos\theta_1 - 2r_3r_1(\cos\theta_1\cos(\mu-\pi) + \sin\theta_1\sin(\mu-\pi)), \\ B_r &= -2r_2r_1\sin\theta_1 + 2r_3r_1(\cos\theta_1\sin(\mu-\pi) - \sin\theta_1\cos(\mu-\pi)), \\ C_r &= r_2^2 + r_3^2 + r_1^2 - r_4^2 + 2r_2r_3\cos(\mu-\pi). \end{aligned} \tag{24}$$

Substituting these coefficients into (19), the solution for θ_{2r} is given by (20). The angle θ_{3r} is then found from (22), and θ_{4r} from (14) and (15):

$$\theta_{4r} = \arctan\Big(\frac{r_2 \sin\theta_{2r} + r_3 \sin\theta_{3r} - r_1 \sin\theta_1}{r_2 \cos\theta_{2r} + r_3 \cos\theta_{3r} - r_1 \cos\theta_1}\Big). \tag{25}$$

As for θ_{2s} the solution for which $\theta_{4r} > 0$ correspond to the configuration where the sprockets rotate in the same direction.

2.10. Span length variation

Calculation of the driven sprocket angular position, velocity and acceleration using both exact and approximate methods can now take into account that the span length r_3 varies according to (13), with the function h defined as:

$$h = h(\theta_4) = \begin{cases} 0 \ \text{ for } \ \theta_{4s} \geq \theta_4 \geq \theta_{4r} \\ 1 \ \text{ for } \ \theta_{4r} \geq \theta_4 \geq \theta_{4s} + 2\alpha_c \end{cases} \tag{26}$$

where θ_4 is decreasing since the driver rotates in clockwise direction. The angles θ_{4s} and θ_{4r} are cumbersome to determine exactly, but simple and accurate approximations can be determined (sections 3.1 and 3.2).

2.11. Input-output angular position

In order to determine the motion of the driven sprocket it is required that the angular position, velocity and acceleration of the driver sprocket are known, i.e. that θ_4, ω_4 and α_4 are given functions of time.

Determining θ_2 as a function of θ_4 follows steps similar to the ones carried out in the above analysis for the seating and release configurations. By squaring and adding (14)-(15) to eliminate θ_3, expanding the squared terms and canceling out terms, the equation governing the output position θ_2 can be written in the form

$$A\cos\theta_2 + B\sin\theta_2 + C = 0, \tag{27}$$

where

$$A = -2r_1r_2\cos\theta_1 - 2r_4r_2\cos\theta_4,$$
$$B = -2r_1r_2\sin\theta_1 - 2r_4r_2\sin\theta_4, \tag{28}$$
$$C = r_1^2 + r_4^2 + r_2^2 - r_3^2 + 2r_1r_4(\cos\theta_1\cos\theta_4 + \sin\theta_1\sin\theta_4).$$

Using these coefficients the solution for θ_2 is given by (20), with $\tau_{1,2}$ determined from (19). For completeness, the solution for θ_3 is found from (14)-(15) to be

$$\theta_3 = \arctan\Big(\frac{r_1\sin\theta_1 + r_4\sin\theta_4 - r_2\sin\theta_2}{r_1\cos\theta_1 + r_4\cos\theta_4 - r_2\cos\theta_2}\Big). \tag{29}$$

There are agin two solution sets, corresponding to the two values of τ, where the two solutions for θ_2 are of opposite sign, and $\theta_2 > 0$ corresponds to the configuration where the sprockets rotate in the same direction. With the chain span assumed to be straight, motion of the chain drive is tooth-periodic, i.e. the position of the four-bar members repeat when the driver angle advances by $2\alpha_c$, the angle between two consecutive teeth. During one period a roller will have been released into, and another one removed, from the span.

2.12. Angular velocity

The angular velocity of the driven sprocket ω_2 generally varies with time, even if the driver sprocket rotates at constant angular velocity ω_4. This velocity variation can be determined from (11): We split (11) into real and imaginary parts, eliminate ω_3 from the real part using the imaginary part, expand the products of trigonometric functions, and find

$$\omega_2 = \omega_4\,\frac{r_4}{r_2}\,\frac{\sin(\theta_4 - \theta_3)}{\sin(\theta_2 - \theta_3)}. \tag{30}$$

When θ_3 is neglected in the above expression, the result agrees with existing approximate result [7]. Note here, that the driver velocity may vary, i.e.

$\omega_4 = \omega_4(t)$. The angular velocity ω_3 of the span can be determined following an approach similar as for the calculation of ω_2. This gives

$$\omega_3 = \omega_4 \frac{r_4}{r_3} \frac{\sin(\theta_2 - \theta_4)}{\sin(\theta_2 - \theta_3)}. \tag{31}$$

2.13. Angular acceleration

Accelerations of the driven sprocket are relevant for calculating forces transmitted to the chain drive components and attached machinery. The angular acceleration α_2 of the driven sprocket depends both on the driver sprocket angular acceleration α_4 and the sprocket angular velocities ω_2 and ω_4. From the real part of (12) we eliminate α_3 using the imaginary part, simplify using sum and products of trigonometric functions, and rewrite to get the result:

$$\alpha_2 = \alpha_4 \frac{\omega_2}{\omega_4} + \frac{\omega_4^2 r_4 \cos(\theta_4 - \theta_3) - \omega_2^2 r_2 \cos(\theta_2 - \theta_3) - \omega_3^2 r_3}{r_2 \sin(\theta_2 - \theta_3)}, \tag{32}$$

where the first term has been simplified using (30).

3. Approximate analysis

The exact results presented above are cumbersome to calculate and parameter dependency is hard to interpret. In the following, we seek simple approximate but accurate formulas for seating and release configurations, as well as angular position, velocity and acceleration of the driven sprocket.

In obtaining approximate solutions it is utilized that contact angles angles θ_2 and θ_4 make small variations about $\pi/2$. This is utilized by introducing shifted angles, marked by a tilde, which are bounded by the angle α, c.f. Fig. 2, thus:

$$\begin{aligned} \theta_2 &= \pi/2 + \varepsilon\tilde{\theta}_2, \quad \varepsilon\tilde{\theta}_2 \in [-\alpha_o, \alpha_o], \\ \theta_4 &= \pi/2 + \varepsilon\tilde{\theta}_4, \quad \varepsilon\tilde{\theta}_4 \in [-\alpha_c, \alpha_c], \end{aligned} \tag{33}$$

where ε here and below is used to bookmark small terms. It will also be used that span slope θ_3 is small, with a conservative estimate for an upper limit given by

$$\tan\theta_3 \le \frac{R_c - r_c + R_o - r_o}{x_c}, \tag{34}$$

obtained by recognizing that the lower and upper limit of a span endpoints are, respectively, the circumscribed circle radius r and the pitch circle radius R. The estimate gives $\theta_3 < 0.015$ rad and $\alpha \simeq 0.25$ in the case $n_o = n_c = 12$ and $N = 7$. Since most real chain drives have sprockets with more than 12 teeth, and spans more than 8 pitches long, these assumptions are indeed appropriate.

All parameters are nondimensionalized to reduce the number of variables and make the order of magnitude of the various terms easily comparable. All lengths are nondimensionalized by L, and nondimensional parameters are identified by over-bars,

$$\bar{R}_c = \frac{R_c}{L}, \quad \bar{R}_o = \frac{R_o}{L}, \quad \bar{r}_c = \frac{r_c}{L}, \quad \bar{r}_o = \frac{r_o}{L}, \quad \bar{p} = \frac{p}{L}, \tag{35}$$

from which it follows that $\bar{x}_c = 1 + f\bar{p}$ and $\bar{y}_c = \bar{r}_o - \bar{r}_c$.

3.1. Approximate seating configuration

Simple expressions for the configuration where a roller seats on the driver sprocket will be obtained from an approximate solution of (17). Looking at Fig. 2 it is expected that θ_{4s} is close to z_3, so we let

$$\theta_{4s} = \frac{\pi}{2} + \alpha_c + \varepsilon\hat{\theta}_{4s}, \tag{36}$$

where the shifted variable is marked with a hat, and $\varepsilon\hat{\theta}_{4s}$ is assumed to be small. We insert this into (17), expand the trigonometric functions and approximate them by the linear part of their Taylor expansions, e.g.

$\sin(\pi/2+\alpha_c+\varepsilon\hat{\theta}_{4s}) \approx 1-\alpha_c\varepsilon\hat{\theta}_{4s}$. With this the approximate solution for $\varepsilon\hat{\theta}_{4s}$ can be expressed as,

$$\varepsilon\hat{\theta}_{4s} \approx \frac{B_s + C_s - A_s\alpha_c}{A_s + B_s\alpha_c}. \tag{37}$$

We then simplify the coefficients A_s, B_s and C_s from (18) by inserting $\sin\theta_1 = y_c/|OC|$, $\cos\theta_1 = x_c/|OC|$, $\gamma = \pi/2 + \alpha_c$ and $r_1 = |OC|$. Next substitute $x_c = L + fp$, $y_c = r_o - r_c$, the lengths given by (13) with $h = 0$ and nondimensionalize using (35). Approximating the resulting coefficients is done by assuming the radius of the inscribed- and pitch circles to be identical. This follows from expressing the radii in (1) using only the first term of the Taylor expansions for the trigonometric functions, i.e. $\tan\alpha \approx \sin\alpha \approx \alpha$. Inserting these approximate expression for the radii as well as $\cos\alpha \approx 1$ gives

$$\begin{aligned}
\hat{A}_s &= \bar{p}\Big(\frac{\bar{p}}{\alpha_c} + 2\alpha_c\Big)f + \frac{\bar{p}}{\alpha_o} + 2\alpha_c, \\
\hat{B}_s &= -2\bar{p}f + \frac{\bar{p}^2}{2}\Big(\frac{1}{\alpha_c\alpha_o} - \frac{1}{\alpha_c^2}\Big) + \bar{p}\Big(\frac{\alpha_c}{\alpha_o} - 1\Big) - 2, \\
\hat{C}_s &= \bar{p}^2 f^2 + 2\bar{p}f + \frac{\bar{p}^2}{2}\Big(\frac{1}{\alpha_c^2} - \frac{1}{\alpha_c\alpha_o}\Big) + 2 + \bar{p}.
\end{aligned} \tag{38}$$

These approximations of the coefficients in (18) are marked with a hat and nondimensionalized by L^2. We then approximate $\varepsilon\hat{\theta}_{4s}$ by a polynomial in f,

$$\varepsilon\hat{\theta}_{4s} = a_0 + a_1 f + a_2 f^2. \tag{39}$$

We substitute this and (38) into (37) and determine the coefficients a_0, a_1 and a_2 by equating to zero like powers of f, which gives:

$$\begin{aligned}
a_0 &= \frac{-4\alpha_c^3\alpha_o}{\bar{p}\big((2\alpha_c^2+\bar{p})(\alpha_c-\alpha_o)+2\alpha_c\big)}, \\
a_1 &= \frac{-2(2\alpha_c^2+\bar{p})\alpha_c\alpha_o}{(2\alpha_c^2+\bar{p})(\alpha_c-\alpha_o)+2\alpha_c}, \\
a_2 &= \frac{2\bar{p}(\bar{p}\alpha_o+\alpha_c)\alpha_o}{(2\alpha_c^2+\bar{p})(\alpha_c-\alpha_o)+2\alpha_c}.
\end{aligned} \tag{40}$$

These coefficients are approximated by retaining only the dominating linear terms, giving $a_o \approx 0$, $a_1 \approx -\bar{p}\alpha_o$, and $a_2 \approx \bar{p}\alpha_o$. With these coefficients substitute (39) into (36) to get

$$\theta_{4s} \approx \frac{\pi}{2} + \alpha_c + \bar{p}\alpha_o f(f-1). \tag{41}$$

Using this, the angle of the span when a roller seats on the driver sprocket can be found from (16):

$$\theta_{3s} \approx \bar{p}\alpha_o f(f-1). \tag{42}$$

With real chain drives, both $\bar{p}$ and α_o are expected to be small.

A simple expression for θ_{2s} is determined using the approximate results for θ_{4s} and θ_{3s}: In (14)-(15), use that $\theta_{3s} \approx 0$ and insert $\cos\theta_3 \approx 1$ and $\sin\theta_3 \approx 0$. Shift to the variable $\varepsilon\tilde{\theta}_{2s}$ using (33) and insert the approximation $\theta_{4s} = \pi/2 + \alpha_c$, including only the first term of the Taylor expansions of the trigonometric functions. Divide the two resulting equations to eliminate r_2 and obtain an equation for $\varepsilon\tilde{\theta}_{2s}$. Nondimensionalize using (13) and (35) with $h = 0$, use $\bar{r}_c \approx \bar{R}_c$ and $\bar{R}_c \approx \bar{p}/(2\alpha_c)$, shift back the variable to obtain:

$$\theta_{2s} \approx \pi/2 + \alpha_o(1-2f). \tag{43}$$

3.2. Approximate release configuration

To determine simple approximate expressions for the release configuration one can proceed as for the seating configuration. In this case however, shift the variable in (23) by introducing $\theta_{2r} = \pi/2 - \alpha_c - \varepsilon\hat{\theta}_{2r}$. Following the same principal steps as in section 3.1 leads to

$$\theta_{2r} \approx \pi/2 - \alpha_o - \bar{p}\alpha_c f(f-1), \tag{44}$$

$$\theta_{3r} \approx -\bar{p}\alpha_c f(f-1), \tag{45}$$

$$\theta_{4r} \approx \pi/2 - \alpha_c(1-2f), \tag{46}$$

where (22) has been used to calculate θ_{3r}.

3.3. Phase between seating and release

The excitation of the chain drive coming from the polygonal effect depends on the phase between the seating and release of the rollers. Such a phase can be defined in various ways, but one choice would be

$$\psi = \theta_{4s} - \theta_{4r} \approx 2\alpha_c(1 - f), \tag{47}$$

where the approximation have been obtained using (46) and (41), in which the small term $\bar{p}\alpha_o$ have been assumed vanishing.

3.4. Approximate I/O-analysis

Expressing the driven sprocket angular position directly as a function of the driver position and span length requires an approximate solution of (27). Shifting to $\varepsilon\tilde{\theta}_2$ using (33) and approximating the trigonometric functions by the linear terms of their Taylor expansion gives

$$\varepsilon\tilde{\theta}_2 \approx \frac{B + C}{A}. \tag{48}$$

We then simplify the coefficients in (28) using $\sin\theta_1 = y_c/|OC|$, $\cos\theta_1 = x_c/|OC|$ and (13), substitute $x_c = L + fp$, $y_c = r_o - r_c$, the lengths given by (13) with $h \neq 0$ and nondimensionalize using (35). Shifting θ_2 and θ_4 according to (33) and approximating the resulting coefficients assuming $R_o \approx r_o$ and $R_c \approx r_c$, and using the first term of the Taylor expansions of the trigonometric functions gives

$$\begin{aligned}
\tilde{A} &= -2\bar{R}_o(1 + f\bar{p}) - 2\bar{R}_c\bar{R}_o\varepsilon\tilde{\theta}_4, \\
\tilde{B} &= -2\bar{R}_o^2, \\
\tilde{C} &= 2R_o^2 + (1 + f\bar{p})^2 - (1 + h\bar{p})^2 - 2R_c(1 + f\bar{p})\varepsilon\tilde{\theta}_4,
\end{aligned} \tag{49}$$

where the approximate coefficients (marked by a tilde) have been nondimensionalized by L^2. Inserting (49) into (48) and shifting back the angles with (33) gives

$$\theta_2 \approx \frac{\pi}{2} + \frac{\bar{p}(f-h)(1+\frac{1}{2}\bar{p}(f+h)) - \bar{R}_c(1+f\bar{p})(\theta_4-\pi/2)}{\bar{R}_o\bar{R}_c(\theta_4-\pi/2) - \bar{R}_o(1+f\bar{p})}, \tag{50}$$

where h varies discontinuously with θ_4 according to (26).

3.5. Velocity

The exact driven sprocket angular velocity given by (30) can be approximated. We do this by neglecting θ_3 in (30), shifting the angles θ_2 and θ_4 using (33), shifting to cosine functions and approximating them using the first two terms of their Taylor expansions. Then substituting the nondimensional radii gives

$$\omega_2 \approx \omega_4 \frac{\bar{R}_c(1-(\theta_4-\pi/2)^2)}{\bar{R}_o(1-(\theta_2-\pi/2)^2)}. \tag{51}$$

Since it is relevant for the approximation of the acceleration, the span velocity ω_3 given by (31) is also considered. The span angle θ_3 is again assumed vanishing and the trigonometric functions are approximated by the first term of their Taylor expansion, which gives

$$\omega_3 \approx \omega_4 \frac{\bar{R}_c}{1+h\bar{p}}\big(\theta_2-\theta_4\big). \tag{52}$$

For a conservative estimate of the order of magnitude of ω_3 assume $|\theta_2-\theta_4| \leq 0.5$ and $1/\bar{R}_c \approx 5$ to get $\omega_3 \approx \omega_4/10$. Thus, ω_3 is one order of magnitude smaller than ω_4 when spans are long compared to the sprocket size $\bar{R}_c$.

3.6. Acceleration

In the exact expression for the angular acceleration given by (32) we assume both θ_3 and ω_3 to be vanishing. Including only the first term of the

Taylor expansions of the trigonometric functions then gives an approximate expression for the angular acceleration of the driven sprocket:

$$\alpha_2 \approx \alpha_4 \frac{\omega_2}{\omega_4} + \omega_2^2(\theta_2 - \pi/2) - \omega_4^2 \frac{R_c}{R_o}(\theta_4 - \pi/2). \tag{53}$$

In the expressions for both angular velocity and acceleration the angles θ_2 and θ_4 jumps discontinuously every time a roller is released from and seated on the sprockets, respectively.

4. Example results

4.1. Test configurations

Three different chain drive configurations are used when presenting results of the kinematic analysis, with properties as listed in Table 1. The

	n_c	n_o	N
Coarse	6	9	4
Medium	12	18	11
Fine	21	63	34

Table 1: Configurations

pitch fraction f = {0, 0.5, 0.75} will be stated explicitly as results are presented. These values of f are chosen because minimum and maximum variation of the driven sprocket velocity occurs for f = 0 and f = 0.5, respectively, [4, 5, 8]. Most previous studies have utilized either f = 0 or f = 0.5, and f = 0.75 have been chosen to illustrate the general case. The coarse configuration was used in [4] and with a different span length also [8]. Experimental measurements of "angular displacement error" (the difference

between angular position and angular position for constant velocity), for the driven sprocket exists for the medium configuration [8]. The fine configuration was also analyzed [10]. A driver angular velocity of $\omega_4 = 100$ rpm ≈ 10 rad/s has been used when calculating driven sprocket angular velocity and acceleration.

4.2. Angular position, velocity and acceleration

Figure 4 shows the exact and approximate results for the coarse, medium and fine configurations in columns C, M and F, respectively. The horizontal axis shows the angular position of the driver normalized so that $[0, 1]$ correspond to one tooth period, starting when a roller seats on the driver. Exact results were obtained by discretizing θ_4 and calculating the configuration of the chain drive for each f. The approximate results for driven sprocket angular position, velocity and acceleration are calculated using Equations (50), (51) and (53), respectively, with seating and release positions obtained from the exact analysis.

Angular position of the driven sprocket is shown in Fig. 4(a-b-c). There is seen to be very good agreement between exact and approximate results, especially for the medium and fine configurations which are of most practical importance. The phase ψ between rollers being seated ($\triangledown$) and released ($\triangle$) is shown with a double arrow in Fig. 4(a). Since the horizontal axis shows one tooth period the phase between seating and release is simply $\psi = 1 - f$, as shown in Equation (47).

The velocity ratio between the driven and driver sprocket varies during one tooth period and is shown in Fig. 4(d-e-f). All three graphs shows excellent quantitative and qualitative agreement between exact and approximate results. For the coarse, medium and fine configurations the variation of the

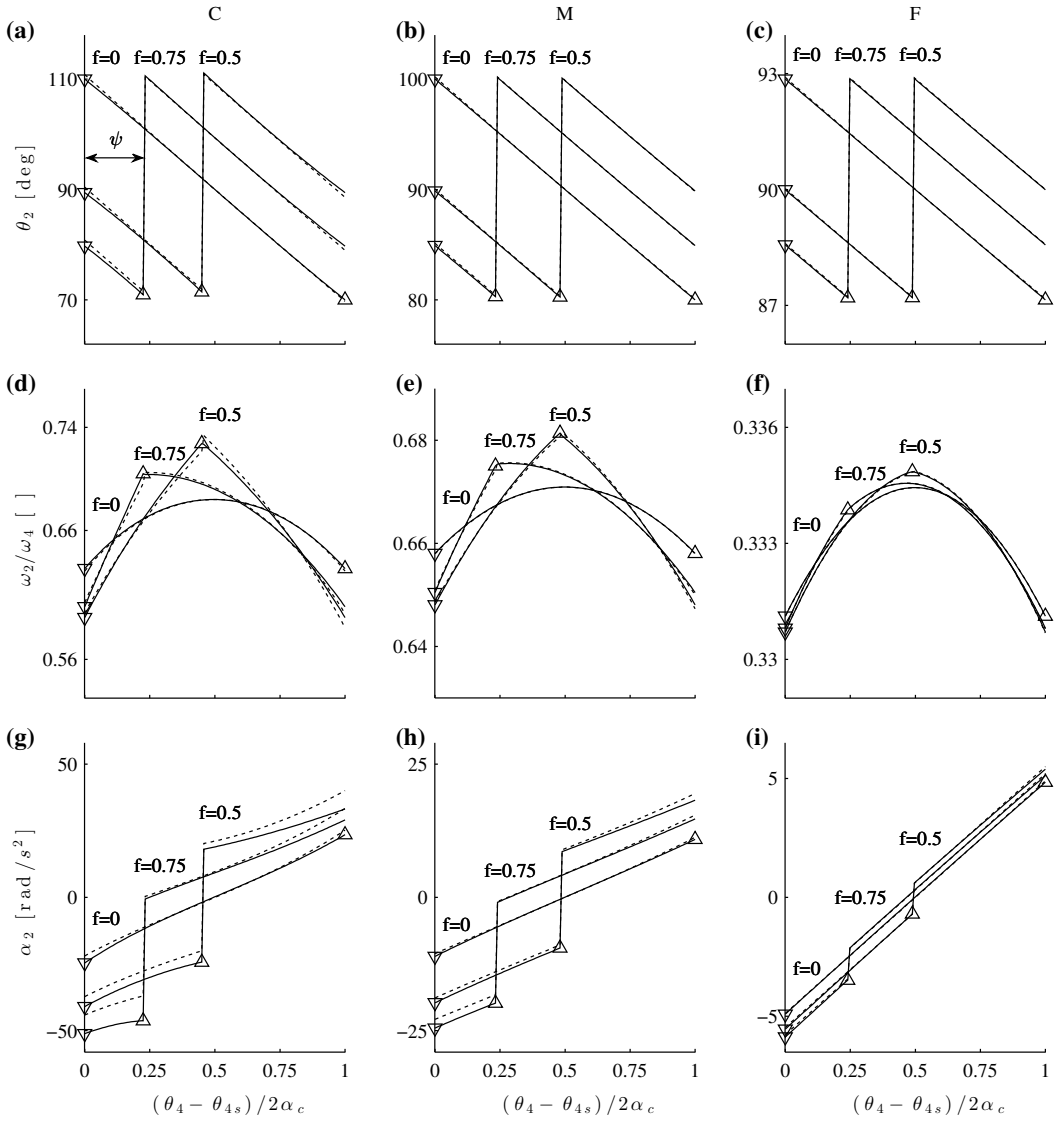

Figure 4: Exact (–) and approximate (- -) angular *position*, *velocity* and *acceleration* (first, second and third row, respectively) of the driven sprocket for one tooth period, for the *coarse*, *medium* and *fine* chain drive configuration (first, second and third column, respectively). A roller seating on the driver sprocket is indicated by $\triangledown$, and the release of a roller from the driven sprocket is indicated by $\triangle$.

velocity ratio is seen to be on the first, second and third decimal point, respectively. This demonstrates how the magnitude of the velocity variation decreases rapidly as the number of teeth is increased. The velocity variation was shown empirically to be inversely proportional to n_c^2, assuming $n_c < n_o$ [8]

In Fig. 4(d-e) one can see the how the velocity ratio variation decreases and smoothens when $f = 0$, compared to $f = 0.5$. However, as the tooth ratio n_c/n_o decreases (smaller than about 1/3), the effect of changing f becomes less significant. This can be seen in Fig. 4(f), where the curves for $f = 0$ and $f = 0.5$ are practically identical. Lastly, the velocity ratio will only be constant in the special case $n_c = n_o$ and $f = 0$, as can be seen from (51).

The driven sprocket angular acceleration in Figures 4(g-h-i) shows good quantitative and qualitative agreement between exact and approximate results. In the results presented here the driver rotates with constant angular velocity, and despite, that two sudden jumps in angular acceleration occurs when $f \neq 0$, whereas for $f = 0$ the acceleration only jumps at the end of the interval. The magnitude of a discontinuous jump occurring when a roller is seated or released decrease rapidly as the number of teeth is increased on the driver- and driven sprocket, respectively. Thus, the discontinuous jumps are most prominent for sprockets with few teeth.

For a driver rotating with constant angular velocity the time between seating and release will be given by $\psi = (1 - f)T$, where T is the tooth period. Seating and release will only happen simultaneously if $f = 0$. Only in the special case where $f = 0$ and $n_c = n_o$ will the angular velocity and acceleration of the driven- and driver sprockets be equal.

In studies of string and roller chain drive dynamics it is often assumed that polygonal action leads to a parametric excitation described by time

harmonic variation of span tension or velocity [17]. However, the driven sprocket acceleration in Fig. 4(g-h-i) is shown to be non-smooth and this could be taken into consideration when modeling chain drive loads.

4.3. Seating and release angles

Figure 5 shows the exact angular seating- and release positions for the coarse configuration, together with the closed form approximations. The phase ψ between seating and release given by (47) is indicated with an arrow in Fig. 5(b). In Fig. 5(a) it is seen that the approximation given

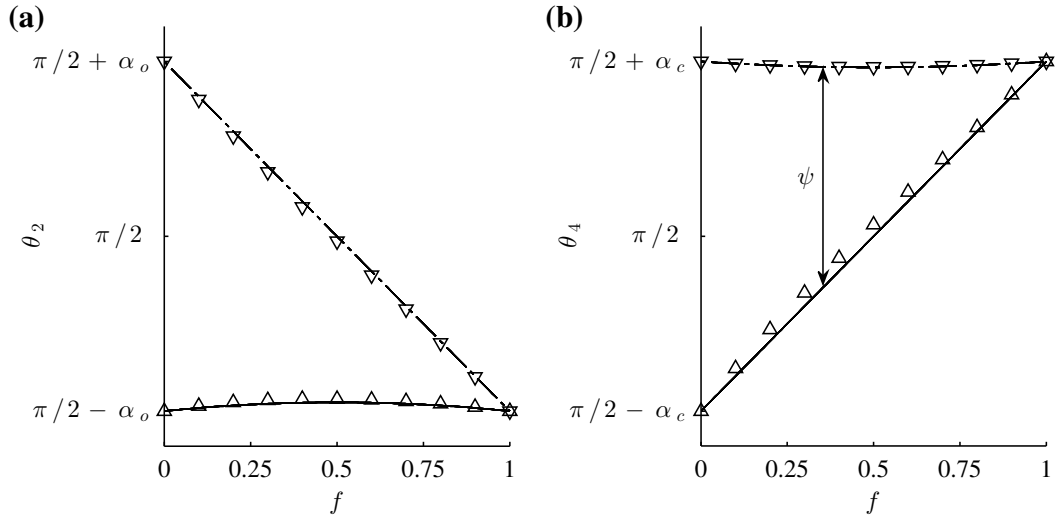

Figure 5: Exact seating $\triangledown$ and release angles $\triangle$ as a function of the pitch fraction f for the coarse configuration. Approximations for seating (–) and release (– · –) are shown for (a) the driven sprocket and (b) the driver sprocket.

by (44) capture correctly that θ_{2r} is almost constant. There is only slight movement toward the horizontal position $\pi/2$ for f around 0.5. This is due to the rise of the span endpoint at the opposite sprocket, e.g. $\theta_{4r} = \pi/2$ for $f = 0.5$. Similarly for θ_{4s} in Fig. 5(b) as predicted by (41).

The driven sprocket angular seating position θ_{2s} is proportional to f and moves between the outer limits given by $z_{1,2} = \pi/2 \pm \alpha_o$ in Fig. 2, as predicted by the approximation in (43). Similarly, the driver sprocket angular position θ_{4r} given by (46) moves between limits $z_{3,4} = \pi/2 \pm \alpha_c$, in agreement with the exact results.

Impact has not been the object of investigation of this work, but it has been shown that the seating position θ_{4s} is close to point z_3 in Fig. 2, as is often assumed in studies of impact and noise [18, 19]. In Fig. 1 the relative velocity between a seating roller and the driver sprocket $\mathbf{u}_1 - \mathbf{u}_2$, is therefore practically independent of f. Assuming the span is a straight line, the main design factor affecting the relative velocity, besides the angular velocity of the driver, is therefore the number of teeth on the driver sprocket (the pitch angle).

Results are not presented here for the medium and fine configurations, but when calculated the curves for θ_{2r} and θ_{4s} straighten and approximations improve slightly as the number of teeth increase.

4.4. Approximation error

The error is calculated between the approximate and exact results for the driven sprocket angular position, velocity and acceleration. The error is calculated as the normalized root mean square deviation:

$$\epsilon_x = \sqrt{\frac{1}{n}\sum_{i=1}^{n}(\tilde{x}_i - x_i)^2} \Big/ \sqrt{\frac{1}{n}\sum_{i=1}^{n} x_i^2}, \tag{54}$$

where $\tilde{x}_i$ represent the approximation and x_i the exact value of sample i. Figure 6 shows approximation errors for angular position θ_2, velocity ω_2 and acceleration α_2.

The errors in Fig. 6 were calculated using a tooth ratio of unity. Since the trigonometric functions were approximated by Fourier expansions the largest errors are to be expected for the chain drive configurations with the lowest number of teeth, hence $n = n_o = n_c$. Obtaining the approximate results made use of the span slope being small, so it is expected that the approximations will improve as span length is increased. The errors presented are the maximum errors obtained for $n = 10..40$, when the span length and pitch fraction are varied as $N = 10 \ldots 40$ and $f = 0.1 \ldots 0.9$. Error calculations for different tooth ratios are not presented here but show both quantitative and qualitative similarity to Fig. 6.

Approximation errors for the driven sprocket angular position $\tilde{\theta}_2$ in Fig. 6(a) are less than 0.5 %, and decreasing when the chain span becomes longer and the number of teeth on the sprockets increase, as expected. Similarly for the approximation of the driven sprocket angular velocity $\tilde{\omega}_2$, where errors are less than 0.1 %. The approximation errors for the driven sprocket angular acceleration $\tilde{\alpha}_2$ are less than 10 % for $n, N > 12$ and reduce to a level of about 5 %.

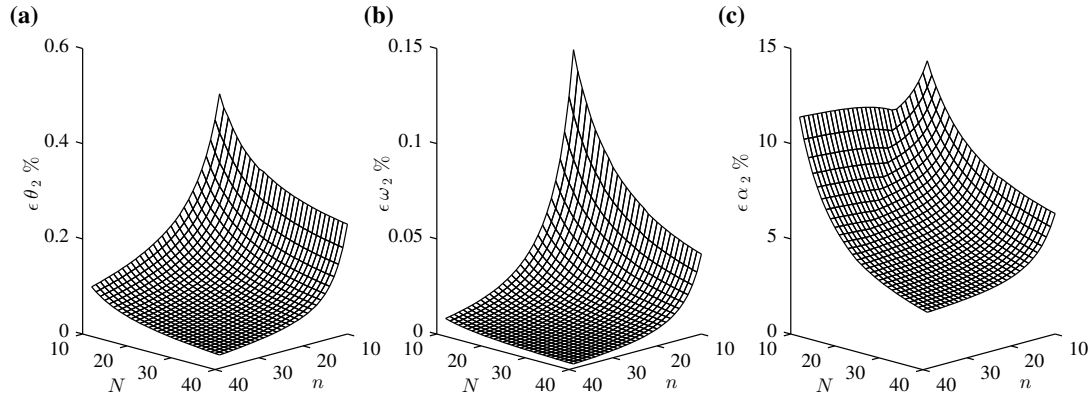

Figure 6: Error between exact and approximate angular (a) position, (b) velocity, (c) acceleration of the driven sprocket.

5. Comparison with multibody simulation

The exact kinematic prediction of the chain span motion is compared with results from multibody simulation of a roller chain drive. multibody simulations are carried out using the program described in [11, 12]. In the multibody model the mass of the chain is lumped at the roller center locations, and springs and viscous dampers with constant stiffness- and damping coefficients model the chain links. Clearances between pin and bushings are neglected as well as rotational inertia of the rollers about their center of gravity. Tooth geometry is Type II per ASA B29.1-1950.

Simulation is carried out for the medium configuration in Table 1 with a chain consisting of 40 links, $p = 0.0254$ m, and for the shaft center distance $f = 0.43$ is chosen to ensure a positive pretension of both the upper and lower spans connecting the two sprockets. Angular velocity of the driver sprocket is 10 rpm and constant. The main parameters for the simulation are chain link stiffness 0.221 GN/m, link mass 0.066 kg and link damping 0.01 Ns/m. The radius of the driven sprocket is 0.073 m, mass is 1.68 kg, rotational inertia 0.046 kg m^2 and the rotational damping coefficient is 0.1 Nms/rad.

Figure 7 shows the curves traced out by the roller centers for the upper span, as the driver sprocket rotates in clockwise direction. Assuming the span moves as a rigid string supported by moving endpoints, the kinematic analysis gives the presented wavy path of the chain span roller centers. The shape of the wavy path depends on the phase between seating and release, i.e. f. In Figure 7 the simulation results shows the chain span endpoints moves as predicted by the kinematic analysis. In the simulation results however, there are transverse vibration of the chain span at the first mode,

but the averaged motion of the span is in excellent agreement with the kinematic prediction.

All together, the comparison demonstrate how the kinematic analysis can be useful for predicting and understanding e.g. simulation and experimental results, even when these include dynamic effects. The results in Figure 7 are comparable to an idealized sketch presented for $f = 0$ in a discussion of the path of the chain span in chapter 13 [6], and existing simulation results [13].

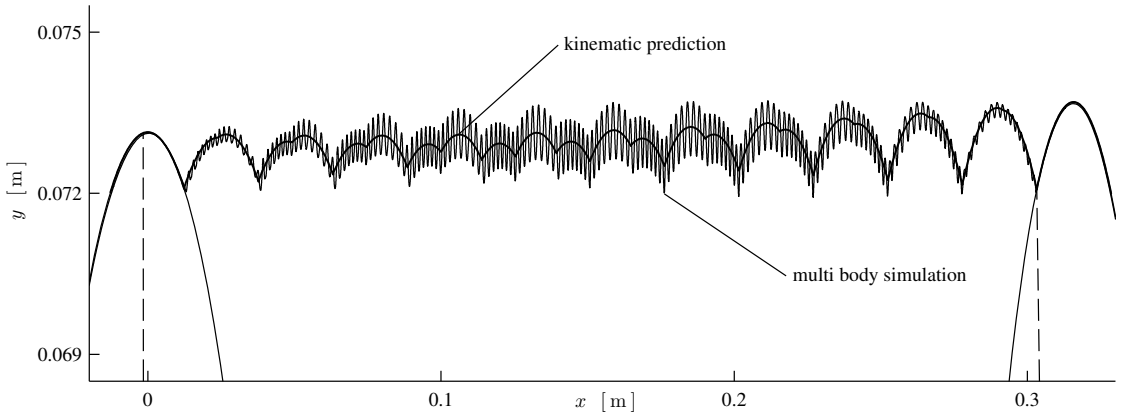

Figure 7: Phase plane for the chain roller centers as predicted by kinematic analysis, and as obtained from multibody simulation. The broken lines −− are drawn from the sprocet centers to the roller centers which are the span endpoints at the instant where a roller seats on the driver sprocket.

Comparison between the kinematic predictions for the angular motion of driven sprocket and multibody simulation results are not presented. In the analysis of multibody simulation results it becomes apparant that the response of the driven sprocket is sensitive to the parameters relating to the dynamics of the sprocket, i.e. inertia, rotational damping and flexibility coming from the connected chain spans. The driven sprocket angular vibration response generally shows resemblence to an impulse respons, where

the discontinous excitation results in a smoothend transient respons. An analytical study which includes the coupled dynamics of transverse chain vibration and angular vibration of the driven sprocket is given by Fuglede and Thomsen [20].

6. Conclusion

A chain drive is modeled as a four-bar mechanism, and equations governing position, velocity and acceleration are presented and solved exactly and approximately. The instantaneous span length is determined, and its discontinuous variation with time is given a simple formulation. It is shown how the chain drive geometry is conveniently nondimensionalized. The seating and release configurations are determined, and simple approximate expressions including only the dominant design parameters are derived.

The driven sprocket angular position, velocity and acceleration is determined, and results presented for a coarse, medium and fine chain drive configurations show very good agreement between exact and approximate results. Errors between exact and approximate results were shown to be small for all practical chain drives. The closed form approximate results provide insight into the effects of changing design parameters, and allows for a convenient estimation of the chain drive kinematics.

An approximate expression for the phase between chain roller seating and release is determined, giving insight into the time intervals between the discontinuous accelerations of the driven sprocket.

Comparison is made between multibody simulation results and analytical kinematic predictions, and there is seen to be very good agreement. It is demonstrated how the kinematic analysis can be used for interpreting e.g.

simulation results.

This study treats the case where the span connects the sprockets such that they rotate in the same direction. However, it is expected that the case where the span connects the two sprockets as the inner tangent could be treated following a similar approach.

References

[1] K. W. Wang and S. P. Liu. On the noise and vibration of chain drive systems. *The Shock and Vibration Digest*, 23(4):8–13, 1991.

[2] J. N. Fawcett. Chain and belt drives, a review. *The Shock and Vibration Digest*, 13(5):5–12, 1981.

[3] Li-Qun Chen. Analysis and control of transverse vibrations of axially moving strings. *Applied Mechanics Review*, 58(2):91–116, 2005.

[4] G. M. Bartlett. Roller chain drives in theory and practice. *Product Engineering*, 2(4):253–255, 1931.

[5] R. A. Morrison. Polygonal action in chain drives. *Machine Design*, 24 (9):155–159, 1952.

[6] R. C. Binder. *Mechanics of the Roller Chain Drive: Based on Mathematical Studies by RC Binder*. Prentice-Hall, 1956.

[7] S. Mahalingam. Polygonal action in chain drives. *Journal of The Franklin Institute*, 265(1):23–28, 1958.

[8] G. Bouillon and G. V. Tordion. On polygonal action in roller chain drives. *Journal of Engineering for Industry*, 87(2):243–250, 1965.

[9] S. R. Turnbull and J. N. Fawcett. An approximate kinematic analysis of the roller chain drive. *Proceedings of the Fourth World Congress on Theory of Machines and Mechanisms*, pages 907–911, 1975.

[10] C. K. Chen and F. Freudenstein. Toward a more exact kinematics of roller chain drives. *Journal of Mechanisms Transmissions and Automation in Design-Transactions of the ASME*, 110(3):269–275, 1988.

[11] S. L. Pedersen, J. M. Hansen, and J. A. C. Ambrosio. A roller chain drive model including contact with guide-bars. *Multibody System Dynamics*, 12(3):285–301, 2004.

[12] S. L. Pedersen. Model of contact between rollers and sprockets in chain-drive systems. *Archive of Applied Mechanics*, 74(7):489–508, 2005.

[13] C. M. Pereira, J. A. Ambrosio, and A. L. Ramalho. A methodology for the generation of planar models for multibody chain drives. *Multibody System Dynamics*, 24(3):303–324, 2010.

[14] J. Ambrósio, C. Pereira, and A. Ramalho. Roller chain drives multibody models using a generalized revolute clearance joint formulation. In *Proceedings of the 23rd International Congress of Theoretical and Applied Mechanics*, 2012.

[15] M. R. Smith and L. Maunder. Inertia forces in four-bar linkage. *Journal of Mechanical Engineering Science*, 9(3):218–225, 1967.

[16] K.J. Waldron and G.L. Kinzel. *Kinematics, dynamics, and design of machinery.* Wiley, 1999.

[17] S. T. Ariaratnam and S. F. Asokanthan. Dynamic stability of chain

drives. *Journal of Mechanisms Transmissions and Automation in Design - Transactions of the ASME*, 109(3):412–418, 1987.

[18] W. Choi and G. E. Johnson. Vibration of roller chain drives at low, medium and high operating speeds. *American Society of Mechanical Engineers, Design Engineering Division (Publication) DE*, 63:29–40, 1993.

[19] H. Zheng, Y. Y. Wang, G. R. Liu, K. Y. Lam, K. P. Quek, T. Ito, and Y. Noguchi. Efficient modelling and prediction of meshing noise from chain drives. *Journal of Sound and Vibration*, 245(1):133–150, 2001.

[20] N. Fuglede and J. J. Thomsen. Kinematic and dynamic modeling and approximate analysis of a roller chain drives. *Submitted for journal publication*, 2014.

P2 Publication 2

The following manuscript [P2] has been submitted for journal publication. It concerns both kinematic and dynamic mathematical modeling of roller chain drive systems. It reports also on novel analytical results on both the kinematic properties of roller chain drives system and the coupled dynamics of chain spans and sprockets.

Kinematic and dynamic modeling and approximate analysis of a roller chain drive

Niels Fuglede, Jon Juel Thomsen[1,]

Department of Mechanical Engineering, Technical University of Denmark, Building 404, DK-2800, Lyngby, Denmark

Abstract

A simple roller chain drive consisting of two sprockets connected by tight chain spans is investigated. First, a kinematic model is presented which include both spans and sprockets. An approach for calculating the chain wrapping length is presented, which also allows for the exact calculation of sprocket center positions for a given chain length. The kinematic analysis demonstrate that the total length of the chain wrapped around the sprockets generally varies during one tooth period. Analytical predictions for the wrapping length are compared to multibody simulation results and shows very good agreement. It is thereby demonstrated that chain drives with tight chain spans must include compliant components to function. Second, a dynamic model is presented which includes the two spans and the driven sprocket. Assuming the presence of a stationary operating state, the presented dynamic model allows for analytical studies of the coupled motion of the chain spans and driven sprocket. Parametric excitation of the spans come from sprocket angular displacements, and the driven sprocket acts as a boundary which can be compliant in the axial direction. External transverse

[1]Corresponding author: jjt@mek.dtu.dk

excitation of the spans comes from polygonal action, and is treated through kinematic forcing at the moving string boundaries. Perturbation analysis of the model is carried out using the method of multiple scales. Results show a multitude of internal and external resonance conditions, and some examples are presented of both decoupled and coupled motion. Together, the kinematic and dynamic model are aimed toward providing a framework for conducting and understanding both numerical, and experimental investigations of roller chain drive dynamics.
Keywords: Roller chain drive, axially moving string, moving boundaries, polygonal action, kinematic analysis, multibody simulation

1. Introduction

Roller chain drives are applied for power transmission in many mechanical systems due to a high energy efficiency, large power capacities, timing capabilities, flexibility in choosing shaft center distance, and ease of installation and maintenance. However, roller chain drives are also challenging due to the presence of undesired noise and vibration, and is therefore subject to ongoing studies [1].

Kinematic studies of roller chain drives are carried out by modeling the sprockets as polygons [2]. The angular motion of two sprockets connected by a chain span is considered to happen through a series of four-bar mechanisms [3]. Because a chain wrapped around a sprocket forms a polygon rather than a circle, several less desirable effects are introduced. These are referred to as polygonal action and include; impact when a roller seats on a sprocket, non-constant torque transmission and velocity ratio between sprockets. The monograph [4] introduces subjects such as tooth geometry, load distribution, friction, wear, and driven sprocket velocity variations. Studies demonstrate

how the center distance can be chosen to minimize velocity variations of the driven sprocket [5]. A procedure for calculating the driven sprocket motion for a general chain drive was developed, and examples demonstrated how design parameters influence the polygonal action [6]. An exact and approximate kinematic analysis of the chain drive modeled as a four-bar mechanism was given [7]. The presentation included the derivation of the driven sprocket angular- position, velocity, and acceleration. Seating and release configurations were also determined, and the analytical results were illustrated using three chain drive configurations.

It is common to the above kinematic studies that the analysis only considers the tight span transferring the torque between two sprockets. In this work, the slack span is also considered, which is relevant for practical roller chain drives where the sprockets are positioned to keep all the chain spans in tension during operation, as in e.g. low speed marine propulsion engines. The kinematic analysis of a roller chain drive presented here is for two sprockets with arbitrary number of teeth and center distance. Our results demonstrate that when sprockets are modeled as polygons, and the chain spans are pretensioned to form straight lines, the total wrapping length of the chain varies periodically with the tooth frequency. This leads to a prediction of a tooth-periodic variation of the axial tension in the chain spans. The analytical kinematic prediction is compared to multibody simulation results and shows very good agreement. Simulation results are obtained using a simulation program which include dynamic effects, flexible contact, and the exact geometry of the sprocket teeth [8, 9]. These results demonstrate that a real roller chain drive must include compliant components for a tensioned chain to wrap around rotating sprockets, as the sprockets are effectively eccentric. The kinematic results allow for the exact prediction of

the shaft center distance, for which a chain with a given number of links wraps tightly around two sprockets.

Under the assumption that the chain span motion decouples from the dynamics of sprockets and attached machinery, the studies of roller chain drive dynamics is found to border the analysis of axially moving strings, which belongs to the class of gyroscopic systems. For a decoupled axially moving string, equations governing non-linear oscillations were derived using Hamiltons principle, and the influence of transport velocity and nonlinearity on the natural frequencies was analyzed [10], along with examples of the modal distributions [11]. Based on the modal analysis of discrete gyroscopic systems [12, 13], the result of exact modal analysis of axially moving continua was presented [14], as well as asymptotic studies of the forced and free response around super- and sub-critical axial velocity [15]. From these studies, the characteristics of axially moving strings are shown to be transport-velocity dependent natural frequencies, the presence of a critical speed, and complex-valued traveling string eigenfunctions utilized by casting the system in a first order form. The complex eigenfunctions are shown to be a superior orthogonal discretization basis, compared to real-valued stationary string eigenfunctions, when predicting parametric instability [16]. For an extensive review of the research on axially moving materials until 2004 we refer to [17].

In this study we analyze the effect of the span being supported by moving boundaries with prescribed endpoint displacements, and demonstrate that a span with a first order variable length introduces a second order effect.

Central to many studies of string dynamics is the presence of parametric excitation from prescribed tension fluctuations, which may lead to parametric instability. Most often these excitations are single frequency har-

monic excitations, but the response have also been analyzed for multiple frequency excitations [18]. Tension variation can have many sources, e.g. camshaft excitation, eccentricity of belt pulleys or variable transport velocity, cf. the review [19]. The study of sprocket and chain span motion introduced in [20, 21] and subsequent studies [22] are based on the assumption that the driven sprocket angular velocity varies time-harmonically at the tooth frequency, due to the excitation coming from the variable velocity ratio between driver and driven sprocket. Comprehensive models are derived for belt drives [23] and engine timing chain drives [24], with non-linear transverse and longitudinal motion of the chain spans coupled to the displacements of pulleys/sprockets with flexible supports. In the case where chain span decouples from the motion of the driven sprocket, the chain span stability was analyzed [24].

Here we present a model which takes into account the coupled motion of span and sprocket angular displacements, i.e. motion of the chain span when it is connected to a sprocket which is compliant, and the sprocket motion is not assumed to be given. We demonstrate how the coupled non-linear system of the spans and driven sprocket can be analyzed analytically using perturbation methods, and predictions are provided for the amplitude frequency response.

Meshing between the chain span and sprockets introduce problems with noise and wear in real chain drives. It is therefore of interest to study the chain span subjected to transverse excitation at, or near, the span boundaries. One approach is to analyze the impulse created when a roller seats on a sprocket, and assume the impulse to be independent of the chain span dynamic response [25, 26]. Noise and vibration problems has also motivated several experimental studies [27, 28]. Including the chain vibrations

in the estimate of the impulse function improves the analytical predictions, and gives better agreement with experimental results [29, 30]. Predictions of meshing noise that compare well with measurements has also been presented [31, 32].

For this study we consider an impulsive excitation acting at the tooth frequency at both span ends, in order to model the kinematic transverse excitation coming from polygonal action. The impulses are assumed to be independent of the span dynamics, and are derived only from the chain geometry and operating speed. The time between the impulses acting at either span end can be determined from the kinematic configuration of the chain drive [7]. This type of excitation is of specific interest to designers of chain drives operating in low-speed marine engines. Our analysis demonstrate how the impulse loading leads to multifrequency excitation, and identifies the operating conditions where the transverse excitation from meshing can be resonant to other excitation sources.

The structure of the paper is as follows: First we present a kinematic model, carry out the analysis for the total wrapping length, and demonstrate the analytical results by some examples. Analytical predictions for the kinematic analysis are then compared to multibody simulation results. Secondly, we derive the governing equations for the coupled chain-sprocket dynamic model, perform an approximate analysis, and present three examples to illustrate the type of results that can be achieved.

2. Kinematic modeling and analysis

First we introduce the model assumptions followed by the definition of the coordinate systems and main kinematic parameters. When defining the

kinematic model we also introduce the seating and release configurations for both spans, as well as the driven sprocket angular position determined as a function of the driver angular position. These kinematic relations provide the initial steps required for the determination of the lower span length, and are based on the analysis [7]. With the seating, release and driven sprocket motion determined, a procedure for determining the lower span length is given. With the lower span length determined, the (approximate) total wrapping length can be calculated, which is the main object of the kinematic analysis.

2.1. Kinematic model assumptions

The kinematic model neglects all dynamic effects. It is assumed that the chain spans are tensioned into straight lines, sprockets are rigid and match the chain such that the sprocket pitch is equal to the chain pitch, and rollers are seated at the center of the seating curves. There are no mechanical clearances, and the system is frictionless.

By modeling the two sprockets and the upper span a as a four-bar mechanism, the length l_b of the lower span b is determined as a function of the driver angle θ. As will be shown, this length is not constant, but varies during each tooth period. The length l_b is calculated by assuming that span b is the only member which can deform, i.e. for the upper span a, as well as the parts of the chain seated on the sprockets, the distance between the rollers equals the chain pitch. It is necessary to make this assumption in order to obtain results for the total wrapping length of a chain using the existing methods, i.e. the chain drive modeled as a four-bar mechanism. In a real chain drive, the deformation would be distributed on all the chain drive components, but taking this into account would require a different

approach, which is not readily apparent.

The method is exact when the total wrapping length equals an integer number of chain links, since in this case, the chain is not deformed. The analysis thereby provides a method for calculating the exact sprocket center positions for a given chain length. This is of practical relevance, since real chains has a high axial stiffness, and the axial span tension is therefore sensitive to the sprocket center positions. With this analysis we identify and *approximately* quantify the property of roller chain drives having a variable wrapping length. This effect has been observed for real chains, but has not previously been treated theoretically.

2.2. Kinematic model

Figure 1 shows the kinematic model of a chain drive consisting of a driven sprocket O connected by the chain to make both sprockets rotate in the clockwise direction, as prescribed by the driver sprocket C. The sprockets are positioned such that the two spans are both in tension and form straight lines. The angular position of the sprockets to the rollers constituting the current span endpoint are given by θ_a and ϕ_a, for the the driver and driven sprockets, respectively; similarly for the lower span, where the span endpoint positions are θ_b and ϕ_b. Subscripts o, c and a, b are used throughout the kinematic analysis to relate variables specific to sprockets O, C and spans a, b respectively, e.g. α_o and θ_b.

As the sprockets rotate, chain links will recurrently be *released* from a sprocket to enter the connecting span and *seated* on a sprocket, thereby being removed from the connecting span; these seat and release configurations are referred to with subscripts r and s, respectively.

A sprocket with n teeth is modeled as a pitch polygon with n sides

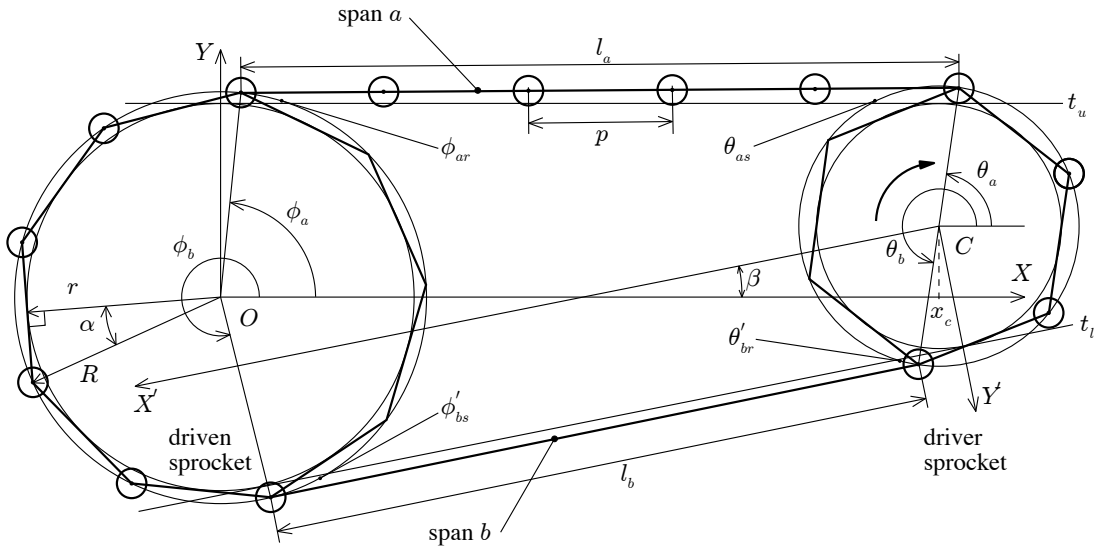

Figure 1: Kinematic model of a chain drive consisting of two sprockets connected by tight spans a and b of instantaneous length l_a and l_b, respectively. The driver sprocket C rotates counter-clockwise.

of length p, where p is the chain pitch length. A chain roller seated on a sprocket is positioned such that the center of the sprocket seating curve and the roller center traces out the *pitch circle* with radius $R = p/(2\sin\alpha)$, circumscribing the pitch polygon. The circle inscribed of the pitch polygon has radius $r = p/(2\tan\alpha)$ and the pitch angle is given by $\alpha = \pi/n$, making the angle between two seated rollers 2α.

The origin of the inertial X, Y coordinate system coincides with the center of sprocket O. It is orientated such that the X-axis is parallel with the upper tangent t_u which is common to the two inscribed circles. The center position of sprocket C is (x_c, y_c), where

$$x_c = (N + 1 + f)p, \quad y_c = r_o - r_c. \tag{1}$$

By this definition of x_c, two parameters have been introduced: The number of chain links $N \in \mathbb{N}$ and the pitch fraction $f \in [0, 1[$. For the lower span,

the X', Y' coordinate system has its origin coinciding with the center of sprocket C, and is orientated such that the X'-axis is parallel to the lower tangent t_l.

For real chain drives, a chain wrapped around two sprockets must contain an inter number of chain pitches. Therefore the pitch fraction f will not be a parameter than can be chosen independently when the spans form straight lines, since the shaft center distance OC must be adjusted to obtain the desired pretension of the chain.

It is necessary to determine the seating and release configurations, as these are required for calculating the chain wrapping length. Seating and release configurations for the upper and lower span can be determined according to [7]: By considering the two sprockets to be connected by one span only, the seating and release configurations are determined from the kinematic analysis of the resulting four-bar mechanism. Following [7], the upper span seating and release configurations are: (θ_{as}, ϕ_{as}) and (θ_{ar}, ϕ_{ar}), and similarly for the lower span, $(\theta'_{bs}, \phi'_{bs})$ and $(\theta'_{br}, \phi'_{br})$. These seating and release configurations are determined in the X, Y and X', Y' coordinate systems, respectively.

It is also necessary to determine the driven sprocket angular position and the span length l_a as a function of the driver angular position, as it is required for calculating the chain wrapping length. The kinematic motion of the four-bar mechanism with span a can determined according to [7]: By considering the two sprockets to be connected by span a only, the angular position of the driven sprocket can be determined as a function of the angular position of the driver sprocket, i.e. $\phi = \phi(\theta)$. Also, the span length $l_a = l_a(\theta)$ can be determined according to [7]. The span length l_a varies discontinuously with the driver angular position, because links enter and leave the span. Here,

and in the following, a variable marked with prime denotes angles given in the X', Y' coordinate system. In the following, a procedure for determining the lower span length l_b will be given.

2.3. Calculating the lower span length

It is convenient to consider one period of the angular motion to start from θ_{as}, the configuration where a roller from the span a seats on the driver sprocket. The upper span length varies according to

$$l_a = (N + 1 + h)p, \quad h = \begin{cases} 0 & \text{for } \theta_{as} \geq \theta_a \geq \theta_{ar}, \\ 1 & \text{for } \theta_{ar} \geq \theta_a \geq \theta_{as} + 2\alpha_c. \end{cases} \tag{2}$$

Note that θ and ϕ decrease as the sprockets rotates in clockwise direction. The angle between the two coordinate systems is $\pi + \beta$, where β is given by

$$\beta = 2 \arccos\left(x_c/|OC|\right). \tag{3}$$

The seating and release configurations provides limits for the angles to the span endpoints. Expressing these limits in the X, Y coordinate system gives

$$\theta_a \in [\theta_{as} - 2\alpha_c,\ \theta_{as}], \tag{4}$$

$$\phi_a \in [\phi_{ar},\ \phi_{ar} + 2\alpha_o], \tag{5}$$

$$\theta_b \in [\theta'_{br} + \pi + \beta,\ \theta'_{br} + \pi + \beta + 2\alpha_c], \tag{6}$$

$$\phi_b \in [\phi'_{bs} + \pi + \beta - 2\alpha_o,\ \phi'_{bs} + \pi + \beta]. \tag{7}$$

These limits will be used to determine the number of rollers seated on the two sprockets. Expressing the angels to span b in terms of the angles to span a and integer increments of 2α gives

$$\theta_b = \theta_a + 2\alpha_c \hat{n}_c, \tag{8}$$

$$\phi_b = \phi_a + 2\alpha_o \check{n}_o - 2h\alpha_o, \tag{9}$$

where the function h ensures that ϕ_b decrease continuously, as ϕ_a jumps discontinuously when a roller is released from the driven sprocket at ϕ_{ar}. In (8)-(9) the total number of sprocket seating curves has been split into being either free or occupied by a chain roller, i.e.

$$n = \check{n} + \hat{n}, \quad \check{n}, \hat{n} \in \mathbb{N}, \tag{10}$$

where the number of seating curves with a roller seated is $\check{n}$ and the number of seating curves with no roller seated is $\hat{n}$. Substituting (8) into (6) gives the number of free seating curves on the driver sprocket:

$$\frac{\theta'_{br} - \theta_a + \pi + \beta}{2\alpha_c} \leq \hat{n}_c \leq \frac{\theta'_{br} - \theta_a + \pi + \beta}{2\alpha_c} + 1. \tag{11}$$

Similarly, by substituting (9) into (7) the number of rollers seated on the driven sprocket can be determined from

$$\frac{\phi'_{bs} - \phi_a + \pi + \beta}{2\alpha_c} - 1 + h \leq \check{n}_o \leq \frac{\phi'_{bs} - \phi_a + \pi + \beta}{2\alpha_c} + h. \tag{12}$$

With $\hat{n}_c$ determined from (11), the contact angle to the lower span at the driver sprocket can be determined from (8). The contact angle to the lower span at the driven sprocket can be determined from (9) with $\check{n}_o$ determined from (12) and h given in (2). The total wrapping length of the chain is then

$$L = l_a + l_b + (\check{n}_c + \check{n}_o)p, \tag{13}$$

with l_a given by (2), $\check{n}_c$ by (10) and the lower span length calculated from

$$l_b = \sqrt{(x_c + R_c \cos\theta_b - R_o \cos\phi_b)^2 + (y_c + R_c \sin\theta_b - R_o \sin\phi_b)^2}. \tag{14}$$

In summary, the total length L of the chain wrapping around both sprockets was determined by assuming that only span b could deform. Because the lower span length varies as the sprockets rotate, it has been shown that

a roller chain drive with tight spans must in general include components to function. To improve the quantitative estimate of the wrapping length variation, the deformation of the other chain drive components should be included, i.e. the deformation of the both spans, and the deformation of chains wrapped on elastic sprockets [33, 34, 35]. The above analysis serves as an initial investigation of this effect of polygonal action, which has not been treated previously. Lastly, the kinematic configuration of all the chain drive components determined when the wrapping length equals an integer number of chain pitches is exact. This is useful for initializing e.g. multi-body simulations of roller chain drives.

3. Example results of the kinematic analysis

Twelve different chain drive configurations are used to present results for the calculation of the wrapping length, with ID and properties as listed in Table 1. For a given pitch length p, number of teeth n_c, n_o, span length given by N and pitch fraction f, the sprocket center positions can be found from (1). The tight span length l_a can be determined from (2), and the total number of links in the chain is given by M. Calculated values for the minimum, mean and maximum wrapping length obtained from (13) are presented, all nondimensionalized with the pitch p. Configuration C_1 has been subject to experimental measurements of "angular displacement error" [5] as well as kinematic studies of driven sprocket angular motion [7]. Note from Table 1, that if both chain spans are to be in tension for a given configuration, the pitch fraction f cannot be chosen freely.

Figure 2 shows how the wrapping length varies during one tooth period for the configurations in Table 1. In general, the magnitude of the wrapping

Table 1: Chain drive configurations

ID	n_c	n_o	N	M	f	$L_{\min}/p$	L_{mean}/p	$L_{\max}/p$
A_1	6	12	4	20	0.3325	20.0020	20.0200	20.0411
A_2			8	28	0.4066	28.0027	28.0162	28.0329
A_3			16	44	0.4516	44.0046	44.0130	44.0236
B_1	12	12	8	31	0.5015	31.0030	31.0032	31.0034
B_2			16	46	0.0024	46.0048	46.0048	46.0048
B_3			24	63	0.5032	63.0064	63.0065	63.0066
C_1	12	18	11	40	0.4302	40.0040	40.0091	40.0149
C_2			22	62	0.4655	62.0066	62.0100	62.0138
C_3			33	84	0.4786	84.0085	84.0110	84.0138
D_1	24	32	16	63	0.4106	63.0064	63.0079	63.0094
D_2			24	79	0.4408	79.0080	79.0095	79.0112
D_3			32	95	0.4569	95.0097	95.0111	95.0126

length variation is seen to decrease as the number of sprocket teeth and span length is increased. For the special configuration B where $n_c/n_o = 1$, it is seen from Figure 2(b) that the length variation decreases significantly, and vanishes completely for configuration B_2, where the number of links M equals an even number and $f \simeq 0$. Except for configurations B, the wrapping length variation resembles a harmonic function, albeit the variations are not completely symmetric. A time-varying wrapping length demonstrates that a chain drive with tight spans must generally include compliant components to function.

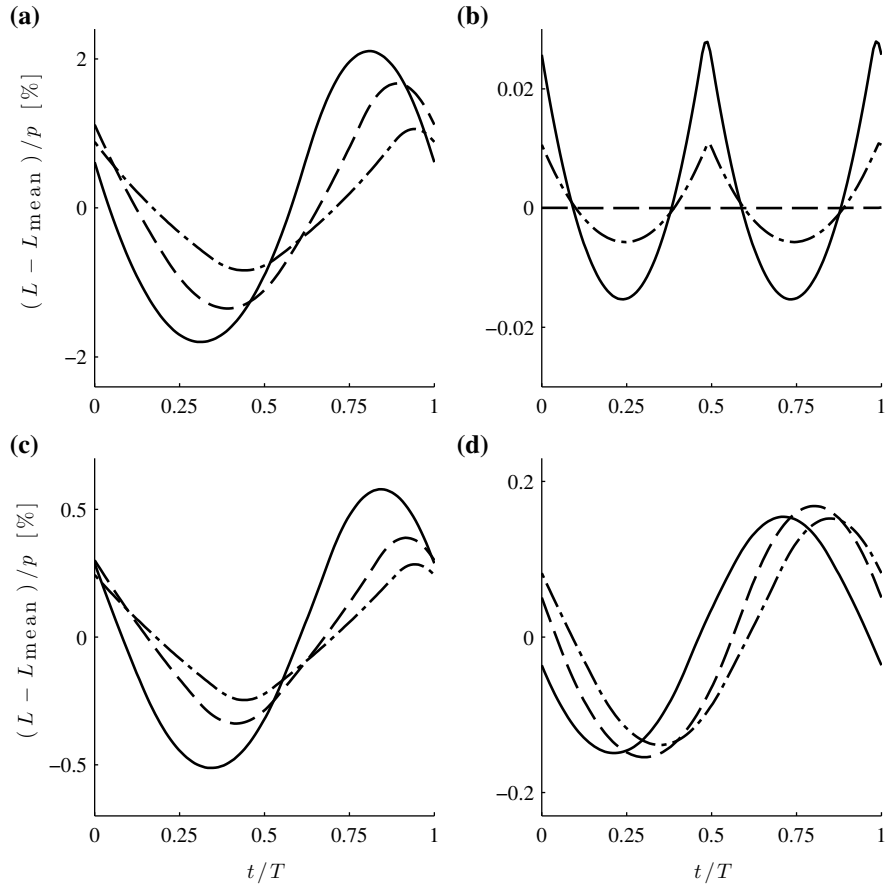

Figure 2: Chain wrapping length variation $L - L_{\text{mean}}$ normalized by pitch p for one tooth period. Configurations A-D are shown in figures (a)-(d), respectively. The line types (—), (−−) and (− · −) identify the, short, medium and long span lengths, respectively.

4. Wrap length comparison with multi body simulation

The kinematic analysis is based on a simplified model of a chain drive and the results describe the motion when deformations, clearances, dissipation and dynamics are neglected. In order to access the potential similarity with chain drives in operation, the kinematic results are compared with results from multibody simulations, which includes both greater detail of the chain drive geometry and dynamic effects. The multibody simulations are carried out using a simulation program developed by Pedersen et al. [8], which

includes a detailed modeling of the tooth geometry and the flexible contact between teeth and chain rollers [9].

In the multibody model, the mass of the chain is assumed to be lumped at the roller locations, and the rotational inertia of the rollers about their centre of gravity is ignored. Springs and dampers with constant stiffness and damping coefficients model the links. Clearances between pin and bushing are neglected. Tooth geometry in the simulation program used to produce the results presented here is Type II per ASA B29.1-1950. For this comparison the chain drive configuration C_1 is used, which has also been analyzed experimentally [5]. Full details of the simulation parameters are comprehensive to present and only the main dynamic parameters are given: Chain pitch 0.0254m, link stiffness 0.221GN/m, link mass 0.066kg, link damping 0.01Ns/m, driven sprocket rotational inertia 0.046kgm^2 and rotational damping 0.1Nms/rad. The driver angular velocity is constant at 10, 100 and 300 rpm, and the simulations show no significant vibratory response of the chain spans or driven sprocket at these driver velocities.

Analytical predictions of the wrapping length given by (13) are compared to the results of multibody simulation and presented in Figure 3. It is seen that the minimum wrapping length predicted by the kinematic analysis is in excellent agreement with the simulation results. The wrapping length variation shows resemblance to harmonic functions, and the simulation and analytical results are in very good qualitative agreement. Quantitatively, the kinematic analysis predicts an amplitude of the wrapping length which is about a two times larger than what is observed in the simulation results. One reason for this could be that the multibody model allows for indentation of the rollers into the sprockets. Finally, it is seen that the phenomena is not limited to quasi static (low speed) operation of the chain drive, as

the simulation results for 10, 100 and 300 rpm all shows a tooth periodic variation of the wrapping length. As the driver velocity increases there is seen to be a slight increase in the minimum wrapping length, and one explanation for this could be an increased axial tension of the chain due to centrifugal effects.

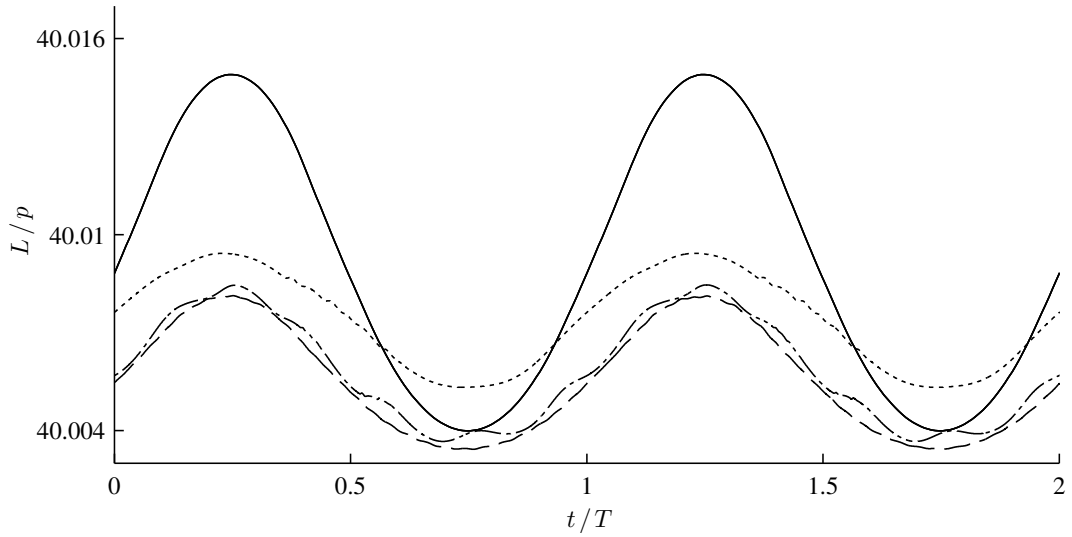

Figure 3: Normalized chain wrapping length L/p for configuration C_1 for two tooth periods. Results in broken lines $(--)$, $(- \cdot -)$ and $(\cdot \cdot \cdot)$ identify results from multibody simulation at a driver speed of 10, 100 and 300 rpm, respectively. Shown in solid line (—) is the analytical kinematic prediction for the chain wrapping length.

During installation of real chain drives, i.e. when the drive is stationary and unloaded, the span tension will depend on the angular position of the driver sprocket. During operation the axial force is then expected to vary periodically with the tooth frequency. The effect appears here for chain drives with only two sprockets, but is also expected for chain drive configurations with more sprockets and spans, and should also not be limited to low-speed chain drives. We hypothesize that multiple sprockets can be positioned to either attenuate or amplify the effect of a variable wrapping length. If this

is the case, careful positioning of e.g. a tensioner sprocket could possibly neutralize the effect of a variable wrapping length, and allow for a constant span tension even for chain drive configurations where the sprockets have few teeth.

5. Dynamic modeling and analysis

First a model is derived which is capable of representing the coupling between the chain span transverse vibrations with the driven sprocket angular vibration. Then we present approximate solutions for the longitudinal displacements, and perform a mode shape expansion leading to coupled equations of motion of the tight span, the slack span and the driven sprocket. This resulting 3-DOF model is analyzed using the method of multiple scales, and three example results are presented.

The tight- and slack chain spans are assumed to have axial tension $P, \tilde{P} > 0$, respectively, thereby providing elastic coupling across the driven sprocket. In real applications of roller chain drives such as low speed marine engines, the roller chain is pretensioned in this way in order to minimize chain span transverse vibrations. Pretension is achieved by the positioning of a fixed tightener sprocket, ensuring that all chain spans in the drive are in positive tension. However, the choice of pretension giving the optimal vibration suppression at various operating conditions is not well understood, and in some designs guide-bars must be applied to limit transverse vibrations.

In roller chain drives both ends of the chain spans are subjected to transverse excitation from chain and sprocket meshing. Axial excitation of the chain span coming from polygonal action, non-uniform motion of the driver sprocket, and external loading of the driven sprocket will be included.

Throughout the modeling and analysis we identify prescribed external forcing to be included in the multiple scales analysis by a star $(\,)^*$. Whenever possible, we do not present equations for the slack span, as for $\tilde{P} > 0$ they are equivalent to equations for the tight span. Parameters and variables for the slack span are identified by a tilde ($\tilde{}$), and their definitions are equivalent to the similar variables for the tight span without a tilde.

5.1. Dynamic model

A simple model consisting of two sprockets is considered, with gravity ignored. The local coordinate systems and definitions of displacements are shown in Figure 4. The dependent variables $U, \tilde{U}, \hat{W}, \hat{\tilde{W}}$ and θ_1 are the displacements measured at a steady state of operation, i.e. the particular solution of the forced response, calculated when the mean of the input torque M_2 equals the mean of the output torque M_1.

The motion of the driving sprocket is assumed to be given, i.e. θ_2^* is a known function of time. This represents the case where angular motion of e.g. a crankshaft is given, and the crankshaft kinematically forces the chain drive, as is relevant with combustion engines, where the chain drive powers auxiliary equipment requiring only a small fraction of the power required at the main output. For example with ship propulsion engines, the chain drive powering the hydraulic pumps is driven directly by the crankshaft, and consumes only about 1% of the power required for driving the propulsion propeller.

At steady state the input torque balances the output torque, such that there is no net transient acceleration and change of velocity of the drive. This is equivalent to the chain drive operating at nominal angular velocity [24]. Assuming the initial total span (pre)tension $P_{\text{tot}} = P_{\text{pre}} + \tilde{P}_{\text{pre}}$ at zero

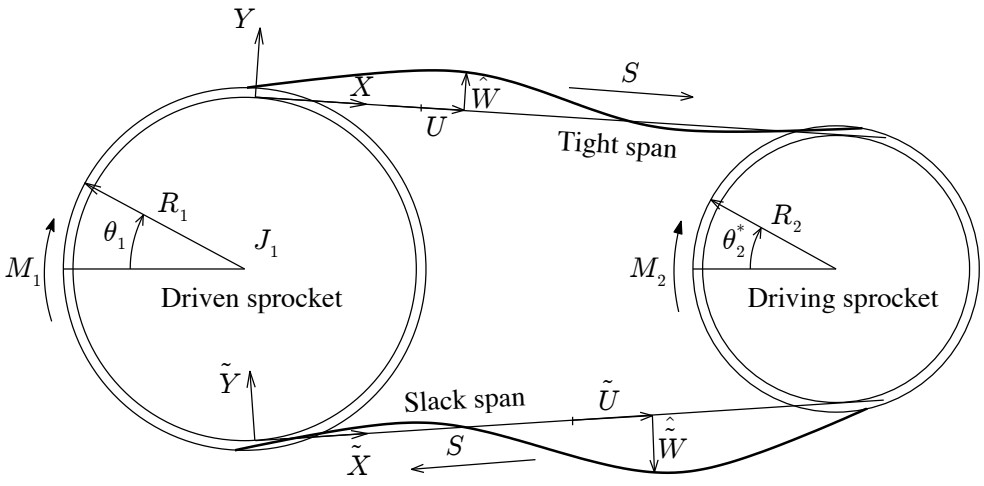

Figure 4: Mechanical model of a chain drive system with two sprockets

external load and zero angular velocity to be known, as well as the nominal span velocity S and input torque $\hat{M}_2$, the longitudinal forces at steady state operation are, for the upper and lower spans

$$P_0 = \tfrac{1}{2}(P_{\text{tot}} + \hat{M}_1/R_1), \tag{15}$$

$$\tilde{P}_0 = \tfrac{1}{2}(P_{\text{tot}} - \hat{M}_1/R_1). \tag{16}$$

The output torque $\hat{M}_1$ can me modeled as comprised of a constant (brake) load $\hat{f}_1$, rotational viscous damping $\hat{d}_1$, and a time dependent torque $\hat{M}_1^*(t)$, where t is time

$$\hat{M}_1 = \hat{d}_1 S/R_1 + R_1\hat{f}_1 + \hat{M}_1^*. \tag{17}$$

For $\hat{M}_1^* = 0$ (15)-(16) with (17) demonstrate how the nominal tension of the chain spans varies with initial pretension, operating speed, and constant external load. Centrifugal forces are not included in this model, which could be relevant for high-speed roller chain drives, and we note that chain wear corresponds to a reduction of P_{tot}.

In the following section, the equations of motion for the chain spans are derived using Hamiltons principle. For the driven sprocket, the equation of motion will be derived using Newtons 2nd law. The governing equations are formulated such that the driven sprocket motion couples the tight and slack span motion through their boundary conditions.

5.2. Equation of motion for the chain spans

The roller chain is modeled as an axially moving string supported by moving boundaries, as illustrated in Figure 5. The coordinate system X, Y is inertial and the moving string endpoint displacements are prescribed from the axial positions $X_1(T)$ and $X_2(T)$. In a chain drive, the chain span travels in the axial direction with the span endpoint constituted by the rollers seated on the rotating sprocket which has a neighboring roller in the free span. As the sprockets rotate, chain links recurrently *enter* and *leave* the span. Therefore the positions of the span endpoints from which the displacements are prescribed moves instantly at these events cf. Figure 1. Consequently, the amount of string material within the boundaries varies, as we see from the periodically varying span length given by (2) for the tight span. To model this, it is necessary to allow the position from which the span endpoint displacements are prescribed from to be functions of time; $X_1(T)$ and $X_2(T)$ models this. Between the seating and release events, the distance $X_2(T) - X_1(T)$ equals the span length, and the boundaries move in the positive x-direction at nominal speed $S \geq 0$.

From the moving span endpoint axial positions X_1, X_2, we denote the span endpoint longitudinal displacements by $U_1(T), U_2(T)$, respectively. In the transverse direction, the string endpoint displacements are given by $Y_1(T), Y_2(T)$.

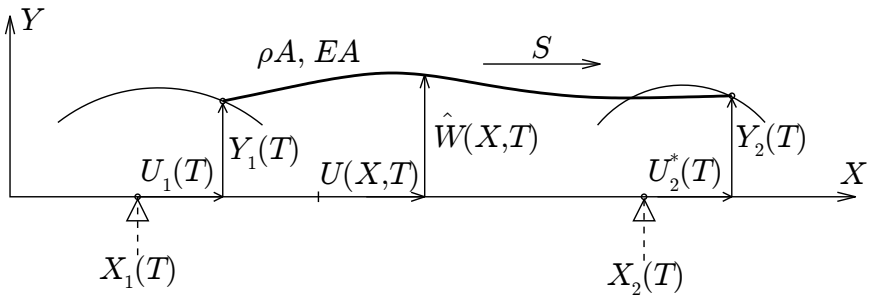

Figure 5: Axially moving chain span supported by moving boundaries

The string is assumed to have constant axial stiffness EA and mass per unit length ρA, and is subjected to axial tension $P > 0$. Longitudinal and transverse displacements of the string are denoted by $U(X,T)$ and $\hat{W}(X,T)$, respectively, while out of plane motion is not considered. Both longitudinal and transverse displacements is possible at the moving span endpoints, i.e. the boundary conditions are inhomogeneous:

$$U(X_1(T),T) = U_1(T), \qquad U(X_2(T),T) = U_2^*(T) \tag{18}$$

$$\hat{W}(X_1(T),T) = Y_1(T), \qquad \hat{W}(X_2(T),T) = Y_2(T). \tag{19}$$

Kinematic forcing from the angular motion of the driver sprocket is assumed prescribed and identified by a star, U_2^*.

The axial and transverse velocity components are $U_{,T} + S(1 + U_{,X})$ and $\hat{W}_{,T} - S\hat{W}_{,X}$, respectively. With this, the kinetic energy of the string is

$$K(T) = \frac{\rho A}{2} \int_{X_1(T)}^{X_2(T)} \left(\left(U_{,T} + S(1 + U_{,X}) \right)^2 + \left(\hat{W}_{,T} - S\hat{W}_{,X} \right)^2 \right) dX. \tag{20}$$

Since $X_2(T) - X_1(T)$ is not constant for all T, the amount of string material within the boundaries varies, and we can investigate the effect of a chain span having a time-varying length. When P_0 is the mean over time of the axial force P, the mean axial strain is $e_0 = P_0/EA$, and the total strain is

$e_0 + e(X,T)$. The approximate nonlinear measure for the dynamical strain is [15]:

$$e(X,T) = U_{,X} + \tfrac{1}{2}\hat{W}_{,X}\,. \tag{21}$$

Using this, the potential energy associated with elastic string deformation is

$$V(T) = \frac{EA}{2}\int_{X_1(T)}^{X_2(T)} \left(\frac{P_0}{EA} + U_{,X} + \tfrac{1}{2}\hat{W}_{,X}^{\,2}\right) dX, \tag{22}$$

where $K(T)$ and $V(T)$ are most accurate when $|\hat{W}_{,X}| = |U_{,X}| = O(\varepsilon)$, $\varepsilon \ll 1$ and $U = O(\hat{W}^2)$, such that nonlinear strain deriving from U is negligible. The equations of motion and the associated boundary conditions can be derived using Hamilton's principle,

$$\delta \int_{T_1}^{T_2} (K - V) dT = 0. \tag{23}$$

By specifying the motion at the boundaries, and requiring the virtual displacements to be kinematically admissible, the displacement variations at the boundaries where motion is prescribed is zero; this ensures that the virtual work done at either boundary is zero [36]. The actual work done by the boundaries is not zero, and not required to be [37]. The total mechanical energy is not constant, even for fixed boundary conditions [38]. But the application of Hamiltons principle presupposes the applied forces to be derivable from a potential; it does not require constant energy. Non-constant energy is usually associated with damping (or external non-potential forces), but there are no dissipative forces in the system so far, and the equations of motion can be derived using (23).

Since the limits of integration in (20) and (22) are time dependent, the usual process of deriving the governing equations [10] using integrations by parts is not possible, and the use of Leibniz rule for differentiation of

integrals is required, as in [39]. This gives:

$$\rho A(U_{,TT}+2SU_{,XT}+S^2U_{,XX})-EA(U_{,X}+\tfrac{1}{2}\hat{W}_{,X}^{2})_{,X}=0, \tag{24}$$

$$\rho A(\hat{W}_{,TT}+2S\hat{W}_{,XT}+S^2\hat{W}_{,XX})-EA\big(\hat{W}_{,X}\,(U_{,X}+\tfrac{1}{2}\hat{W}_{,X}^{2}+\frac{P_0}{EA})\big)_{,X}=0, \tag{25}$$

with boundary conditions given by (18)-(19). The functions $U_1(T)$ and $U_2^*(T)$ relates to the non-constant angular motion of the driven and driver sprockets, respectively; $U_2^*(T)$ is assumed to be given, and $U_1(T)$ will be formulated in terms of the angular displacements of the driven sprocket in section 5.5. Equations (24)-(25) are non-dimensionalized with all lengths measured relative to the length l,

$$(x,u,\hat{w},x_1,x_2,y_1,y_2)=\frac{(X,U,\hat{W},X_1,X_2,Y_1,Y_2)}{l}, \tag{26}$$

where $l=|OC|$, and time is non-dimensionalized by the fundamental frequency of a fixed-fixed string of length l under constant axial tension P_t,

$$t=\sqrt{\frac{P_t}{\rho Al^2}}T. \tag{27}$$

Here we do not specify P_t, as the convenient choice for P_t depends on the object of the analysis; e.g. engine builders usually normalize to the driver frequency, in which case P_t can be chosen accordingly. The corresponding non-dimensional equation of motion for the transverse motions $\hat{w}$ of the tight span becomes

$$\hat{w}_{,tt}+2s\hat{w}_{,xt}+s^2\hat{w}_{,xx}-\alpha\left(\hat{w}_{,x}\,(u_{,x}+\tfrac{1}{2}\hat{w}_{,x}^{2}+\gamma)\right)_{,x}=0, \tag{28}$$

while longitudinal motions u of the tight span are governed by

$$u_{,tt}+2su_{,xt}+s^2u_{,xx}-\alpha(u_{,x}+\tfrac{1}{2}\hat{w}_{,x}^{2})_{,x}=0, \tag{29}$$

where dimensionless parameters have been introduced as

$$s = \frac{S}{\sqrt{\frac{P_t}{\rho A}}},\ \alpha = \frac{EA}{P_t},\ \gamma = \frac{P_0}{EA},\ \tilde{\gamma} = \frac{\tilde{P}_0}{EA}. \tag{30}$$

Note that, if $P_t = P$, then $\alpha\gamma = 1$ and $\alpha\tilde{\gamma} = \tilde{P}/P$. The non-dimensional boundary conditions are

$$\hat{w}(x_1(t), t) = y_1(t), \qquad \hat{w}(x_2(t), t) = y_2(t), \tag{31}$$

$$u(x_1(t), t) = u_1(t), \qquad u(x_2(t), t) = u_2^*(t), \tag{32}$$

where u_1 depends on the driven sprocket angular displacements and u_2^* is given by the driving sprocket angular displacements.

5.3. Solution for the longitudinal displacement and axial tension

The transverse wave speed for at roller chain under axial tension P_0 and mass per unit length ρA is $c_w = \sqrt{P_0/\rho A}$. The natural frequencies of a stationary ($s = 0$) fixed-fixed string with length l are $f_n = nc_w/2l, n = 1, 2, \ldots$. Assuming EA and ρA to be constant, the longitudinal wave speed is $c_u = EA/\rho A$. The analysis is restricted to roller chain spans operating under low or moderate loads, and with a maximum allowable tension P_{max} being small compared to the axial stiffness EA. The longitudinal waves propagate much faster than the lower transverse waves, and the influence of longitudinal inertia is small. Under this assumption the axial force is only time dependent, i.e. $N_{,x} = 0$.

The instantaneous axial tension N can be identified from (28) as the coefficient to $\hat{w}_{,xx}$:

$$N(x, t) = \alpha(u_{,x} + \tfrac{1}{2}\hat{w}_{,x}^{\,2} + \gamma) - s^2. \tag{33}$$

Using $N_{,x} = 0$ gives

$$(u_{,x} + \tfrac{1}{2}\hat{w}_{,x}^{\,2})_{,x} = 0, \tag{34}$$

which shows that the strain is also constant along the axial direction, $e_{,x} = 0$. Integrating (21) with the boundary conditions (32), the axial dynamic dynamic strain becomes:

$$e(t) = \frac{u_2^*(t) - u_1(t) + \frac{1}{2}\int_{x_1(t)}^{x_2(t)} \hat{w}_{,x}^{\,2}\, dx}{x_2(t) - x_1(t)}. \tag{35}$$

Integrating (21) from $x_1(t)$ to x gives the solution for the axial displacement

$$u(x,t) = u_1(t) + e(t)\big(x - x_1(t)\big) - \tfrac{1}{2}\int_{x_1(t)}^{x} \hat{w}_{,x}^{\,2}\, dx. \tag{36}$$

Which shows how u depends nonlinearly on the transverse motion $\hat{w}_{,x}$. The axial force is then given by

$$N(t) = \alpha\big(e(t) + \gamma\big) - s^2, \tag{37}$$

which becomes useful when deriving the equation of motion for the driven sprocket.

5.4. Obtaining homogeneous boundary conditions for the transverse motion

To obtain homogeneous boundary conditions we employ a linear transformation

$$\hat{w}(x,t) = w(x,t) + y_1(t)\big(1 - x\big) + y_2(t)x. \tag{38}$$

Substituting into (28) and (35) for the dynamic strain, the equation of transverse motion becomes

$$w_{,tt} + 2sw_{,xt} - (\alpha\gamma - s^2)w_{,xx} - \alpha e(t)w_{,xx} = -y_{,tt}\,(1-x) - y_{2,tt} - 2s(y_{2,t} - y_{1,t}), \tag{39}$$

with boundary conditions

$$w\big(x_1(t),t\big)=0,\ w\big(x_2(t),t\big)=0. \tag{40}$$

Although homogeneous, the boundary conditions are specified from a moving position. For roller chain drives the change in span endpoint position is small compared to the span length; it is therefore reasonable to limit the analysis to small axial variations of the support positions. They are assumed to be of the form

$$x_1(t)=\varepsilon\Delta x_1(t),\ x_2(t)=1+\varepsilon\Delta x_2(t), \tag{41}$$

where $\varepsilon \ll 1$ denotes smallness of terms. Taylor expanding the boundary conditions (40) around $x=0$ and $x=1$ gives

$$w(x_1(t),t)=w(0,t)+\varepsilon\Delta x_1(t)w(0,t)_{,x}+O(\varepsilon^2) \tag{42}$$

$$w(x_2(t),t)=w(1,t)+\varepsilon\Delta x_2(t)w(1,t)_{,x}+O(\varepsilon^2). \tag{43}$$

When deriving the kinetic and potential energies it was used that $|U_{,x}|=|\hat{W}_{,x}|=O(\varepsilon)$, which is fulfilled when $|w_{,x}|=O(\varepsilon)$. Then (42)-(43) reduce to

$$w(x_1(t),t)=w(0,t)+O(\varepsilon^2), \tag{44}$$

$$w(x_2(t),t)=w(1,t)+O(\varepsilon^2). \tag{45}$$

For roller chain drives the transverse displacements of the chain span endpoints is also small compared to the span length, and it is reasonable to specify the displacements of the boundaries to satisfy $|y_2-y_1|=O(\varepsilon)$ and $|x_1-x_2|=O(1)$. Then the dynamic strain (35) reduces to

$$e(t)=u_2^*-u_1+\tfrac{1}{2}\int_0^1 w_{,x}^2\,dx+O(\varepsilon^2), \tag{46}$$

and the equation of motion for the transverse motion of the tight span becomes

$$w_{,tt} + 2sw_{,xt} - (\alpha\gamma - s^2)w_{,xx} - \varepsilon\alpha\Big(u_2^* - u_1 + \tfrac{1}{2}\int_0^1 w_{,x}^2\, dx\Big)w_{,xx} = -y_{1,tt}\,(1-x) - y_{2,tt}\,x - 2s(y_{2,t} - y_{1,t}) + O(\varepsilon^2). \quad (47)$$

with boundary conditions

$$w(0,t) = 0 + O(\varepsilon^2), \quad (48)$$

$$w(1,t) = 0 + O(\varepsilon^2). \quad (49)$$

Thus, the effect of boundary positions moving in the axial and transverse direction by a small amount $O(\varepsilon)$ leads to a second order effect in the equation of motion and boundary conditions for transverse vibrations of the chain span.

5.5. Driven sprocket equation of motion

For the driven sprocket it is assumed that the sprocket center is fixed such that only rotation around the sprocket center is possible. The equation of motion can be obtained using Newton's second law, which gives

$$\hat{J}_1\theta_{1,TT} + \hat{d}_1\theta_{1,T} = R_1(N - \tilde{N}) + \hat{M}_1, \quad (50)$$

where $\hat{J}_1$ is the mass moment of inertia for the driven sprocket and attached machinery, $\hat{d}_1$ is the coefficient of viscous rotational damping of sprocket motion, $\hat{M}_1$, is the externally applied torque, and $N, \tilde{N}$ are the axial reaction forces from the upper and lower chain span, respectively. Assuming a purely kinematic relationship between the sprocket angular displacements $\theta_{1,2^*}$ and the span endpoint longitudinal displacements $u_{1,2^*}$ allows us to write

$$\theta_1 = \frac{l}{R_1}u_1, \quad \theta_2^* = \frac{l}{R_2}u_2^*. \quad (51)$$

Inserting this, and using (27) and (33) gives

$$J_1 u_{1,tt} + d_1 u_{1,t} = \alpha \left(u_{,x} + \tfrac{1}{2}\hat{w}_{,x}^{\,2} + \gamma - \frac{s^2}{\alpha} \right) - \alpha \left(\tilde{u}_{,x} + \tfrac{1}{2}\hat{\tilde{w}}_{,x}^{\,2} + \tilde{\gamma} - \frac{s^2}{\alpha} \right) + M_1, \tag{52}$$

where

$$J_1 = \frac{\hat{J}_1}{\rho A l R_1^2},\ d_1 = \frac{\hat{d}_1}{R_1^2 \sqrt{\rho A P_t}},\ M_1 = \frac{\hat{M}_1}{R_1 P_t}. \tag{53}$$

When the mean axial forces P and $\tilde{P}$ in (30) are chosen such that they balance the nominal output torque (17), (52) reduces to

$$J u_{1,tt} + d u_{1,t} = \alpha(u_{,x} + \tfrac{1}{2}\hat{w}, x^2) - \alpha(\tilde{u}_{,x} + \tfrac{1}{2}\hat{\tilde{w}}_{,x}^{\,2}) + M_1^*(t), \tag{54}$$

where $M_1^*(t)$ is the time dependent driven sprocket torque with zero mean. The two terms multiplied by α can be recognized to be the dynamic axial strains of the upper and lower spans. Under the already made assumptions of $e_{,x} = 0$ and small endpoint displacements these are given by (46). Assuming rigid connection of the upper and lower span across the sprocket, i.e.

$$u_1 = -\tilde{u}_1,\ u_2^* = -\tilde{u}_2^*, \tag{55}$$

and inserting the dynamic strains given by (46), using (55) to eliminate $\tilde{u}_1, \tilde{u}_2$, (54) becomes

$$J u_{1,tt} + d u_{1,t} + 2\alpha u_1 = 2\alpha u_2^* + \frac{\alpha}{2} \int_0^1 (w_{,x}^{\,2} - \tilde{w}_{,x}^{\,2}) dx + M_1^*(t). \tag{56}$$

This is an inhomogeneous ordinary second order differential equation for the driven sprocket angular displacements u_1 measured from steady state operating conditions. The equation is nonlinearly coupled to the upper and lower span transverse displacements w and $\tilde{w}$.

5.6. Mode shape expansion

Because the main focus is to study the coupling between the two spans and the driven sprocket it is chosen to use stationary mode shapes for the discretization of the equations governing the transverse vibrations of the string. As noted in the introduction, using complex mode shapes provides a better basis for estimating parametric instability. However, to simplify the algebra and produce results which are more easily interpreted, and still valid at lower speeds s, (47) is discretized using the standard Galerkin method with test functions chosen as mode shapes for transverse vibrations of an axially non-moving uniform string:

$$w(x,t) = \sum_{n=1}^{N} \xi_n(t)\phi_n(x), \quad \phi_n(x) = \sin n\pi x. \tag{57}$$

Following the standard Galerkin procedure, the equation governing the modal amplitudes ξ_m, $m = 1, 2, \ldots, N$ becomes

$$\xi_{m,tt} + 2sC_{mn}\zeta_{m,t} + (\alpha\gamma - s^2)(m\pi)^2\xi_m + \alpha(m\pi)^2\Big(u_2^* - u_1 + \tfrac{1}{4}\sum_{n=1}^{N}\xi_n^2(n\pi)^2\Big)\xi_m$$
$$= -(y_{1,tt} - 2s(y_{2,t} - y_{1,t}))G_m + (y_{1,tt} - y_{2,tt})E_m, \tag{58}$$

where

$$C_{mn} = \frac{2mn\,(1-(-1)^{m+n})}{m^2+n^2},\ G_m = \frac{2\,(1-(-1)^m)}{m\pi},\ E_m = \frac{-2(-1)^m}{m\pi}. \tag{59}$$

It is seen here that the non-linear term introduces modal coupling. The Coriolis term (with C_{mn}) will only be included with an expansion including an even and an odd mode.

5.7. Single mode approximation

For the purpose of this analysis, where there is modal coupling between the tight and slack span, only a single mode expansion will be used for

each span. For a single m mode, the equation for the corresponding modal coordinate becomes:

$$\xi_{m,tt} + 2\mu_m \xi_{m,t} + \omega_m^2 \xi_m + \varepsilon \alpha_m \big(u_2^* - u_1 + p_o^*(t)\big)\xi_m + \varepsilon \kappa_m \xi_m^3 \\ = -(y_{1,tt} - 2s(y_{2,t} - y_{1,t}))G_m + (y_{1,tt} - y_{2,tt})E_m, \quad (60)$$

where

$$\omega_m^2 = (\alpha\gamma - s^2)(m\pi)^2,\ \alpha_m = (m\pi)^2\alpha,\ \kappa_m = \tfrac{1}{4}(m\pi)^4\alpha, \quad (61)$$

linear modal damping with coefficient $2\mu_m$ has been added, and axially varying tension coming from the varying wrapping length as specified by the function $p_o^*(t)$ has been included.

5.8. Modeling transverse excitation

The span endpoint positions y_1, y_2 follows curves which resemble a cycloid. At the instant where a roller enters (or leaves) the chain span, the projections of the nominal tangential velocity s in the y-direction changes discontinuously, cf. Figure 1. Therefore, the endpoint transverse velocities are non-smooth in time, and the span endpoint accelerations also jumps discontinuously in time, which leads to impulsive loading of the chain spans from meshing. The external non-dimensional modal forcing f_m depends on the transverse velocity and acceleration of the span endpoints, and is given by the right hand side of (60):

$$f_m(t) = -(y_{1,tt} - 2s(y_{2,t} - y_{1,t}))G_m + (y_{1,tt} - y_{2,tt})E_m, \quad (62)$$

where $G_m = 0$ for m even, while $E_m \neq 0$ for all m. To represent the impulsive loading at the span endpoints, the acceleration jumps are modeled

using Dirac pulse trains,

$$y_{1,tt} = \sum_{j=-\infty}^{\infty} Q_1 \delta(t - j\tau_o), \quad y_{2,tt} = \sum_{j=-\infty}^{\infty} Q_2 \delta(t - (\psi + j)\tau_o), \tag{63}$$

where $\tau_o = \sqrt{P_t/\rho A l^2}(n_2 f_2)^{-1}$ is the non-dimensional tooth period, f_2 is the driver frequency in Hz, and n_2 the number of teeth on the driver sprocket. The acceleration jump at the driven sprocket Q_1 occurs at the instant where a roller is released from the sprocket. Similarly, the acceleration jump Q_2 occurs at the instant where a roller seats on the driver sprocket. The Dirac pulses of the two endpoint accelerations are separated in time by a phase ψ, which relates to the shaft center distance, specifically the pitch fraction f [7]. Assuming the span to remain straight, the relative velocities between two neighbouring rollers at the instant of seating and release, respectively, are given by

$$Q_1 = 2s \sin \alpha_1 = \frac{sp}{R_1}, \quad Q_2 = 2s \sin \alpha_2 = \frac{sp}{R_2}, \tag{64}$$

where α_1, α_2 are the pitch angles, R_1, R_2 are the pitch circle radius, p is the pitch length, and it has been used that $R_1 = p/(2 \sin \alpha_1)$ and $R_2 = p/(2 \sin \alpha_2)$. The same relative velocities are used in [32] for the study of impact between a roller seating at the driver sprocket. It is seen from (64) that increased sprocket radius, shorter pitch length and lower velocities reduce the endpoint acceleration discontinuities. Assuming the acceleration terms to be dominating, the terms proportional to s are neglected in (62), and the approximation of the modal forcing becomes

$$f_m(t) = (E_m - G_m) \sum_{j=-\infty}^{\infty} Q_1 \delta(t - j\tau_o) - E_m \sum_{j=-\infty}^{\infty} Q_2 \delta(t - (\psi + j)\tau_o). \tag{65}$$

Since the forcing is time-periodic, it can be written as a (complex-valued) Fourier series,

$$f_m(t) = \sum_{p=-\infty}^{\infty} k_p e^{i2\pi pt/\tau_o}, \tag{66}$$

where

$$k_p = \frac{1}{\tau_o}\big((E_m - G_m)Q_1 - E_m Q_2 e^{-i2\pi p\psi}\big). \tag{67}$$

The Fourier coefficients have the same value for all p, due to the properties of the Dirac pulse train. The coefficient k_m is complex, due to the phase ψ and forcing can be obtained as the real part of (66). For high-speed drives, the loading coming from Q_2 will be dominant, as intertial forces reduce the discontinuous velocity jump at the driven sprocket. The approximate forcing introduced here is suitable for the purpose of investigating the tooth-periodic impulsive loading inherent to chain drives; shown here to lead to multi-frequency external transverse excitation.

5.9. Multiple scales perturbation analysis

The vibrations of the chain spans and the driven sprocket are governed by coupled non-linear equations. To analyze the dynamics of this system the Method of Multiple Scales is employed. This relies on the sorting of terms into orders of magnitude, and the results and solution procedure depends on this ordering. Here, aiming at identifying and analyzing possible resonance conditions, we assume damping, parametric coupling and excitation to be weak, as well as non-linearity, and the forcing on the chain spans from impact loading. Under these assumptions, with smallness of terms identified by a book keeping parameter $\varepsilon \ll 1$, the governing equations for transverse vibrations of the upper and lower span given by (60) with external forcing

(66), and rotational vibrations of the driven sprocket (56) are:

$$\xi_{m,tt} + 2\varepsilon\mu_m\xi_{m,t} + \omega_m^2\xi_m + \varepsilon\alpha_m\big(u_2^* - u_1 + p_o^*(t)\big)\xi_m + \varepsilon\kappa_m\xi_m^3 = \varepsilon\sum_{j=-\infty}^{\infty} k_m e^{ij\Omega_o t}, \quad (68)$$

$$\tilde{\xi}_{n,tt} + 2\varepsilon\tilde{\mu}_n\tilde{\xi}_{n,t} + \tilde{\omega}_n^2\tilde{\xi}_m + \varepsilon\tilde{\alpha}_n\big(u_1 - u_2^* + p_o^*(t)\big)\tilde{\xi}_n + \varepsilon\tilde{\kappa}_n\tilde{\xi}_n^3 = \varepsilon\sum_{j=-\infty}^{\infty} \tilde{k}_n e^{ij\Omega_o t+\phi}, \quad (69)$$

$$u_{1,tt} + 2\varepsilon\mu_\theta u_{1,t} + \omega_\theta^2 u_1 + \varepsilon\eta_n\tilde{\xi}_n^2 - \varepsilon\eta_m\xi_m^2 = \varepsilon\omega_\theta^2 u_2^* + \varepsilon M_1^* J^{-1}, \quad (70)$$

where (57) has been inserted in (56), $\Omega_o = 2\pi/\tau_o$, a phase $\phi \in [0, \tau_o]$ has been introduced between the upper and lower span external loading (which depends on the chain drive configuration), and

$$2\mu_\theta = \frac{d}{J}, \quad \omega_\theta = \sqrt{\frac{2\alpha}{J}}, \quad \eta_m = \frac{\alpha(m\pi)^2}{4J}, \quad \tilde{\eta}_n = \frac{\alpha(n\pi)^2}{4J}. \quad (71)$$

We seek solutions in the form of uniformly valid expansions:

$$\xi_m(t) = q_0(T_0, T_1) + \varepsilon q_1(T_0, T_1) + O(\varepsilon^2), \quad (72)$$

$$\tilde{\xi}_n(t) = \tilde{q}_0(T_0, T_1) + \varepsilon\tilde{q}_1(T_0, T_1) + O(\varepsilon^2), \quad (73)$$

$$u_1(t) = \nu_0(T_0, T_1) + \varepsilon\nu_1(T_0, T_1) + O(\varepsilon^2), \quad (74)$$

where $T_0 = t$ and $T_1 = \varepsilon t$ is the slow time. Substituting into (68)-(70) and equating to zero like powers of ε gives, to order ε^0:

$$D_0^2 q_0 + \omega_m^2 q_0 = 0, \quad (75)$$

$$D_0^2\tilde{q}_0 + \tilde{\omega}_n^2\tilde{q}_0 = 0, \quad (76)$$

$$D_0^2\nu_0 + \omega_\theta^2\nu_0 = 0, \quad (77)$$

where $D_i^i \equiv \partial^j / \partial T_i^j$, and to order ε^1:

$$D_0^2 q_1 + \omega_m^2 q_1 = -2D_0 D_1 q_0 - 2\mu_m D_0 q_0 + \alpha_m(\nu_0 - u_2^* + p_o^*(T_0))q_0 - \kappa_m q_0^3 + \sum_{j=-\infty}^{\infty} k_m e^{ij\Omega_o t}, \quad (78)$$

$$D_0^2 \tilde{q}_1 + \tilde{\omega}_n^2 \tilde{q}_1 = -2D_0 D_1 \tilde{q}_0 - 2\tilde{\mu}_n D_0 \tilde{q}_0 + \tilde{\alpha}_n(u_2^* - \nu_0 + p_o^*(T_0))\tilde{q}_0 - \tilde{\kappa}_n \tilde{q}_0^3 + \sum_{j=-\infty}^{\infty} \tilde{k}_n e^{ij\Omega_o t + \phi}, \quad (79)$$

$$D_0^2 \nu_1 + \omega_\theta^2 \nu_1 = -2D_0 D_1 \nu_0 - 2\mu_\theta D_0 \nu_0 + \eta_m q_0^2 - \tilde{\eta}_n \tilde{q}_0^2 + \omega_\theta^2 u_2^* + M_1^*/J. \quad (80)$$

The general solutions to (75)-(77) are

$$q_0 = A(T_1)e^{i\omega_m T_+} + cc, \quad (81)$$

$$\tilde{q}_0 = \tilde{A}(T_1)e^{i\tilde{\omega}_n T_+} + cc, \quad (82)$$

$$\nu_0 = V(T_1)e^{i\omega_\theta T_0} + cc, \quad (83)$$

where the unknown functions $A, \tilde{A}, V$ are complex functions of slow time to be determined, and *cc* complex conjugates of preceeding terms.

So far, the parametric excitation $p_o^*(t)$, the kinematic forcing of the driver sprocket $u_2^*(t)$ and the external excitation of the driven sprocket $M_1^*(t)$ has been assumed to have a zero mean, but otherwise arbitrary. Assuming each of them to be mono-frequency harmonic,

$$p_o^* = p_0 \cos(\Omega_0 T_0), \quad (84)$$

$$M_1^*/J = p_1 \cos(\Omega_1 T_0), \quad (85)$$

$$u_2^* = p_2 \cos(\Omega_2 T_0), \quad (86)$$

and substituting (81)-(83) into (78)-(80), gives

$$\begin{aligned} D_0^2 q_1 + \omega_m^2 q_1 = \frac{1}{2}k_m - (2i\omega_m A' + 2i\mu_m\omega_m A + 3\kappa_m A^2\bar{A})e^{i\omega_m T_0} \\ + \alpha_m(AVe^{i(\omega_m+\omega_\theta)T_0}) + \bar{A}Ve^{i(\omega_\theta-\omega_m)T_0}) \\ - \frac{1}{2}\alpha_m p_2(Ae^{i(\Omega_2+\omega_m)T_0} + \bar{A}e^{i(\Omega_2-\omega_m)T_0}) \\ + \frac{1}{2}\alpha_m p_0(Ae^{i(\Omega_0+\omega_m)T_0} + \bar{A}e^{i(\Omega_0-\omega_m)T_0}) \\ - \kappa_m A^3 e^{3i\omega_m T_0} + \sum_{j=1}^{\infty} k_m e^{ij\Omega_o t} + cc \end{aligned} \quad (87)$$

$$\begin{aligned} D_0^2 \tilde{q}_1 + \tilde{\omega_n}^2 \tilde{q}_1 = \frac{1}{2}\tilde{k}_n - (2i\tilde{\omega}_n\tilde{A}' + 2i\tilde{\mu}_n\tilde{\omega}_n\tilde{A} + 3\tilde{\kappa}_n\tilde{A}^2\tilde{\bar{A}})e^{i\tilde{\omega}_n T_0} \\ - \tilde{\alpha}_n(\tilde{A}Ve^{i(\tilde{\omega}_n+\omega_\theta)T_0}) + \tilde{\bar{A}}Ve^{i(\omega_\theta-\tilde{\omega}_n)T_0}) \\ + \frac{1}{2}\tilde{\alpha}_n p_2(\tilde{A}e^{i(\Omega_2+\tilde{\omega}_n)T_0} + \tilde{\bar{A}}e^{i(\Omega_2-\tilde{\omega}_n)T_0}) \\ + \frac{1}{2}\tilde{\alpha}_n p_0(\tilde{A}e^{i(\Omega_0+\tilde{\omega}_n)T_0} + \tilde{\bar{A}}e^{i(\Omega_0-\tilde{\omega}_n)T_0}) \\ - \tilde{\kappa}_n\tilde{A}^3 e^{3i\tilde{\omega}_n T_0} + \sum_{j=1}^{\infty} \tilde{k}_n e^{i(j\Omega_o t+\phi)} + cc \end{aligned} \quad (88)$$

$$\begin{aligned} D_0^2\nu_1 + \omega_\theta^2\nu_1 = \eta_m A\bar{A} - \eta_n\tilde{A}\tilde{\bar{A}} - (2i\omega_\theta)V' + 2i\mu_\theta\omega_\theta V)e^{i\omega_\theta T_0} \\ + \eta_m A^2 e^{i2\omega_m T_0} - \tilde{\eta}_n\tilde{A}^2 e^{i2\tilde{\omega}_n T_0} + \frac{1}{2}\omega_\theta^2 p_2 e^{i\Omega_2 T_0} + \frac{1}{2}p_1 e^{i\Omega_1 T_0} + cc \end{aligned} \quad (89)$$

The external sources of parametric excitation of the spans are from p_0 and p_2. When $p_1 = 0$ and $p_0 \neq 0$ there will be parametric excitation of the spans, and the driven sprocket is only forced by span transverse vibration. When $p_1 \neq 0$ or $p_2 \neq 0$, there is parametric excitation of the spans and also direct excitation of the driven sprocket. To proceed with the solution of the coupled equations (87)-(89) it is necessary to identify resonant terms

for each equation. For (87), certain right hand terms are resonant to the homogeneous part under conditions of:

$$\begin{aligned} &\text{External resonance: } j\Omega_0 \approx \omega_m, \\ &\text{Primary parametric resonance: } \Omega_2 \approx 2\omega_m \text{ and/or } \Omega_0 \approx 2\omega_m, \\ &\text{Internal two-to-one resonance: } \omega_\theta \approx 2\omega_m. \end{aligned} \tag{90}$$

Similarly for (88):

$$\begin{aligned} &\text{External resonance: } j\Omega_0 \approx \tilde{\omega}_n, \\ &\text{Primary parametric resonance: } \Omega_2 \approx 2\tilde{\omega}_n \text{ and/or } \Omega_0 \approx 2\tilde{\omega}_n, \\ &\text{Internal two-to-one resonance: } \omega_\theta \approx 2\tilde{\omega}_n, \end{aligned} \tag{91}$$

and for (89):

$$\begin{aligned} &\text{External resonance: } \Omega_2 \approx \omega_\theta \text{ and/or } \Omega_1 \approx \omega_\theta, \\ &\text{Primary parametric resonance: } \Omega_2 \approx 2\tilde{\omega}_n \text{ and/or } \Omega_0 \approx 2\tilde{\omega}_n, \\ &\text{Internal two-to-one resonance: } 2\tilde{\omega}_n \approx \omega_\theta \text{ and/or } 2\omega_m \approx \omega_\theta. \end{aligned} \tag{92}$$

Thus, a multitude of resonance - and combined resonance cases exists, which involves one, two or all three degrees of freedom $q_1, \tilde{q}_1$, and ν_1. Note that for e.g. the tight span motion q_1, primary parametric and external resonance coming from polygonal action (p_0 and k_m terms) cannot exist simultaneously, since primary parametric resonance requires $\Omega_0 \approx \omega_m$, in which case the external forcing is has frequency $j\Omega_0 \approx j2\omega_m$, i.e. non-resonant. Primary parametric resonance of both spans simultaneously is practically possible when there is no torque on the driven sprocket, as in the case of a guide or coupler sprocket; under these conditions the natural frequency of the two spans will be nearly identical, and coupling could occur across the

driven sprocket if it is compliant. This case, as well as resonant transverse span excitation (k_m terms), possibly in combination with other resonant excitations, are left for future studies.

In the following we investigate three resonance cases which are of practical interest, but also demonstrate how the motions (de)couple in this model; primary parametric resonance of the tight span is treated first, then external resonance of the driven sprocket, and lastly, the two cases combined, i.e. primary parametric resonance of the tight span along with internal resonance of the driven sprocket.

5.10. Primary parametric resonance of the tight span

This example is relevant, since it demonstrates how decoupled transverse vibration of a single chain span, coming from a harmonic variation of axial tension leading to parametric resonance, could be realized in a real roller chain drive. We consider primary parametric resonance of the tight span q_1 coming from p_2. There are no other external or internal resonances, and the tight and slack span are detuned such that ω_m is away from $\tilde{\omega}_n$. For the external forcing coming from p_2, the nearness to primary parametric resonance of the tight span is quantified by a detuning parameter σ_2, such that

$$\Omega_2 = 2\omega_m + \varepsilon\sigma_2, \tag{93}$$

Inserting into (87)-(89) and requiring secular terms to vanish gives the solvability conditions:

$$2i\omega_m(A' + \mu_m A) + 3\kappa_m A^2\bar{A} + \tfrac{1}{2}\alpha_m p_2 \bar{A} e^{i\sigma_2 T_1} = 0, \tag{94}$$

$$2i\tilde{\omega}_n(\tilde{A}' + \tilde{\mu}_n\tilde{A}) + 3\tilde{\kappa}_n\tilde{A}^2\tilde{\bar{A}} = 0, \tag{95}$$

$$2i\omega_\theta(V' + \mu_\theta V) = 0, \tag{96}$$

where a prime denotes differentiation with respect to T_1. Letting

$$A = \tfrac{1}{2} a e^{i\varphi}, \quad a, \varphi \in \mathbb{R}, \tag{97}$$

$$\tilde{A} = \tfrac{1}{2} \tilde{a} e^{i\tilde{\varphi}}, \quad \tilde{a}, \tilde{\varphi} \in \mathbb{R}, \tag{98}$$

$$V = \tfrac{1}{2} v e^{i\rho}, \quad v, \rho \in \mathbb{R}, \tag{99}$$

and substituting first into (94) gives, when separating real and imaginary parts:

$$a' = -\mu_m a - \frac{1}{4\omega_m} \alpha_m p_2 a \sin \psi_2, \tag{100}$$

$$\psi_2' = \sigma_2 - \frac{3}{4\omega_m} \kappa_m a^3 + \frac{1}{2\omega_m} \alpha_m p_2 \cos \psi_2, \tag{101}$$

where

$$\psi_2 = \sigma_2 T_1 - 2\varphi. \tag{102}$$

Substituting (102), (97) and (93) into (72), then gives

$$\xi_m = a \cos(\tfrac{1}{2}\Omega_0 T_0 + \tfrac{1}{2}\psi_2) + O(\varepsilon), \tag{103}$$

from which it is seen, that in seeking a stationary response of ξ_m where the amplitude and phase does not change, we must require $a' = \psi_2' = 0$. In this case (100)-(101) has a trivial solution

$$a = 0, \quad \cos(\psi_2) = \frac{2\sigma_2 \omega_m}{\alpha_m p_2}, \tag{104}$$

that is, a solution exists for which the span does not vibrate. A non-trivial solution also exists:

$$a^2 = \frac{4\omega_m}{3\kappa_m} \left(\sigma_2 \pm \sqrt{\left(\frac{\alpha_m p_2}{2\omega_m}\right)^2 - 4\mu_m^2} \right), \quad \tan \psi_2 = \frac{2\mu_m}{\frac{4\omega_m a^2}{3\kappa_m} - \sigma_2}, \tag{105}$$

when the following conditions are fulfilled,

$$\left(\frac{\alpha_m p_2}{2\omega_m}\right)^2 \geq 4\mu_m^2 \text{ and } \sigma_2 \pm \sqrt{\left(\frac{\alpha_m p_2}{2\omega_m}\right)^2 - 4\mu_m^2} \geq 0. \tag{106}$$

For the solution of $\tilde{A}$ we substitute (98) into (95) and readily solve to find:

$$\tilde{a} = \tilde{a}_0 e^{-\tilde{\mu}_n T_1}, \tag{107}$$

$$\tilde{\varphi} = \tilde{\varphi}_0 - \frac{3\tilde{\kappa}_n \tilde{a}_0^2}{\tilde{\mu}_n T_1} e^{-2\tilde{\mu}_n T_1}, \tag{108}$$

where $\tilde{a}_0$ and $\tilde{\varphi}_0$ are arbitrary real-valued constants. Equation (107) shows that $\tilde{a} \to 0$ as $T_1 \to \infty$, since $\tilde{\mu}_n > 0$, and consequentially $\tilde{\xi}_n$ remain small under the specified loading conditions. For the driven sprocket (96) gives the solution

$$v = v_0 e^{-\mu_\theta T_1}, \tag{109}$$

$$\rho = \rho_0, \tag{110}$$

where v_0 and ρ_0 are arbitrary real-valued constants. Here equation (109) shows that $v \to 0$ as $T_1 \to \infty$, since $\mu_\theta > 0$. Therefore also the driven sprocket angular displacements u_1 remain small under the specified loading conditions.

Inserting (102) and (93) in (97)-(99) and substituting according to (93) in the oscillatory terms of (88)-(89) the solutions to (81)-(83) can be expressed as

$$\begin{aligned}\xi_m = a\cos(\tfrac{1}{2}\Omega_0 T_0 + \tfrac{1}{2}\psi_2) + \varepsilon\Bigg[&\frac{k_m}{\omega_m^2} + \frac{\alpha_m p_2 a}{16\omega_m^2}\cos(\tfrac{3}{2}\Omega_0 T_0 - \tfrac{1}{2}\psi_2) \\ &+ \frac{\alpha_m p_0 a}{\Omega_0(2\omega_m - \Omega_0)}\cos((\Omega_0 + \tfrac{1}{2}\Omega_2)T_0 - \tfrac{1}{2}\psi_2) \\ &- \frac{\alpha_m p_0 a}{\Omega_0(2\omega_m + \Omega_0)}\cos((\Omega_0 - \tfrac{1}{2}\Omega_2)T_0 + \tfrac{1}{2}\psi_2) \\ &+ \frac{\kappa_m a^3}{4\omega_m^2}\cos(\tfrac{3}{2}(\Omega_2 T_0 - \psi_2)) \\ &+ \sum_{j=1}^{\infty}\frac{2k_m}{\omega_m^2 - (j\Omega_0)^2}\cos(j\Omega_o T_0)\Bigg] + O(\varepsilon^2),\end{aligned} \tag{111}$$

$$\tilde{\xi}_n = \varepsilon\left[\frac{\tilde{k_n}}{\tilde{\omega}_n^2} + \sum_{j=1}^{\infty} \frac{2\tilde{k}_n}{\tilde{\omega}_n^2 - (j\Omega_0)^2}\cos(j\Omega_0 T_0 + \phi)\right] + O(\varepsilon^2), \tag{112}$$

$$u_1 = \varepsilon\left[\frac{2\eta_m a^2}{\omega_\theta^2} + \frac{2\eta_m a^2}{\omega_\theta^2 - \Omega_2^2}\cos(\Omega_2 T_0 - \psi_2)\right.$$
$$\left. + \frac{\omega_\theta^2 p_2}{\omega_\theta^2 - \Omega_2^2}\cos(\Omega_0 T_0) + \frac{p_1}{\omega_\theta^2 - \Omega_1^2}\cos(\Omega_1 T_0)\right] + O(\varepsilon^2). \tag{113}$$

By assuming the external excitation of the driven sprocket coming from p_2 to be non-resonant and of order $O(\varepsilon)$, as prescribed by the term $\varepsilon\omega_\theta^2 u_2$ in (70), we in effect render the driven sprocket with a zero vibratory response, i.e. the driven sprocket is not compliant to the driver sprocket excitation. For this to hold in the case where the external excitation of the driven sprocket coming from p_2 is *not* weak, but $O(1)$, the frequencies Ω_2 and ω_θ should be so far apart that the driven sprocket forced response given by $\omega_\theta^2 p_2/(\omega_\theta^2 - \Omega_2^2)\cos(\Omega_2 T_0)$ becomes $O(\varepsilon)$. With this we have demonstrated under which conditions span vibrations decouple from the remaining system, with the response being similar to the decoupled motion of an axially moving string.

5.11. Primary external resonance of driven sprocket

During normal operation of a real chain drive, the nominal (angular) velocity varies according to the desired operating conditions. As the excitation from the driver is often period with the driver nominal angular velocity, it is relevant to examine the case where the external excitation is near-resonant to the driven sprocket, $\Omega_2 \approx \omega_\theta$. The other direct and parametric excitations are assumed non-resonant. To describe the nearness of external resonance, we introduce the detuning parameter σ_θ by

$$\omega_\theta = \Omega_2 + \varepsilon\sigma_\theta. \tag{114}$$

Inserting into (87)-(89) and requiring secular to terms vanish we obtain the solvability conditions,

$$2i\omega_m(A' + \mu_m A) + 3\kappa_m A^2 \bar{A} = 0, \tag{115}$$

$$2i\tilde{\omega}_n(\tilde{A}' + \tilde{\mu}_n \tilde{A}) + 3\tilde{\kappa}_n \tilde{A}^2 \tilde{\bar{A}} = 0, \tag{116}$$

$$2i\omega_\theta(V' + \mu_\theta V) - \tfrac{1}{2}\omega_\theta^2 p_2 e^{-i\sigma_\theta} = 0, \tag{117}$$

which are decoupled. Equations (115) and (116) have the same form as (95), thus the response for ξ_m and $\tilde{\xi}_n$ will decay to zero in the stationary state. Inserting (99) into (117), and introducing

$$\psi_\theta = \sigma_\theta T_1 + \rho, \tag{118}$$

the modulation equations becomes

$$v' = -\mu_\theta v - \tfrac{1}{2}\omega_\theta p_2 \sin\psi_\theta, \tag{119}$$

$$v\psi_\theta' = v\sigma_\theta - \tfrac{1}{2}\omega_\theta p_2 \cos\psi_\theta. \tag{120}$$

Back substitution as in the previous case gives $\nu_0 = v\cos(\Omega_2 T_0 + \psi_\theta)$, from which we require $v' = \psi_\theta' = 0$ for stationary solutions. Using this in (119)-(120) we note that $v = 0$ is not a solution, and the stationary amplitude and phase are given by

$$v = \frac{1}{2}\frac{\omega_\theta p_2}{\sqrt{\mu_\theta^2 + (\omega_\theta - \Omega_2)^2}}, \quad \tan\psi_\theta = \frac{-\mu_\theta}{\omega_\theta - \Omega_2}. \tag{121}$$

With $A = \tilde{A} = 0$ and V given by (99) with (121)-(121) and (118), the solution of (87)-(89) and (81)-(83) becomes

$$\xi_m = \varepsilon\Big[\frac{k_m}{\omega_m^2} + \sum_{j=1}^{\infty} \frac{2k_m}{\omega_m^2 - (j\Omega_0)^2} \cos(j\Omega_o T_0) + O(\varepsilon^2)\Big], \tag{122}$$

$$\tilde{\xi}_n = \varepsilon\Big[\frac{\tilde{k_n}}{\tilde{\omega}_n^2} + \sum_{j=1}^{\infty} \frac{2\tilde{k}_n}{\tilde{\omega}_n^2 - (j\Omega_0)^2} \cos(j\Omega_0 T_0 + \phi) + O(\varepsilon^2)\Big], \tag{123}$$

$$u_1 = v\cos(\Omega_2 T_0 + \psi_\theta) + \varepsilon\Big[\frac{p_1}{\omega_\theta^2 - \Omega_1^2}\cos(\Omega_1 T_0)\Big] + O(\varepsilon^2). \tag{124}$$

This case demonstrates that for-near resonant excitation of the driven sprocket there will be no transverse vibrations of the spans, if the excitation frequency is not near primary parametric resonance of the spans. However, this is under the assumption that the parametric excitation of the chain spans is small compared to the linear axial stiffness of the chain spans, as assumed in (68)-(69), which might not be fulfilled under large resonant vibrations of the driven sprocket. However, in real chain drives, the ratio between linear axial stiffness and parametric excitation can be decreased by increasing the pretension P_{tot}. We note from (121) that, with the present model, rotational damping of the driven sprocket is the only mechanism which will limit the response of the driven sprocket subjected to resonant excitation. For a real roller chain drive this case indicates that for a chain drive in operation, passing a natural frequency of the driven sprocket does not lead to transverse span vibrations if the excitation is not near parametric resonance of the spans, and that rotational damping of the driven sprocket may reduce the resonant response.

5.12. Combined parametric and internal resonance between span and sprocket

In the first example (section 5.10) we analyzed the span response when the driven sprocket is not compliant, i.e. the driver excitation let to a

vibratory response of the chain span only. The second example (section 5.11) demonstrated the response in the case where the driver excitation caused a vibratory response of the driven sprocket only. Here we analyze the case where the driver excitation may cause a vibratory response of both the driven sprocket and the chain span. This is both of practical interest, and novel to the study of the dynamics of axially moving strings.

Thus we consider primary parametric excitation of the tight span $\Omega_2 \approx 2\omega_m$ combined with internal two-to-one resonance between span and the driven sprocket $\omega_\theta \approx 2\omega_m$. All remaining excitations are assumed non-resonant, and the two spans are detuned by loading of the driven sprocket, such that ω_m is away from $\tilde{\omega}_n$. To describe the nearness to primary parametric resonance we introduce the detuning parameter σ_2 defined by (93). Similarly, to describe the nearness to internal resonance we introduce the detuning σ_θ defined by

$$\omega_\theta = 2\omega_m + \varepsilon\sigma_\theta. \tag{125}$$

Inserting into (87)-(89) and equating to zero the resulting secular terms gives the solvability conditions,

$$2i\omega_m(A' + \mu_m A) + 3\kappa_m A^2\bar{A} - \alpha_m \bar{A} V e^{i\sigma_\theta T_1} + \tfrac{1}{2}\alpha_m p_2 \bar{A} e^{i\sigma_2 T_1} = 0, \tag{126}$$

$$2i\tilde{\omega}_n(\tilde{A}' + \tilde{\mu}_n\tilde{A}) + 3\tilde{\kappa}_n\tilde{A}^2\bar{\tilde{A}} = 0, \tag{127}$$

$$2i\omega_\theta(V' + \mu_\theta V) - \eta_m A^2 e^{-i\sigma_\theta T_1} - \tfrac{1}{2}\omega_\theta^2 p_2 e^{i(\sigma_2 - \sigma_\theta)T_1} = 0. \tag{128}$$

The condition for $\tilde{A}$ is decoupled, and when represented in polar form (95) the solution is given by (107)-(108), showing that $\tilde{A} \to 0$ as $T_1 \to \infty$. The two other conditions are coupled. Using (97) and (99) the modulation

equations (126) and (128) becomes:

$$a' = -\mu_m a - \Lambda_1 a v \sin\psi_1 - f_1 a \sin\psi_2, \tag{129}$$

$$v' = -\mu_\theta v + \Lambda_2 a^2 \sin\psi_1 - f_2 \sin(\psi_2 - \psi_1), \tag{130}$$

$$a\varphi' = \Lambda_0 a^3 + \Lambda_1 a v \cos\psi_1 + f_1 a \cos\psi_2, \tag{131}$$

$$v\rho' = \Lambda_2 a^2 \cos\psi_1 + f_2 \cos(\psi_2 - \psi_1), \tag{132}$$

where

$$\psi_1 = \sigma_\theta T_1 - 2\varphi + \rho, \tag{133}$$

$$\psi_2 = \sigma_2 T_1 - 2\varphi, \tag{134}$$

$$\Lambda_0 = \frac{3\kappa_m}{8\omega_m},\ \Lambda_1 = \frac{-\alpha_m}{4\omega_m},\ \Lambda_2 = \frac{-\eta_m}{4\omega_\theta},\ f_1 = \frac{\alpha_m p_2}{4\omega_m},\ f_2 = -\tfrac{1}{2}\omega_\theta p_2. \tag{135}$$

Back substitution gives $q_0 = a\cos(\frac{1}{2}\Omega_2 T_0 - \frac{1}{2}\psi_2)$ and $\nu_0 = v\cos(\Omega_2 T_0 + \psi_2 - \psi_1)$. Thus, for stationary solutions of (129)-(132) we require $a' = v' = \psi_1' = \psi_2' = 0$, which with (133)-(134) gives the equations governing stationary amplitudes:

$$0 = -\mu_m a - \Lambda_1 a v \sin\psi_1 - f_1 a \sin\psi_2, \tag{136}$$

$$0 = -\mu_\theta v + \Lambda_2 a^2 \sin\psi_1 - f_2 \sin(\psi_2 - \psi_1), \tag{137}$$

$$\tfrac{1}{2} a\sigma_2 = \Lambda_0 a^3 + \Lambda_1 a v \cos\psi_1 + f_1 a \cos\psi_2, \tag{138}$$

$$v(\sigma_2 - \sigma_\theta) = \Lambda_2 a^2 \cos\psi_1 + f_2 \cos(\psi_2 - \psi_1). \tag{139}$$

There is a trivial solution given by,

$$a = 0, \quad v^2 = \frac{f_2^2}{\mu_\theta^2 + (\sigma_2 - \sigma_\theta)^2}, \quad \tan(\psi_2 - \psi_1) = \frac{\mu_\theta}{\sigma_\theta - \sigma_2}, \tag{140}$$

Representing pure rotational motion of the driven sprocket without transverse vibrations of the upper span, as examined in section 5.11. As for

non-trivial solutions $a \neq 0$, corresponding to coupled motions of the driven sprocket and the tight span, the algebraic set of nonlinear equations (136)-(139) are not readily solved for a and v; here we must rely on numerical solution.

6. Example results of the dynamic analysis

To illustrate results of the above three resonance cases, we present solutions for a specific chain drive, using configuration C_1 in Table 1 with pitch $p = 0.0254$ m, and mass, stiffness, damping and loading parameter values as listed in Table 2. We consider the first mode $m = 1$. With a stationary angular velocity of the driver of 400 rpm there will then be internal resonance between the tight span and the driven sprocket.

Table 2: Dynamic parameters

P_{tot}	1000	N
EA	0.56e6	N
ρA	2.61	kg/m
$\hat{J}_1$	0.6	kg m^2
$\hat{f}_1$	200	N
$\hat{d}_1$	1.1	Nms/rad
θ_2^*	0.005	rad
μ_θ	0.02	
μ_m	0.02	

6.1. Parametric resonance of the tight span

Here we present an example of the results derived in section 5.10 for the response of the tight span under primary parametric excitation. The

analysis demonstrated that the tight span transverse motion decouples, because the driven sprocket is non-compliant. The solution for the steady state span vibration amplitude a given by (105) is shown in Figure 6 along with numerical solutions of the modulation equations (100)-(101) shown with circles $\circ$. Broken and full lines identifies stable and unstable solution states, respectively.

The resonance peak near $\Omega_2/\omega_m = 2$ bends to the right due to non-linear hardening coming from increased axial tension at large amplitudes, represented by the cubic nonlinearity in the model. Increased parametric excitation amplitude p_2 and decreased damping μ_m widens the resonance peak. It is seen that as the upper branch bends to the right, there are two co-existing stable solutions; one with zero amplitude and another with a large amplitude. Since this is a non-linear response, the solution to which the system converges depends on the initial conditions, which for the numerical solutions were chosen at random, to demonstrate the presence of coexisting solution branches.

In real chain drives, adjusting the span tension to change the natural frequency of the span can be used as an approach to ensure that the the span does not operate near the critical excitation frequencies.

6.2. Resonant excitation of driven sprocket

The solution for the driven sprocket steady state amplitude v given by (121) is shown in Figure 7 for the resonant excitation of the driven sprocket, as analyzed in section 5.11. Near $\Omega_2/\omega_\theta = 1$ there is a clearly defined maximum amplitude. The analysis showed that increased damping reduces the height of the resonance peak.

In this example the sprocket motion decouples since the spans are ten-

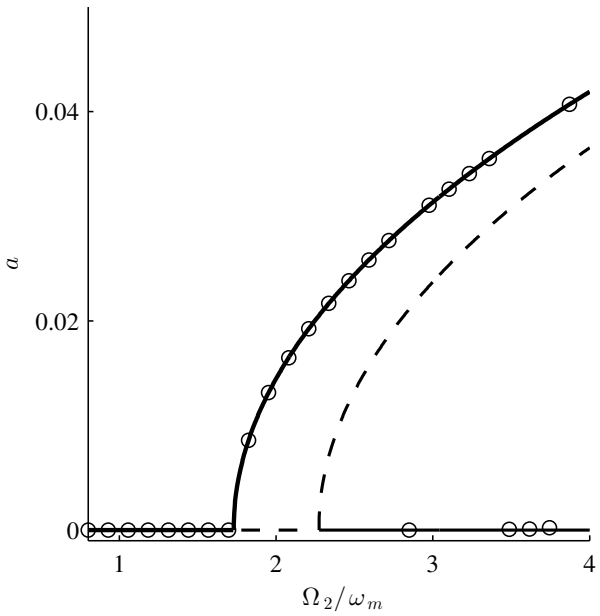

Figure 6: The tight span transverse vibration amplitude a at primary parametric resonance according to perturbation results (105) (solid lines stable, dashed line unstable), and numerical solution of the modulation equations (100)-(101) (circles).

sioned to prevent transverse vibration. Therefore, the response is essentially linear, and the numerical solution confirms there is only a single, independent of initial conditions. The analysis presupposes that the parametric excitation amplitude of the spans is small compared to the span linear stiffness, and the solution is only a good approximation when these conditions are fulfilled; they could be violated during large resonant vibration amplitudes of the driven sprocket, which should therefore still be avoided in real roller chain drives.

6.3. Combined parametric resonance and internal resonance

The combination of internal resonance and parametric resonance was investigated in section 5.12. The solution for the span and sprocket steady state response is obtained through numerical integration of the modulation

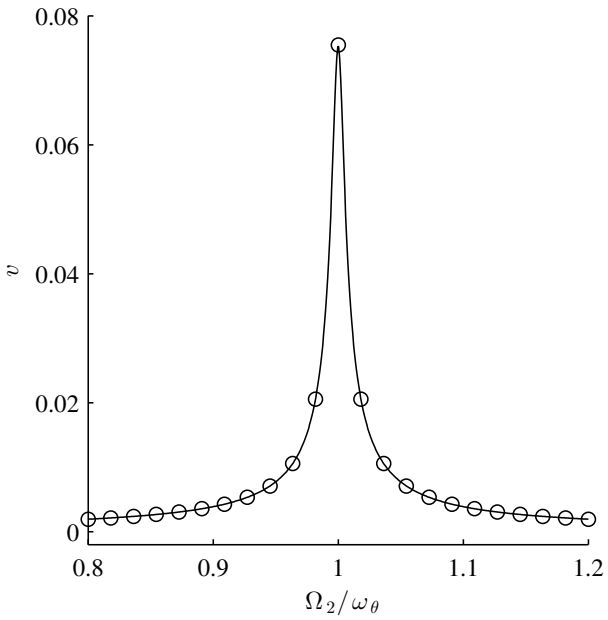

Figure 7: The driven sprocket angular vibration amplitude v at resonant direct external excitation according to the perturbation results (121) (solid line), and numerical solutions of the modulation equations solutions (119)-(120) (circles).

equations (129)-(132). Results for the stationary amplitudes a of the span and v of the driven sprocket are shown in Figures 8 and 9, respectively. In these figures exact parametric resonance occurs for $\sigma_2 = 0$, and exact internal resonance occurs on the line running diagonally across the graphs where $\sigma_\theta = \sigma_2$. Figure 8(a) shows three projections of the span vibration amplitude for three values of the detuning of internal resonance σ_θ, as indicated by bold lines in Figure 8(b). First we point to the qualitative and quantitative similarity between the bended resonance peak in the response of the decoupled span motion in Figure 6 and the response drawn with solid bold lines for $\sigma_\theta/\omega_m = -1.9$ in Figure 8(a) and at the edge of Figure 8(b). For $\sigma_\theta/\omega_m = -1.9$ the amplitude a is zero until $\sigma_2/\omega_m > -0.3$. For $\sigma_2/\omega_m > 0.5$ the stationary amplitude jumps between two solution states. This is similar to what is shown in Figure 6, where the span motion was decoupled, and

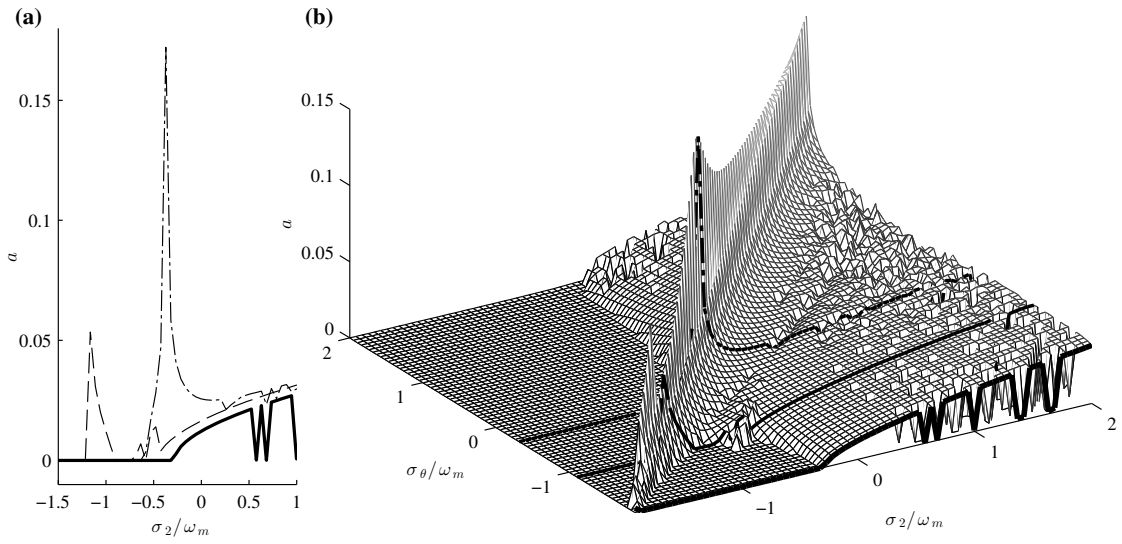

Figure 8: Span transverse vibration a under combined primary parametric resonance and internal resonance obtained by integration of the modulation equations (129)-(132). In (a) cross sections of (b) for values $\sigma_\theta/\omega_m \simeq [-1.9,\ -1.1,\ -0.3]$ are shown with lines $[-,\ --,\ -\cdot-]$, respectively.

it also appears from Figure 8 that for $\sigma_2/\omega_m > 0.5$ there are two coexisting solutions between which the response jumps between depending on the initial conditions.

Secondly, we observe in Figure 8 that there is a large upright amplitude peak running diagonally across Figure 8(b) near exact internal resonance $\sigma_\theta = \sigma_2$. As $\sigma_\theta/\omega_m = \sigma_m/\omega_m$ increase from below to approach zero, the upright resonant peak combines with the bended resonance peak and the amplitude reaches maximum for $\sigma_\theta/\omega_m = \sigma_m/\omega_m \simeq -0.3$. The upright peak is present for values of σ_2/ω_m much lower than zero, and the upright and bended resonance peaks are separated for $\sigma_\theta/\omega_m < -1.1$. This indicate that when the driven sprocket is compliant, chain span vibrations excited by parametric excitation can occur for much lower values of σ_2/ω_m than when the span is decoupled, which is a significant and novel result. In real

chain drives, this means that span transverse vibration can be excited at frequencies lower than parametric resonance when the driven sprocket has a vibratory response.

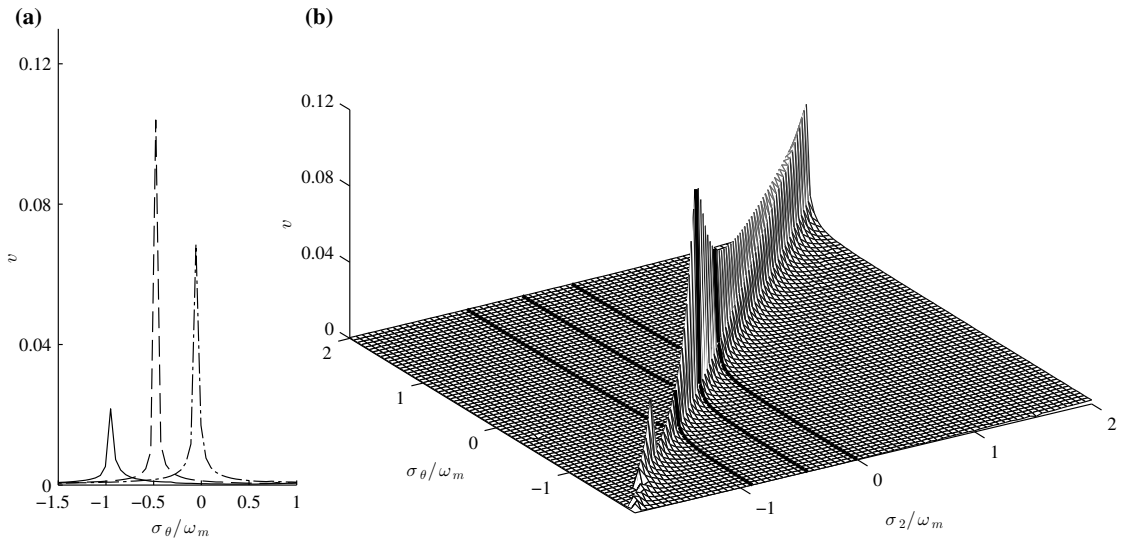

Figure 9: Driven sprocket angular vibration v under combined parametric and internal resonance obtained by integration of the modulation equations (129)-(132). In (a) cross sections of (b) for values $\sigma_2/\omega_m \simeq [-0.9,\ -0.5,\ 0]$ are shown with lines $[-,\ --,\ -\cdot-]$, respectively.

Figure 9(a) shows three projections of the driven sprocket amplitude for three values of the detuning of parametric resonance σ_2 indicated with bold lines in Figure 9(b). We observe a qualitative and partly quantitative similarity to the upright resonance peak in the response of driven sprocket motion in Figure 7 and the cross sections in Figure 9(a). The maximum value of v is observed for $\sigma_2/\omega_m \simeq -0.5$.

In both Figure 8(b) and 9(b) we observe an amplitude peak around $\sigma_\theta/\omega_m = \sigma_2/\omega_m \simeq -1.5$. The explanation for this may require further analysis. For all the presented examples we note that the response is obtained using a perturbation method assuming near-resonance. Thus, predictions

will be most accurate near $\sigma_\theta = \sigma_m = 0$.

7. Conclusion(s)

1. A kinematic model of a two-sprocket roller chain drive with straight spans was presented, along with a procedure for calculating the total chain wrapping length. Analytical predictions were compared to multibody simulation results and demonstrated that the total wrapping length of the chain generally varies periodically with the tooth frequency. The chain wrapping length was shown to be constant for a configuration where both sprockets have the same number of teeth and the chain consists of an even number of chain links.
2. Since the chain wrapping length generally varies during rotation of the sprockets, it is hypothesized (and left for future studies) that careful positioning of more than two sprockets can be done so as to attenuate or amplify the effect of a variable wrapping length.
3. Deriving the equations of motion for the chain spans we treated the problem of an axially moving string supported by moving boundaries, and showed that a first order variable string length leads to a second order effect.
4. We presented a new dynamic model for the coupled motion of the tight chain spans transverse vibration and the driven sprocket angular displacement. The model assumed the presence of a steady operation state from which displacements are measured.
5. The dynamic model provides insight into resonance conditions and amplitude responses, and was analyzed approximately using a mode shape expansion and perturbation analysis.

6. Three example results of the dynamic analysis were presented, illustrating the conditions where the motions of the span and sprockets decouple. Results for a case of combined internal and parametric resonance showed that large span vibrations can occur due to compliance of the driven sprocket.
7. Though the model is simple, it provides useful insight into the coupled dynamics of chain drives, and may aid the design and interpretation of numerical and experimental results.
8. Due to the systematic structure of multiple scales analysis presented here, where the modulation equations decouple for non-resonant excitation, it is expected that the dynamics of chain drives with more than two sprockets could be analyzed using a similar modeling and analysis approach. In the analysis presented here, the coupled motion of transverse span vibrations happens across a single degree of freedom oscillator, which is the driven sprocket with a given natural frequency. For a larger chain drive with more sprockets, this would correspond to modal excitation near the natural frequencies of the coupled rotational motion of the sprockets with the spans acting as linear springs.

References

[1] K. W. Wang and S. P. Liu. On the noise and vibration of chain drive systems. *The Shock and Vibration Digest*, 23(4):8–13, 1991.

[2] G. M. Bartlett. Roller chain drives in theory and practice. *Product Engineering*, 2(4):253–255, 1931.

[3] R. A. Morrison. Polygonal action in chain drives. *Machine Design*, 24 (9):155–159, 1952.

[4] Raymond Charles Binder. *Mechanics of the Roller Chain Drive: Based on Mathematical Studies by RC Binder*. Prentice-Hall, 1956.

[5] G. Bouillon and G. V. Tordion. On polygonal action in roller chain drives. *Journal of Engineering for Industry*, 87(2):243–250, 1965.

[6] C. K. Chen and F. Freudenstein. Toward a more exact kinematics of roller chain drives. *Journal of Mechanisms Transmissions and Automation in Design*, 110(3):269–275, 1988.

[7] N. Fuglede and J. J. Thomsen. Kinematics of roller chain drives - exact and approximate analysis. *Submitted for Journal Publication*, 2014.

[8] S. L. Pedersen, J. M. Hansen, and J. A. C. Ambrosio. A roller chain drive model including contact with guide-bars. *Multibody System Dynamics*, 12(3):285–301, 2004.

[9] S. L. Pedersen. Model of contact between rollers and sprockets in chain-drive systems. *Archive of Applied Mechanics*, 74(7):489–508, 2005.

[10] A. L. Thurman and C. D. Mote, Jr. Free periodic nonlinear oscillation of an axially moving strip. *Journal of Applied Mechanics*, 36(1):83–91, 1969.

[11] C. D. Mote, Jr. and A. L. Thurman. Oscillation modes of an axially moving material. *Journal of Applied Mechanics*, 38(1):279–280, 1971.

[12] L. Meirovitch. A new method of solution of the eigenvalue problem for gyroscopic systems. *AIAA Journal*, 12(10):1337–1342, 1974.

[13] L. Meirovitch. Modal analysis for response of linear gyroscopic systems. *Journal of Applied Mechanics*, 42(2):446–450, 1975.

[14] J. A. Wickert and C. D. Mote, Jr. Classical vibration analysis of axially moving continua. *Journal of Applied Mechanics*, 57(3):738–744, 1990.

[15] J. A. Wickert. Nonlinear vibration of a traveling tensioned beam. *International Journal of Non-Linear Mechanics*, 27(3):503–517, 1992.

[16] E. M. Mockensturm, N. C. Perkins, and A. G. Ulsoy. Stability and limit cycles of parametrically excited, axially moving strings. *Journal of Vibration and Acoustics*, 118(3):346–351, 1996.

[17] Li-Qun Chen. Analysis and control of transverse vibrations of axially moving strings. *Applied Mechanics Review*, 58(2):91–116, 2005. ISSN 00036900, 10888535.

[18] R. G. Parker and Y. Lin. Parametric instability of axially moving media subjected to multifrequency tension and speed fluctuations. *Journal of Applied Mechanics*, 68(1):49–57, 2001.

[19] J. A. Wickert and C. D. Mote, Jr. Current research on the vibration and stability of axially-moving materials. *The Shock and Vibration Digest*, 20(5):3–13, 1988.

[20] S. Mahalingam. Transverse vibrations of power transmission chains. *British Journal of Applied Physics*, 8(4):145–148, 1957.

[21] S. Mahalingam. Polygonal action in chain drives. *Journal of The Franklin Institute*, 265(1):23–28, 1958. ISSN 00160032.

[22] S. T. Ariaratnam and S. F. Asokanthan. Dynamic stability of chain drives. *Journal of Mechanisms Transmissions and Automation in Design*, 109(3):412–418, 1987.

[23] K. W. Wang and Jr. Mote, C. D. Vibration coupling analysis of band/wheel mechanical systems. *Journal of Sound and Vibration*, 109 (2):237–258, 1986. ISSN 0022460x, 10958568.

[24] K. W. Wang. On the stability of chain drive systems under periodic sprocket oscillations. *Journal of Vibration and Acoustics*, 114(1):119–126, 1992.

[25] R.C. Binder and W.V. Covert. Impact between chain roller and sprocket in chain drive. *Franklin Institute – Journal*, 245(4):319–329, 1948.

[26] G. K. Ryabov. Inertia effects of impact loading in chain drives. *Russian Engineering Journal*, 48(8):17–19, 1968.

[27] J. N. Fawcett and S. W. Nicol. Vibration of a roller chain drive operating at constant speed and load. *Proceedings of the Institution of Mechanical Engineers*, 194:97–101, 1980.

[28] J. C. Conwell and G. E. Johnson. Experimental investigation of link tension and roller-sprocket impact in roller chain drives. *Mechanism and Machine Theory*, 31(4):533–544, 1996.

[29] K. W. Wang, S. P. Liu, S. I. Hayek, and F. H. K. Chen. On the impact intensity of vibrating axially moving roller chains. *Journal of Vibration and Acoustics*, 114(3):397–403, 1992.

[30] G K Ryabov and A V Kryukov. Shock loads in chain transmissions. *Russian Engineering Research*, 17(6):15, 1997.

[31] S. P. Liu, K. W. Wang, S. I. Hayek, M. W. Trethewey, and F. H. K. Chen. A global-local integrated study of roller chain meshing dynamics. *Journal of Sound and Vibration*, 203(1):41–62, 1997.

[32] H. Zheng, Y. Y. Wang, G. R. Liu, K. Y. Lam, K. P. Quek, T. Ito, and Y. Noguchi. Efficient modelling and prediction of meshing noise from chain drives. *Journal of Sound and Vibration*, 245(1):133–150, 2001.

[33] Mohammad R. Naji and Kurt M. Marshek. Analysis of sprocket load distribution. *Mechanism and Machine Theory*, 18(5):349–356, 1983.

[34] Mohammad R. Naji and Kurt M. Marshek. Effects of the pitch difference on the load ditribution of a roller chain drive. *Mechanism and Machine Theory*, 24(5):351–362, 1989.

[35] Mahn Shik Kim and Glen E. Johnson. Mechanics of roller chain-sprocket contact: a general modelling stragegy. *American Society of Mechanical Engineers, Design Engineering Division (Publication) DE*, 43(2):689–695, 1992.

[36] L. Meirovitch. *Fundamentals of Vibrations*. McGraw-Hill Higher Education, 2001.

[37] Cornelius Lanczos. *The variational principles of mechanics*. University of Toronto Press, 1966.

[38] J. A. Wickert and C. D. Mote, Jr. On the energetics of axially moving continua. *Journal of the Acoustical Society of America*, 85(3):1365–1368, 1989.

[39] W. D. Zhu and J Ni. Energetics and stability of translating media with an arbitrarily varying length. *Journal of Vibration and Acoustics*, 122 (3):295–304, 2000.

P3 Publication 3

The following abstract [P3] was submitted to and presented at the 3rd International Conference on Vibro Impact Systems and Systems with Non-smooth Interactions (ICOVIS 2013) held in Leinsweiler, Germany, July 2013. It reports on the results of the kinematic analysis and the treatment of the boundaries as non-smooth functions.

Roller chain drive vibration analysis based on a string model with boundaries moving non-smoothly

N. Fuglede[1,*] **and J. J. Thomsen**[1]

[1] Department of Mechanical Engineering, Technical University of Denmark, Building 404, DK-2800, Lyngby, Denmark, *nfug@mek.dtu.dk

A general kinematic analysis of roller chain drives is presented. We analyze the inherent non-smooth properties of chain drives, which causes impact loading of the drive components. Chain span vibrations are then analyzed by considering the chain as a string, forced by boundaries moving non-smoothly as determined by the kinematic analysis. Resonance phenomena are identified, and conclusions about critical operation parameters such as pretension, axial velocity, and impact frequency are presented.

General kinematic analysis of roller chain drives

Chains wrapped around sprockets form polygons rather than circles. This introduce several effects, collectively known as *polygonal action*. Some of these effects are less desirable, e.g. non-smooth transfer of torques between sprockets, and impact between chain rollers and sprockets during meshing. By modeling the sprockets as polygons, and the chain drive as a four-bar mechanism, the configurations are determined for which a) a roller loses contact with the driven sprocket, and b) a roller gets in contact with the driving sprocket. It is shown how the span endpoints move discontinuously in time, leading to impulsive loading as rollers are released into- or removed from the free span. When the driver sprocket rotates at constant speed, the driven sprocket speed and acceleration is shown to generally vary discontinuously in time, leading to a non-smooth excitation of the drive system. The analysis is carried out analytically, and main parameters are shown to be shaft center distance and pitch fraction.

Vibrations of axially moving strings supported by moving boundaries

Vibrations of a chain span are analyzed approximately by modeling the chain as an axially moving string, supported by boundaries moving as prescribed by the above mentioned kinematic analysis. The equation governing transverse string vibrations is nonlinear due to axial stretching with gyroscopic terms, and parametric as well as external excitation. By employing a single-mode approximation in terms of velocity dependent mode shapes, the response is approximated using The Method of Multiple Scales. The external loading is described as a temporal Dirac pulse train. This makes it possible to describe analytically the response of the string subjected to periodic impact loading.

Currently work is in progress to include the effects of modal coupling, internal resonance and dissipation of impact energy into higher modes, using a two-mode approximation. Furthermore, we intend to study the case where excitation frequencies are much higher than the underdamped natural frequencies, which is relevant for chain drives operating at high speeds of revolution. This analysis will be carried out using The Method of Direct Partition of Motion; it should give insight into how system properties such as stiffness, natural frequencies and stability change under this type of excitation.

February 14th 2013

P4 Publication 4

The following extended abstract [P4] was submitted and presented at the 1st International Colloquium on Time-periodic Systems, Current trends in theory and application (EUROMECH 532) held in Darmstadt, Germany, August 2012. It reports on analyzing the dynamics of an axially moving string supported by moving boundaries. At this point the expansion utilized complex mode shapes obtained as eigen solutions to the gyroscopic system.

EUROMECH 532 – 1st International Colloquium on Time-periodic Systems
Current trends in theory and application, TU Darmstadt, Germany, August 27–30, 2012

Vibrations of axially moving strings with in-plane oscillating supports

N. Fuglede[1,*] **and J. J. Thomsen**[1]

[1] Department of Mechanical Engineering, Technical University of Denmark, Building 404, DK-2800, Lyngby, Denmark, *nfug@mek.dtu.dk

Abstract

For a traveling string moving in the plane we analyze analytically the transverse vibrations arising from oscillation of the string supports. Of special interest is the excitation typical of roller chain drives, where meshing between chain and sprockets cause both noise and vibration. Considering a uniform, heavy string moving at subcritical speed with prescribed endpoint motion, and ignoring longitudinal inertia, one obtains a continuous, nonlinear, gyroscopic, parametrically and externally excited system. By employing a single-mode approximation, using velocity dependent mode shapes, the system response is approximated using the method of multiple scales. Vibrations from support oscillations characteristic of roller chain drives are investigated. Conclusions about critical values for chain drive parameters such as pretension and meshing frequency are sought and identified.

INTRODUCTION

Research in the field of axially moving strings has been motivated by applications like chain saws, belt drives, roller chains and fibre winding. Fluctuation of transport speed and string tension both leads to parametric excitation. Usually mono-frequency excitation has been considered, but meshing impacts, attached machinery and crankshaft powered drives may introduce multifrequency excitation [1]. The discrete nature of chain drives introduce effects known as polygonal action [2]. In this work we recognize that polygonal action leads to combined non-smooth longitudinal and transverse excitation, corresponding to parametric and direct excitation, respectively, of transverse string vibration. A model is presented capable of including these effects by prescribing the positions of the string endpoints in the plane. The formulation utilizes velocity dependent mode shapes and analysis of nonlinear effects is done using the method of multiple scales. For a comprehensive review of research on transverse vibrations of axially moving strings see e.g. [3].

MATHEMATICAL MODEL

Figure 1a shows meshing between a roller chain and a sprocket. Relative velocity between the impact roller and the tangential velocity of the sprocket causes impact, which is a significant source of noise and vibration. A mathematical model is formulated in order to analyze transverse vibration arising from this type of excitation. Figure 1b shows a uniform string with mass per unit length ρA, axial stiffness EA moving with constant velocity V between supports positioned in the inertial coordinate system (X, Y) at $\big(\tilde{x}_0(\tilde{t}), \tilde{y}_0(\tilde{t})\big)$ and $\big(\tilde{x}_L(\tilde{t}), \tilde{y}_L(\tilde{t})\big)$. Transverse and longitudinal deformations are given by (U, W) in (X, Y)-directions, respectively.

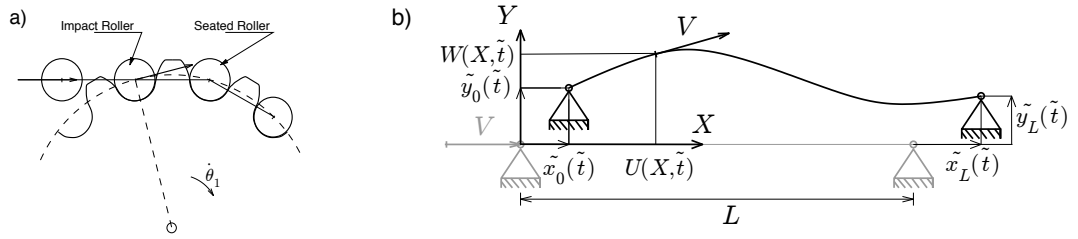

Figure 1. a) Meshing between chain and sprocket. The discrete nature of a chain leads to non-smooth contact between the chain roller and sprocket. b) Tensioned string traveling longitudinally between two supports moving in the plane. Shown in grey is the undeformed string moving between stationary supports.

The equation of motion is formulated using Hamilton's principle. Since finite amplitude vibration response during resonant excitation is of interest, the mathematical model is formulated using the approximate nonlinear strain measure

$$\epsilon(X,T) = U_X + \frac{1}{2}W_X^2. \tag{1}$$

In a roller chain, wear affects chain tension, and therefore pretension $P_0 > 0$ is an important parameter, defined here as the tension of the undeformed stationary string. The potential energy for the string can be formulated using the approximate strain measure and the pretension. Kinetic energy is formulated using the transverse- and longitudinal velocity components of a string element $V_1 = V(1+U_X) + U_{\tilde{t}}$ and $V_2 = VW_X + W_{\tilde{t}}$, valid for small $|U_X|$, $|W_X|$, where $(\cdot)_{X,T}$ denotes partial differentiation with respect to X, T, respectively. Requiring the virtual displacements to be kinematically admissible means that their variation is zero at the supports where motion is specified, i.e. $\delta U|_0^L = \delta W|_0^L = 0$. Therefore, virtual work at the supports become zero and Hamilton's principle can be applied in its standard form. The actual work done by the reaction forces are not zero, the system is non-conservative, and the support conditions classify as rheonomic. The non-dimensional equations of motion governing longitudinal and transverse vibration become, respectively,

$$\tilde{u}_{tt} + 2v\tilde{u}_{xt} + v^2 u_{xx} - \mu(u_x + \tfrac{1}{2}\tilde{w}_x^2)_x = 0, \tag{2}$$

$$\tilde{w}_{tt} + 2v\tilde{w}_{xt} + v^2 w_{xx} - \left[\left(1 + \mu(\tilde{u}_x + \tfrac{1}{2}\tilde{w}_x^2)\right)\tilde{w}_x\right]_x = 0 \tag{3}$$

with dimensionless parameters

$$x, \tilde{u}, \tilde{w} = \frac{X, U, W}{L}, \quad t = \sqrt{\frac{P_0}{\rho A L^2}}\tilde{t}, \quad \bar{v} = V \Big/ \sqrt{\frac{P_0}{\rho A}}, \quad \mu = \frac{EA}{P_0} \tag{4}$$

and inhomogeneous support conditions

$$\tilde{u}(0,t) = x_0(t), \quad \tilde{u}(1,t) = x_1(t), \quad \tilde{w}(0,t) = y_0(t), \quad \tilde{w}(1,t) = y_1(t), \tag{5}$$

$$x_0, x_1, y_0, y_1 = \left(\tilde{x}_0, \tilde{x}_L, \tilde{y}_0, \tilde{y}_L\right) L^{-1}. \tag{6}$$

In the case where transverse wavespeed $v_0 = \sqrt{P_0/\rho A}$ is much lower than longitudinal wave speed $c = \sqrt{E/\rho}$, changes in tension $N(x,t) = 1 + \mu(\tilde{u}_x + \frac{1}{2}\tilde{w}_x^2)$ propagates nearly instantaneously and dynamic tension can be approximated as being independent of x. Utilizing this by requiring $N_x = 0$ leads to $\epsilon_x = 0$, and integration of (1) from 0 to x with respect to x and use of the support conditions leads to a solution of (2), thus neglecting longitudinal inertia. The strain independent of x is found by integrating (1) over the interval. Support conditions for (3) are made homogeneous by introducing the transformation $\tilde{w}(x,t) = w(x,t) + y_0(t)\big(1-x\big) + y_1(t)$. Inserting this and the time dependent strain into (3) yields

$$w_{tt} + 2vw_{xt} - (1-\bar{v}^2)w_{xx} - \mu\big[p(t) + \frac{1}{2}\int_0^1 \tilde{w}_x^2 dx\big]w_{xx} = f(x,t) \tag{7}$$

where

$$p(t) = x_1(t) - x_0(t) + \frac{1}{2}\big(y_0(t) + y_1(t)\big)^2, \tag{8}$$

$$f(x,t) = -y_{0,tt}(t)\big(1-x\big) - y_{1,tt}(t) - 2v\big(y_{1,t}(t) - y_{0,t}(t)\big) \tag{9}$$

and boundary (support) conditions for (7) are $w(0,t) = w(1,t) = 0$. Equation (7) governs the transverse motion of the string. It is a second order partial differential equation which is non-linear due to effects of longitudinal stretching, parametrically excited from longitudinal support motion and directly excited due to transverse support motion.

ANALYSIS

Linear solution

The analysis of (7) is carried out using eigenvalues and eigenvectors obtained from the corresponding linear unforced system; $\lambda_n = i\omega_n = in\pi(1-v^2), \psi_n = \frac{1}{n\pi\sqrt{1-v^2}}e^{in\pi vx}\sin(n\pi x)$, where $i = \sqrt{-1}$ is the imaginary unit [5]. Velocity dependent eigenpairs are chosen because the (non-dimensional) transport speed $\bar{v}$ depends on pretension, which may decrease significantly due to chain wear, thus affecting chain tension. Furthermore, the Coriolis acceleration is proportional to $\bar{v}$ and therefore has an increased significance as pretension is reduced.

Nonlinear perturbation analysis

An approximate solution of (7) valid for small nonlinearity and parametric excitation is determined using a single term Galerkin approximation based on the n'th (complex) mode. As is customary, [1], the system is analyzed in state space formulation, with $\mathbf{v} = \{w_t, w\}^T$. Introducing the excitation vector $\mathbf{q} = \{f, 0\}^T$ and using the standard notation [5] the equation of motion (7) becomes

$$\mathbf{A}\mathbf{v}_t + \mathbf{B}\mathbf{v} + \varepsilon\mathbf{C}(\mathbf{w})\mathbf{v} = \mathbf{q} \tag{10}$$

where the non-standard nonlinear matrix operator is defined as

$$\mathbf{C} = \begin{bmatrix} 0 & Q\big(p(t) + N(w_x)\big) \\ 0 & 0 \end{bmatrix} \quad \text{with} \quad Q = -\mu\frac{\partial^2}{\partial x^2}, \quad N(w_x) = \frac{1}{2}\int_0^1 w_x^2 dx. \tag{11}$$

For $\varepsilon \ll 1$ an approximate solution of (10) is sought using the method of multiple scales.

RESULTS

The aim of the analysis is to obtain approximate analytical solutions for the frequency response and resulting stability properties. Periodic support motion is analyzed by decomposing parametric and direct excitation terms into spectral components using (truncated) Fourier series. Solutions are sought for support motion such as

$$x_0 = r_1 \sin(\Omega t),\ y_0 = r_1 \cos(\Omega t) \quad x_1 = r_2 \sin(\Omega t + \varphi),\ y_1 = r_2 |\cos(\Omega t + \varphi)|. \tag{12}$$

Load case (12) represents the typical case where a chain roller experiences smooth motion when it enters the free span at $x = 0$ (looses contact with a sprocket) and impact as it leaves the free span at $x = L$ (gets in contact with the sprocket). Two events generally happening out of phase. In this case, a one term Fourier decomposition of (8) gives frequency components of both Ω and 2Ω. This combined with direct excitation (9) of frequency Ω may lead to parametric amplification. Similar types of support motion introduce cases of combination resonance. Using such examples, relevant conclusions for safe operation of roller chain drives are sought, e.g. critical excitation- frequencies, motion patterns and pretension effects.

Physical approximations will be tested against simulation software for detailed chain drive simulation. If possible, results will also be tested using commercially available simulation software for analyzing chain drives. Mathematical approximations will be tested by applying numerical continuation.

CONCLUSION

This work is in progress. So far a model has been established for theoretically analyzing the dynamics of a moving string fixed between supports undergoing simultaneous transverse and longitudinal motion. The method of multiple scales will be used for analyzing the nonlinear system to obtain analytical results useful for understanding the dynamics of roller chain drives.

REFERENCES

[1] Parker, R. G. and Lin, Y., Parametric instability of axially moving media subjected to multifrequency tension and speed fluctuations, *Journal of Applied Mechanics -Transactions of the ASME* **68**(1) (2001) pp. 49–57.

[2] Chen, C. K. and Freudenstein, F., Toward a more exact kinematics of roller chain drives, *Journal of Mechanisms Transmissions and Automation in Design -Transactions of the ASME* **110**(3) (1988) pp. 267–275.

[3] Chen, Li-Qun, Analysis and control of transverse vibrations of axially moving strings, *Applied Mechanics Review* **58**(2) (2005) pp. 91–116.

[4] Wickert, J. A., Nonlinear vibration of a traveling tensioned beam, *International Journal of Non-Linear Mechanics* **27**(3) (1992) pp. 503–517.

[5] Wickert, J. A. and Mote, C. D., Classical vibration analysis of axially moving continua, *Journal of Applied Mechanics* **57**(3) (1990) pp. 738–744.

P5 Publication 5

The following extended abstract [P5] was submitted to and presented at the 7th European Nonlinear Oscillations Conferences (ENOC) in Rome, Italy 2011. It reports on the early stages of analyzing the span dynamics using axially moving strings.

Roller chain drive analysis: simplified modeling and analysis of the dynamic effects of meshing

Niels Fuglede* and Jon Juel Thomsen*
*Department of Mechanical Engineering, Technical University of Denmark, Building 404, DK-2800 Lyngby, Denmark

Summary. Transverse vibration of a roller chain and the effects of the interaction with sprockets is examined analytically. Modeling the chain as a uniform string, we consider the meshing process either as a moving boundary, or as boundary impacts and apply perturbation methods to predict dynamical responses.

Introduction

We analyze the transverse vibrations of a traveling string subjected to the excitation at the boundaries that is typical of roller chain drives. Meshing of a roller chain with a sprocket causes noise and vibration, and by modeling the chain as a moving, heavy, uniform string we present two approaches to how the dynamical effects of meshing can be analyzed. Modeling a roller chain as a uniform heavy string and studying the transverse vibrations for simple harmonic excitation was considered already by [1]. Traveling strings in general is a rich field which has been subject to many studies, see e.g. the comprehensive review by [2]. In a roller chain drive, the chain is subjected to complicated excitation when it interacts with the sprockets, because of the discrete nature of the chain and sprockets, known as polygonal action. A detailed study of the kinematic characteristics of roller chain drives is given in [3] and studies of impact intensities between roller and sprockets were carried out by [4]. Linear transverse vibrations of moving strings was considered by [5] and also weak nonlinearity has been investigated [6]. Here, it is demonstrated how the interaction between a chain and two sprockets is nonlinear. We present a simplified model of the chain, and two methods for how the system can be analyzed by considering the meshing process as equivalent to a) kinematically forced boundary conditions, or b) boundary impacts.

Physical system

Figure 1a shows a schematic of a chain drive consisting of two sprockets and illustrates the discrete nature of the drive. The driving sprocket rotates at an angular velocity $\dot{\theta}_1$ and the chain travels axially with velocity v. Relative velocities between the approaching roller, $\oplus$ and the sprocket seat $\times$ causes impacts, and this meshing process is a significant source of noise and vibration. This and e.g. a periodically varying chain tension are inherent for roller chain drives, owing to the sprockets forming polygons instead of circles. Meshing is shown in greater detail in Figure 1b, and here it is seen that the chain and sprocket interaction is nonlinear, because it depends on the vibration of the axially moving chain. Similarly, guide bars installed to limit transverse vibrations of chain spans may also introduce impact effects. We aim at analyzing the transverse vibration of the chain when subjected to this characteristic excitation, specifically the *effects* of meshing, and we consider only the dynamics of a single chain span, i.e. the tight chain span is analyzed while the dynamic responses of the sprockets and other chain drive components are not considered.

Analysis

Fundamental mathematical model

Our first approximations for a model to analyze transverse vibrations of a roller chain span is to assume that the chain can be modeled as a uniform heavy string, with mass per unit length m, i.e. the periodic variation of chain density and cross sectional area are both neglected, and the bending stiffness is assumed to be vanishing. Chain tension T and length L are considered to be constant, and we assume $\dot{\theta}_1$ is given such that the axial velocity v is constant and lower than the speed

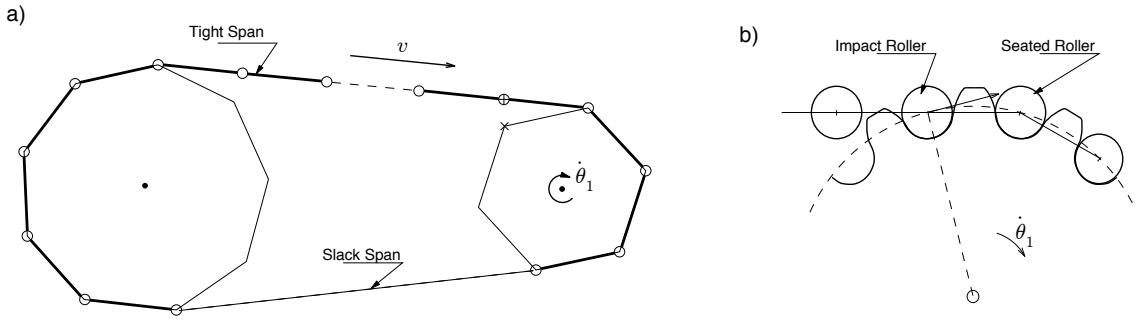

Figure 1: a) Principal sketch of a chain drive consisting of two sprockets. Sprockets form polygons, and impact happens between the approaching chain roller $\oplus$ and the sprocket seat $\times$. b) Sketch showing a more realistic drawing of the situation where the impact roller, suspended between the seated roller and the remaining chain span gets into contact with the sprocket seat.

of propagating transverse waves, $v_0 = \sqrt{T/m}$. The equation of motion governing the transverse displacement $w(x,t)$ of the traveling string is [1]:

$$w_{,tt} + 2vw_{,xt} + (v_0^2 - v^2)w_{,xx} + N(w) = 0, \tag{1}$$

where a comma subscript denotes partial differentiation and $N(w)$ has been added to contain nonlinear operators of w. With $N = 0$ equation (1) is linear, but nonlinearity must be included if e.g. finite vibration amplitudes between axially fixed boundaries are to be considered, as could be necessary for obtaining realistic solutions at resonant excitation.

Kinematically forced boundaries

First, we analyze the effect of chain and sprocket meshing by making the string kinematically forced, that is by specifying boundary motion as a function of time, i.e. $w(0,t) = \delta_1(t)$ and $w(L,t) = \delta_2(t)$, as illustrated in Figure 2a. Such a system is conveniently analyzed by applying the transformation $w(x,t) = \tilde{w}(x,t) + \delta_1(t)(1 - x/L) + \delta_2(t)x/L$, which renders the boundary conditions homogeneous while the excitation at the boundaries is moved to the differential equation for $\tilde{w}$. When $N(w) = 0$ equation (1) has exact closed form solutions for arbitrary excitation and this will be used as a basis for a perturbation solution when nonlinearity is included.

Boundary impact forces

As an alternative to the kinematic forcing described above, we analyze the effect of meshing by specifying the position of an impact surface $w_0 = w_0(x,t)$, allowing for contact between the chain and sprocket away from the boundaries. This contact will depend on the vibration of the chain and is a nonlinear force $g(w - w_0)$ of the discontinous clearance type. Boundary conditions for equation (1) are homogeneous in this case, and of special interest are the effects of nonlinear terms of the clearance type, see Figure 2b. A system of this type can be analyzed through, e.g., discontinuous transformations, by doing a Fourier expansion of the nonlinear terms, or by use of numerical methods such as continuation. As a first step, we aim towards a perturbation solution of (1) when nonlinearity of the clearance type is included, and treated analytically by Fourier expansion.

Expected results

By making simplified mathematical models of a chain span and examining specific phenomena, we aim at contributing with simple predictions that are relevant for understanding the complexity of full chain drive systems. With perturbation solutions obtained by the approaches outlined above, we aim towards analytical predictions of frequency responses, and effects of nonlinearity to be investigated for, e.g., slow- medium- and fast excitation frequencies. Approximate analytical results will be tested against numerical simulation of the simple models. Furthermore we aim to examine the validity of the physical approximations by comparing analytical results with detailed Multibody Dynamics Simulations, and possibly with existing experimental results.

Conclusions

This work is in progress. We expect to find an analytical expression for the transverse vibrations of a traveling string subjected to the characteristic excitation from chain and sprocket meshing.

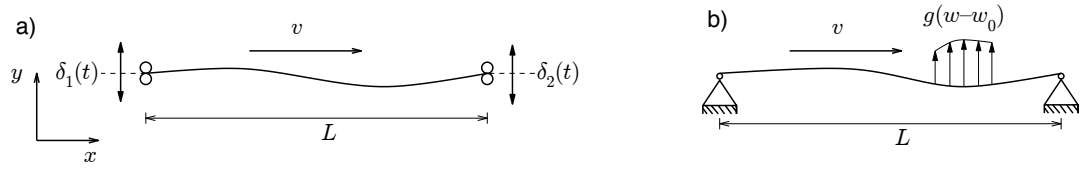

Figure 2: The chain is modeled as a moving string and the effect of meshing is examined by a) specifying the motion of the boundaries, or b) by specifying the motion of a contact surface $w_0(x,t)$ away from the boundaries with a nonlinear forcing of the clearance type $g(w - w_0)$ used to examine the effects of meshing.

References

[1] Mahalingam, S. (1957). Transverse vibrations of power transmission chains. *British Journal of Applied Physics*, **8**(4):145–148.

[2] Chen, L.-Q. (2005) Analysis and control of transverse vibrations of axially moving strings. *Applied Mechanics Reviews* **58**(2):91–116.

[3] Chen, C. K. and Freudenstein, F. (1988) Toward a more exact kinematics of roller chain drives. *Journal of Mechanisms Transmissions and Automation in Design-Transactions of the ASME*, **110**(3):269–275.

[4] Wang, K. W., Liu, S. P., Hayek, S. I., and Chen, F. H. K. (1992). On the impact intensity of vibrating axially moving roller chains. *Journal of Vibration and Acoustics-Transactions of the Asme*, **114**(3):397–403.

[5] Wickert, J. A. and Mote, C. D. (1990). Classical vibration analysis of axially moving continua. *Journal of Applied Mechanics-Transactions of the ASME*, **57**(3):738–744.

[6] Moon, J. and Wickert, J. A. (1997) Non-linear vibration of power transmission belts. *Journal of Sound and Vibration*, **200**(4):419–431.

Appendices

A Input file for SIMCH

A.1 Configuration C, 10 rpm

 # ————————————————————————————————
 # Filename: two_10rpm.dap
 # Type: Inputfile for SIMCH
 # Author: Niels Fuglede
 # Edited: 06/03/2014
 # Purpose: Generate the medium 12-18 configuration, c.f. kinematics paper.
 # Purpose: Comparison with analytical kinematic and dynamics results.
 # Purpose: Calculate 10 tooth periods for t≥3 with 2048 samples per tooth period.
 # Purpose: Correct chain stiffness to LINK STIFFNESS, correct yc position
 # Purpose: Reduce chain damping, both longitudinal and rotational
 # Purpose: Increase pretension; move driver sprocket in + x-direction
 # Purpose: Create Velocity Sweep Set
 # ————————————————————————————————
 # DEFINING CHAIN DRIVE - Geometry and Mechanics
 # 1.1) Declaration of datasets for the "Continous contact force method"
 # Syntax: continousforcedata number <number> [power_n <n>] equivalent_stiffness <Keq> restitution_coefficient <e> [friction <μ>]
contin num 2 eq 5.5D8 power_n 1.5 rest 0.5 fric 0.1D0
 # 2.1) Declaration of Sprockets
 # Syntax: sprocket name <text> geometric_center <X> <Y> [center_mass <X> <Y>] teeth <number> radius <radius> [mass <mass>] inertia <inertia> status <1=driver—2=driven> dataset <number> externalforces <value> <value> <value> direction <1—-1> [damping <coefficient>]
spro nam spro2 geo 0.0 0.0 cen 0.0 0.0 te 18 rad 0.0731393 mass 1.68 /

in 0.046 sta 2 ext 0. 0. 0. dat 2 dir -1 damp 0.1
spro nam spro4 geo 0.315980 0.024628233853020 /
cen 0.315980 0.024628233853020 te 12 rad 0.0490728 mass 0.68 /
in 0.000867 sta 1 ext 0. 0. 0. dat 2 dir -1 damp 0.1
 # 2.2) Declare Sprocket Tooth (Optional, default is BSreal)
 # Syntax: Tooth [BSreal — real — non — beta — circle — 2BSreal — 2real]
tooth real
 # 2.3) Declare friction method (Optional, default 1heaviside v0=0.1D0, v1=0.3D0, v2=0.01D0)
 # Syntax: friction linear — polynomial — bezier — 1heaviside — 2heaviside — 3heaviside <value> <value> <value>
friction 1heaviside 0.5D0 0.6D0 0.05D0
 # 3.1) Declaration of Chain
 # Syntax: chain number_of_links <number> pitch <pitch> radius <r> stiffness <K> mass_pr_link <mass> damping <LD> rotdamping <RD>
chain num 40 pitch 0.0254 radius 0.0079375 /
sti 0.221D9 mass 0.066 da 0.01 Rotdamp 0.001
 # 4.1) Declaration of Guidebars (Optional), delta = 0.003
 # guid num 1 data 2 si 1 sj 2 ri 1.75 rj 2.25 inde 0.005 roun 0.55 end 0.2 angle 0.0
 # guid num 2 data 2 si 2 sj 1 ri 2.25 rj 1.75 inde 0.005 roun 0.55 end 0.2 angle 0.0
 # 5.1) Declaration of Tightner Mechanism (Optional, use only when tightner involves mass, spring and dampers)
 # ————————————————————————————————
 # LOADING AND EXITATION
 # 6.1) Declaration of chain pre-tension
 # Syntax: tension sprocket <name1> circle — linear <value2> <value3> <value4> pretension <value5> [tolerance <value6>] [method <value7>] [relaxparameter <value8>]
 # tens spro spro4 lin -1.0 1.0 0.049069 preten 40 meth 1 tolera 0.001 relax 1.00
 # 7.1) Declaration of Torsional Vibration (Applied to driver, from data file)
 # Syntax: TorsionalVibration file <file.name> [acc_vs_angle — vel_vs_angle — acc_vs_time — vel_vs_time][scaletime <value>] [phase <value>] [convel_time <value>] [amplitudescale <value>]
 # From 4T40MX: TorsionalVibration file time_vs_ang_100rpm_GTORSI.txt acc_vs_time scaletime 10.0 phase 0 convel_time 0.0 amplitudescale 1.0
 # Declare angular acceleration file
 # torsion file sineAngAcc120rpm.txt acc_vs_angle scale 2.0
 # phase 0.0 convel_time 20.0
 # 8.1) Declaration of Contramoment (From file containing angle vs. acceleration in two collums)
 # Syntax: contramoment file <file name> sprocket <sprocket name>
 # contramoment file forcing_Acc_vs_Angle.txt sprocket spro1

 # 9.1) Declaration of Gravity (Default is off)
 # Syntax: gravity <on—off>
gravity off
 # 10.1)Declaration of Move Sprocket
 # Syntax: movesprocket sprocket <name> centre <value1> <value2> <circle <value3>
<value4> <value5> — line > time <value6>
 # 11.1)Declaration of orbit sprocket
 # Syntax: Orbit_spro sprocket <value1> file < value2>
 # ————————————————————————————————
 # PROGRAM EXECUTION
 # 12.1) Declaration of simulation time
 # Syntax: Time BegTime <value> EndTime <value> DeltaTime <value>
driver_frequency <value>
time beg 0.0 end 8.0 delta 0.00001 driv 10.0
 # 14.1) Declaration of Integrator
 # Syntax: Integrator abserr <value> relerr <value>
 # 15.1) Declaration of static equillibrium
 # static_equilibrium
 # 16.1) Declaration of LinScaleVelocity
 # Syntax: linscalevelocity startvelocity <rpm1> endvelocity <rpm2> starttime <time1>
 # endtime <time2> [minorder <min>] maxorder <max> amplitude <mag> [cosine]
 # 17.1) Declaration of NewPositionsFile
 # Syntax: newpositionsfile <filename>
 # newpositionsfile t17/two_stateq.out
 # 18.1) Declaration of newpvfile
 # newpvfile sim2014/t07/two_posvel.out
 # ————————————————————————————————
 # PLOTTING AND REPORTING
 # 27) Declaration of what to report
 # Syntax: report roller <pos — vel — acc > — sprocket <pos — vel — acc > —
LinkForce <number> — Displacement — Energy — AverageForce — Tightener
report rol pos rol vel rol acc spro pos spro vel spro acc linkforce 1 linkforce 40 displ ener aver
 # 28) Declaration of Animation
 # Syntax: animation <on—off>
ani on
 # 29) Declaration of what to plot
 # Syntax: plot [sprocket] [segment] [chain] [configuration] [forceconfiguration]
 # [window <value1> <value2> <value3> <value4>] [roller_numbers] [scaleforce <value5>
<value6> <value7>]
 # [win1] [win2] [win3] [win4] [xwin] [?] [zoomOff] — [gif] — [close] — [closeall]

plot forceconfiguration scaleforce 0.300E-03 0.300E-03 0.3000E-02
 # ————————————————————————————————
 # 13.1) Declaration of Simulation (default windows)
 # Syntax: Simulation [gif — xwin — windows — win1 — win2 — win3 — win4 <rate>] [plot_time <start> <end>]
 # [report_time <start> <end>] [roller_numbers <value>] [SampleFrequency <value>] [ScreenOutMin]
 # [tolerance <tolerance>] [time <value>] [tzero <value>]
sim gif 1.0 plot_time 0.0 60.0 report_time 3.0 8.0 samplefrequency 4096

DTU Mechanical Engineering
Section of Solid Mechanics
Technical University of Denmark

Nils Koppels Allé, Bld. 404
DK- 2800 Kgs. Lyngby
Denmark
Phone (+45) 4525 4250
Fax (+45) 4593 1475
www.mek.dtu.dk
ISBN: 978-87-7475-399-5

DCAMM
Danish Center for Applied Mathematics and Mechanics

Nils Koppels Allé, Bld. 404
DK-2800 Kgs. Lyngby
Denmark
Phone (+45) 4525 4250
Fax (+45) 4593 1475
www.dcamm.dk
ISSN: 0903-1685